Title
Mechanisms of inhibitory transmission at hippocampal synapses

Author
Nguyen, Quynh Anh

Publication Date
2017

Peer reviewed|Thesis/dissertation

Mechanisms of inhibitory transmission at hippocampal synapses

by

Quynh Anh Nguyen

DISSERTATION

Submitted in partial satisfaction of the requirements for the degree of

DOCTOR OF PHILOSOPHY

in

Neuroscience

in the

[redacted]

For my parents

Acknowledgments

First and foremost I would like to thank my thesis advisor, Roger Nicoll, for his support and guidance these past six years of graduate school. His love and enthusiasm for science, the rigor and meticulousness in which he approaches science, and his dedication to sharing and espousing his wealth of knowledge to his students and postdocs has indelibly left an impression on me and influenced my desire to continue to pursue scientific research in academia. Throughout the countless frustrations and difficulties encountered with experiments, Roger has provided stable reassurance and through our constructive discussions showed me ways in which to tackle the problems at hand. His passion for science and training the next generation of researchers are standards that I will carry with me throughout my scientific career.

I have been fortunate to be surrounded by a community of amazing, engaging, and inspiring people throughout my time in graduate school. I would like to thank the various members of the Nicoll lab who were there with me to share in the joys and frustrations of science. I joined the lab in the middle of two what I would call generations of trainees. Most of the first generation had come to the lab at least two years before I did, many of them well before that. They were invaluable in providing me the guidance and advice I needed from the start to become successful in the lab. I am grateful for the mentorship from my rig neighbors John Gray, Alexander Jackson, and Bruce Herring who were postdocs when I first started and have since moved on to start their own labs. The first project I worked on was in collaboration with John Gray and while the project itself did not bear much fruit I gained invaluable knowledge in electrophysiology and conveying scientific knowledge and ideas, allowing me to write and be successful in obtaining a fellowship to

fund my graduate studies. I am also thankful for the presence of multiple senior graduate students in the lab when I first started who provided help, guidance, and camaraderie, including Carleton Goold, Kathryn Lovero, Jonathan Levy, Adam Granger, and Seth Shipman. In particular, Seth's work on neuroligins at excitatory synapses provided the basis for my graduate work on neuroligins at inhibitory synapses and I am thankful for the helpful discussions and feedback he has provided on the subject. Other members include postdocs Wei Lu and Yun Shi who left to start their own labs soon after I joined yet have maintained welcome communication with the lab since. The second generation of trainees include graduate students Samantha Ancona-Esselmann and Meryl Horn, and it has been great to watch them develop into strong, independent scientists and thinkers. Meryl especially has been a welcome rig neighbor and collaborator as we were the only two people in the lab working on inhibition among a sea of projects on excitatory synapses. Also among this cohort are postdocs Nengyin Sheng, Javier Diaz-Alonso, Wucheng Tao, Argentina Lario Lago, and Salvatore Incontro. Argentina has been a source of helpful scientific and non-scientific advice and feedback. Salvatore has been helpful in discussions regarding the use of CRISPR and Wucheng has been helpful in discussions utilizing his background working in GABA receptor function. I would also like to thank the lab managers and laboratory technicians that I have been a part of this lab throughout the years. The tireless efforts of Kirsten Bjorgan, Manuel Cerpas, and Dan Qin in preparing our organotypic hippocampal slices, dissociated cultures, and maintaining the lab have been invaluable.

In addition I would like to thank the collaborators who have helped make this work possible. In particular I would like to thank the Roche lab at NIH and Michael Bemben,

who is now a postdoc in the Nicoll lab, for bringing me on to work on the neuroligin 4X project. Michael has also provided helpful advice regarding biochemistry experiments I needed to perform to finish up my neuroligin 2 paper.

I would also like to thank my committee members for their advice and guidance during graduate school. Peter Sargent provided helpful comments and guidance before and during my qualifying examination, and I greatly enjoyed being a teaching assistant for his Cell Physiology course at the UCSF School of Dentistry. Anatol Kreitzer has been helpful in discussions encompassing a range of topics regarding my present work, my aspirations for the science I want to do in the future, and advice regarding choosing a postdoctoral position. Kevin Bender has provided helpful feedback regarding experiments and the inclusion of certain unpublished yet thought-provoking data into this thesis. Robert Edwards has provided helpful guidance and advice regarding many aspects of science, from providing his expertise with regard to experiments, to discussing the nuances of grant writing, to his mentorship and feedback regarding finding a postdoc.

Outside of lab and school my friends have provided a continual source of joy and an outlet for discussion regarding work, life, and everything in-between. Their willingness to meet up, even at short notice, for a quick bite or to chat has been invaluable in providing relief both mentally and emotionally during graduate school. In particular I would like to thank May Tran, Austin Chou, Ada Yee, Ashley Smart, Bryan Seybold, and especially Raymond Wu for endless opportunities to play board games, go out for boba, eat good food, and watch terrible movies.

Last but not least I would like to thank my family for providing the source of inspiration for everything I do, including my mother, father, and younger brother. This thesis is largely a result of my parents' efforts to build a better life in America as refugees and the values that they fostered in me to utilize the opportunities available in this country to pursue knowledge and education.

Contributions

The experiments in Figures 1 and 2 of Chapter 3 were done in collaboration with Meryl Horn. The biochemistry and imaging experiments in Chapter 4 were performed by Michael Bemben from the laboratory of Katherine Roche. Mass spectrometry data in Chapter 4 was acquired by Yan Li from the Protein/Peptide Sequencing Facility at NINDS. Tongguang Wang from the Translational Neuroscience Center at NINDS performed research on and provided reagents for human neuronal cultures. All other experiments were carried out by Quynh Anh Nguyen.

The work presented in Chapter 3 has previously been published in *eLife* and is reproduced with permission:

> Nguyen, QA, Horn, ME, Nicoll, RA. Distinct roles for extracellular and intracellular domains in neuroligin function at inhibitory synapses. *eLife*. 5: e19236 (2016).

The work presented in Chapter 4 has previously been published in Proceedings of the National Academy of Science and is reproduced with permission:

> Bemben, MA, Nguyen, QA, Wang, T, Li, Y, Nicoll, RA, Roche, KW. Autism-associated mutation inhibits protein kinase C-mediated neuroligin-4X enhancement of excitatory synapses. *Proc. Natl. Acad. Sci*. 112: 2551-2556 (2015).

ABSTRACT OF THE DISSERTATION

Mechanisms of inhibitory transmission at hippocampal synapses

By Quynh Anh Nguyen

Doctor of Philosophy in Neuroscience

University of California, San Francisco, 2017

The human brain contains billions of individual cells called neurons which are responsible for controlling all functions from breathing to complex thought. These neurons communicate with each other via the synapse, locations where signals from the presynaptic cell are relayed to the postsynaptic cell. Depending on the type of cell transmitting the signal and the receptors activated on the cell receiving the signal, each instance of communication either relays an excitatory or inhibitory response to increase or decrease the firing of the postsynaptic cell respectively. Each cell receives both excitatory and inhibitory connections from multiple different neurons. Cells that transmit inhibitory signals are much more diverse than the cells that transmit excitatory signals. Adding to this complexity is the vast diversity of proteins expressed at the synapse of inhibitory connections, varying from the composition of the receptors receiving the signal to the presence of multiple transsynaptic adhesion molecules stabilizing and mediating the line of communication. Recent advances have given us the molecular tools in which to probe the function of these proteins overall and with respect to particular connections they may be involved in. Here, I examine the function of two isoforms of the neuroligin family of cell adhesion molecules at inhibitory synapses. I find that one isoform, neuroligin 3, is

unable to function at the inhibitory synapse without the presence of the other isoform, neuroligin 2, and that this difference could be attributed to a domain within the extracellular region. I also show that neuroligin 2 can function in both a gephyrin-dependent and gephyrin-independent manner and identify key residues mediating these interactions. I also characterize an autism-associated mutation in the neuroligin 4X isoform and show that it prevents the function of this neuroligin at excitatory synapses by blocking its phosphorylation by PKC. Lastly, I utilize CRISPR/Cas9 technology and optogenetic methods to characterize the function of the different β subunit isoforms of the $GABA_A$ receptor in inhibitory transmission. I find that a functional $GABA_A$ receptor requires the β subunit and that knockout of the β3 subunit in particular significantly impairs inhibitory transmission coming from PV but not SOM interneurons.

Table of Contents

List of Figures

CHAPTER 1:

General Introduction

"As long as our brain is a mystery, the universe, the reflection of the structure of the brain will also be a mystery."

— Santiago Ramón y Cajal

More than a century ago a Spanish scientist by the name of Santiago Ramón y Cajal peered through his microscope and saw with amazing clarity the organization of the nervous system as being comprised of billions of separate cells. His sketches of what he observed remain, to this day, used as examples showcasing neural anatomy and neuronal diversity. His observations became the basis for the neuron doctrine, a central tenant of modern neuroscience which states that the nervous system is comprised of individual brain cells. These individual cells communicate with one another through a synapse, a structure that enables one neuron, the presynaptic neuron, to pass an electrical or chemical signal to another neuron, the postsynaptic neuron. The precise, coordinated assembly of the interfaces between cells enabling their communication involves the function of multiple different types of molecules. The various molecules expressed at each synapse determine the properties of that synapse, and there are many different types of synapses mediating communication to each cell.

The most common mechanism for neuronal signaling is via the chemical synapse. Here, an action potential travels down the axon of the presynaptic cell to the presynaptic terminal where it enables depolarization of the membrane and the opening of channels that are permeable to calcium ions. This local increase in calcium activates calcium-sensitive proteins located on vesicles containing neurotransmitters and leads to the fusion of these vesicles with the membrane of the presynaptic cell. This fusion event causes the neurotransmitters to be released outside of the cell where they then diffuse across the narrow space between the pre- and postsynaptic cell and eventually bind to receptors located on the postsynaptic cell. Activation of these receptors leads to the opening of ion channels in the postsynaptic membrane which in turn change the electrical potential of the postsynaptic cell.

The type of signal propagated through these synapses are determined by the specific molecules involved. The majority of fast, excitatory synaptic transmission in the brain occurs at glutamatergic synapses where synaptic vesicles filled with glutamate are released and bind to ionotropic glutamate receptors which causes depolarization of the postsynaptic neuron and propagation of the signal. Conversely, the majority of inhibitory synaptic transmission occurs at GABAergic synapses where synaptic vesicles filled with the neurotransmitter gamma-aminobutyric acid (GABA) are released and bind to GABA receptors which cause hyperpolarization of the postsynaptic neuron and prevents propagation of the signal. Each neuron receives multiple excitatory and inhibitory inputs. The precise coordination and integration of excitatory and inhibitory signals enable the emergence of network activity and complex function in the brain.

Establishing the synapse: The role of cell adhesion molecules

Before a synapse can perform its function in mediating neuronal communication, it has to first be formed and established. A central question is what determines the formation of an excitatory versus an inhibitory synapse. In addition, after it is formed what enables the maintenance of that synapse and its changes throughout development?

Cell adhesion molecules have a critical role in coordinating the precise specialization of either an excitatory and inhibitory synapse. In particular, an extensively studied type of cell adhesion molecule, the Neuroligin (NLGN) family of proteins, has been shown to be essential for proper synapse formation and development (Bemben et al., 2015b). Neuroligins come in multiple different isoforms: NLGN1, NLGN2, NLGN3, and NLGN4. NLGN1 is thought to mostly be at excitatory synapses (Song et al., 1999), NLGN2 is thought to be mostly at inhibitory synapses (Varoqueaux et al., 2004), and NLGN3 and NLGN4 are thought to be at both inhibitory and excitatory synapses (Budreck and Scheiffele, 2007; Graf et al., 2004; Hoon et al., 2011).

The critical role of neuroligins for proper synaptic development was shown by characterizing mice deficient in NLGN1, 2, and 3 or by employing methods to knockdown expression of these neuroligins. First, knockout mice display low rates of viability and this has been attributed to severe deficits in development and functioning of essential neuronal networks which control breathing and other autonomic tasks (Varoqueaux et al., 2006). In addition, knockdown of the neuroligins results in a significant reduction of inhibitory and excitatory synapse number (Chih et al., 2005). Single knockouts and knockdown of the neuroligins display minor effects, owing to the possibility of compensation by other neuroligins.

Neuroligins function via binding their corresponding adhesion molecule partner, the neurexin family of proteins, across the synapse (Nguyen and Sudhof, 1997). The synaptogenic nature of this interaction was shown by co-cultures of non-neuronal cells, which do not endogenously express neuroligins or neurexins, with neurons. Transfection of the non-neuronal cells to express either neuroligins or neurexins enables the respective axons or dendrites of the contacting neurons to form post- or presynaptic specializations onto the cell (Fu et al., 2003; Graf et al., 2004). Neurexins themselves encompass multiple isoforms and splice variants, with more than 1000 possible isoform combinations (Ullrich et al., 1995). The sheer number of isoforms for both neurexins and neuroligins reinforces the idea that these molecules could function as a code for defining synapses.

The expression of particular isoforms to mediate extracellular interactions between cell adhesion molecules is only an initial step in establishing a synapse. The particular intracellular molecules recruited to these sites of interactions are also another key point in which the function of particular synapses can be refined. Multiple scaffolding molecules, such as PSD-95 at excitatory synapses and gephyrin at inhibitory synapses have been suggested to interact directly with the intracellular c-terminus of the neuroligins (Irie et al., 1997; Poulopoulos et al., 2009). Interestingly, all neuroligins contain domains for interaction with both excitatory and inhibitory scaffolding molecules, and it is thought that post-translational modifications such as phosphorylation govern the accessibility and involvement of one domain over another dependent on the particular intracellular environment of either an excitatory or inhibitory synapse (Giannone et al., 2013).

E/I balance

Neurons receive multiple excitatory and inhibitory synaptic inputs. It is the balance between these two opposing signals that govern the firing properties of the cell and the dynamics of the neuronal network. Each excitatory input a cell receives is only able to contribute minimally to the local depolarization of the membrane. It is through coordinated excitation from many synapses that there is enough depolarization to enable the cell to fire. Critical to this is the activation of inhibitory synapses which hyperpolarize the cell to counter the excitation and prevent overly long and sustained firing. It is this ability to control the temporal dynamics of neuronal firing that is the basis for the generation of neuronal oscillations, the rhythmic activity of networks of neurons, which underlie complex thought and behavior such as wakefulness, attention, and memory. The balance between excitation and inhibition at the basal level is critical for these oscillations. Too much basal excitation lowers the dynamic range in terms of perceiving different types of neural oscillations due to an increase in the overall noise of the network whereas too much inhibition prevents firing and the generation of oscillations at all.

Diversity of inhibitory cell populations

GABA is the main inhibitory neurotransmitter in the brain. Most GABAergic neurons are thought to be local inhibitory cells called interneurons. Despite being only a small population of the total number of neurons, for example about 10-20% of the total population of neurons in the cortex, interneurons encompass a wide diversity of cell types

with 21 different types of interneurons in the CA1 region of the hippocampus alone (Klausberger and Somogyi, 2008; Rudy et al., 2011).

Interneurons can be classified largely based on their firing properties, molecular expression profiles, and the spatial region on the cell they target. For example, there are a subset of interneurons which express the molecular marker parvalbumin (PV). In the hippocampus, PV+ cells can be further subdivided into distinct groups based on their targeting profiles onto pyramidal cells: basket cells innervate the soma, axo-axonic cells innervate the axon initial segment, and bistratified cells innervate the dendrites (Klausberger and Somogyi, 2008). While the majority of PV+ cells are basket cells in the CA1 area of the hippocampus, the contribution of axo-axonic and bistratified cells are crucial for the generation of complex neuronal oscillations (Bezaire et al., 2016; Klausberger et al., 2003; Klausberger et al., 2004). Converse to the PV+ cells are the somatostatin (SOM) cells which by and large target the distal dendrites of neurons and are a separate population of interneurons (Kawaguchi and Kubota, 1997; Scheyltjens and Arckens, 2016).

Diversity of inhibitory receptors

The diversity of inhibitory cells is complemented by the diversity in the receptors that mediate their signal in the postsynaptic cell. The type-A GABAergic receptors ($GABA_A$ receptors) which bind GABA and are the principal mediators of fast inhibitory synaptic transmission in the brain are heteropentameric ion channels comprised of five subunits (Jacob et al., 2008). There are 19 different genes encoding the different subunit

members: α1-6, β1-3, γ1-3, δ, ε, θ, π, and ρ1-3 (Simon et al., 2004). While this genetic diversity enables the possibility of many subunit combinations, only a limited number of combinations have actually been found to exist in nature (Sigel and Steinmann, 2012). Canonically $GABA_A$ receptors are composed of two α subunits, two β subunits, and one other subunit (Chang et al., 1996; Sieghart and Sperk, 2002).

Much of the work on properties of $GABA_A$ receptors containing different subunit compositions have been done using overexpression of various subunits in non-neuronal cells (Macdonald and Olsen, 1994). For example, expression of different α subunit isoforms in heterologous cells resulted in different receptor kinetics dependent on the particular isoform involved, with α1 containing receptors possessing faster decay kinetics than α2 containing receptors (Lavoie et al., 1997). In addition, these recombinant expression systems have enabled identification of the sites of action for multiple pharmacological targets of the $GABA_A$ receptors such as benzodiazepines and barbiturates (Sieghart, 1995; Sigel et al., 1990).

Endogenous expression of the different $GABA_A$ receptor subunits varies across multiple brain regions and throughout development (Fritschy and Panzanelli, 2014; Laurie et al., 1992; Sieghart and Sperk, 2002). For example, the β3 subunit is the major β subunit in the fetal brain while in the adult brain the β2 subunit is more dominant (Laurie et al., 1992; Zhang et al., 1991). In addition, while the β2 subunit is the most abundant subunit expressed in the adult brain, its expression in the hippocampus is noticeably minimal (Sieghart and Sperk, 2002).

There is even region specific expression of particular subunit compositions within a cell itself. $GABA_A$ receptors can be located either synaptically or extrasynaptically.

Synaptic GABAergic transmission is responsible for the fast, phasic inhibitory signaling that underlies generation of synchronized neural activity and network oscillations whereas extrasynaptic tonic signaling is responsible for setting the membrane conductance of the cell (Cherubini, 2012; Walker and Kullmann, 2012). Synaptic activation of $GABA_A$ receptors requires precisely coordinated, transient release of GABA from the presynaptic terminals whereas activation of extrasynaptic receptors is largely due to ambient GABA within the extracellular space persistently activating these populations of receptors (Farrant and Nusser, 2005). Synaptic $GABA_A$ receptors are thought to require the γ2 subunit whereas the δ subunit is thought to only be found within extrasynaptic receptors (Brickley and Mody, 2012; Schweizer et al., 2003)

The ability to study the effect of specific subunits on the native function of $GABA_A$ receptors is limited by the availability of genetic knockout animals. In addition, the possibility of compensation by other isoforms may mask more serious phenotypes expected in global knockouts. For example, approximately 90% of knockout mice for the β3 subunit die within 24 hours of birth and the remaining mutants display epilepsy, deficits in motor coordination, and have a reduced life span (Homanics et al., 1997). Conversely, mice lacking the β2 subunit display grossly normal phenotypes despite losing about 50% of the total population of $GABA_A$ receptors (Sur et al., 2001).

Relevance to health and disease

The importance of molecules governing the balance between excitation and inhibition and the function of synapses is most apparent when defects in these molecules

lead to disease. Mutations in the neuroligins have been associated with various diseases ranging from autism, to schizophrenia, to mental retardation (Sudhof, 2008). $GABA_A$ receptors are thought to play a role in epilepsy, anxiety disorders, and even insomnia (Mohler, 2006). Making sense of these associations requires basic knowledge of the functions of these diverse synaptic molecules in normal conditions before we can determine what exactly goes awry in disease.

Individual synapses comprise specific neuronal circuits which are part of larger neuronal networks. The diversity inherent in synaptic molecules suggests that their individual properties help define the differences between specific connections. At the most basic level neurological disease is due to impairments in particular connections, in particular brain regions, and during particular windows of development. Defining how deficits in specific molecules affects synaptic transmission both broadly and at particular circuits will help identify areas, connections, and cells to target for treatment of neurological disorders.

I started off my graduate work trying to characterize how neuroligins function at inhibitory synapses. This led me to become interested in how individual mutations within the neuroligins affect their function. Finally, I was able to study the $GABA_A$ receptors themselves and define the requirements for their function.

The general approach of my studies is to use sparse transfection of organotypic hippocampal slice cultures and perform simultaneous electrophysiological recordings from a transfected and nearby untransfected control pyramidal cell in the CA1 region of the

hippocampus. This enables quantitative and internally controlled comparison of the cell-autonomous effects of each manipulation. Each particular manipulation is guided by the principal that the structure of a protein determines its function. Thus, expression of chimeric constructs or mutants possessing point mutations at regions of interest will enable understanding of the basic biology underlying those regions and how they contribute to the function of the protein overall. These general approaches can be combined with recently developed molecular tools to manipulate the expression of proteins to provide further clarity in showcasing fundamental principles underlying the function of synaptic proteins.

In chapter three I identify differences between the ability of neuroligin 2 and neuroligin 3 to function at inhibitory synapses. I hone in on a particular domain in the extracellular region of neuroligin 2 that is sufficient to confer its ability to independently function at inhibitory synapses onto neuroligin 3. In addition, I show that the intracellular region of any neuroligin including neuroligin 1 is able to confer function as long as it is linked to the extracellular region of neuroligin 2. I identify distinct residues within the intracellular region of the neuroligin that enables it to interact with downstream molecules in gephyrin-dependent and gephyrin-independent pathways to mediate proper synaptic transmission at inhibitory synapses.

In chapter four, I characterize the effects of phosphorylation by protein kinase C (PKC) at a specific site on the intracellular c-terminus of neuroligin 4X at excitatory synapses. I show that blocking phosphorylation at this site by expressing a phospho-null mutation prevents the potentiation of excitatory currents seen with overexpression of neuroligin 4X whereas introducing a phospho-mimetic mutation enhances the degree of potentiation observed. Furthermore, I show that an autism-associated mutation located near

the site of phosphorylation has the same effect as the phospho-null mutation, providing a basis for how this autism-associated mutation affects synaptic transmission.

Finally, in chapter five I use CRISPR/Cas9 technology to knockout expression of the β subunits of the $GABA_A$ receptor. I find that indeed, functional assembly of a $GABA_A$ receptor requires the presence of a β subunit. In addition, I find that presence of the β3 subunit is most important for maintaining proper inhibitory synaptic transmission in the absence of the other β subunits and that expression of β3 alone is sufficient to rescue inhibition that is lost when all endogenous β subunits are knocked out. I investigate synapse-specific requirements for β3 containing $GABA_A$ receptors using optogenetic approaches to isolate inhibitory responses from either PV or SOM interneurons. I found that inhibition from PV cells and not SOM cells are preferentially affected by loss of β3.

CHAPTER 2:

Methods

Mouse genetics

All animals were housed according to the IACUC guidelines at the University of California, San Francisco. To obtain channelrhodopsin (ChR2) expression in PV positive interneurons, *PV-ires-Cre* mice were bred with *Ai32* mice. To obtain ChR2 expression in SOM positive interneurons, *Sst-ires-Cre* mice were bred with *Ai32* mice. Mice that were either heterozygous or homozygous for each gene were used for preparation of organotypic slice cultures. *PV-ires-Cre* and *Sst-ires-Cre* mice were generously donated by Dr. V.S. Sohal, while *Ai32* mice were generously donated by Dr. Z.A. Knight.

Experimental constructs

Neuroligin overexpression constructs have previously been described and were based on RNAi-proofed HA-tagged rat NLGN2 and human NLGN3 (Shipman et al., 2011). We used an RNAi-proof NLGN1 isoform containing the B splice site. All neuroligin constructs were cloned into the pCAGGS expression plasmid by either PCR for truncations or overlap extension PCR for chimera, deletions, and point mutations followed by In-Fusion cloning (Takara Bio). All NLGN2 constructs contained an HA-tag and all chimera retained the NLGN2 version of the transmembrane domain. The triple microRNA construct to knockdown neuroligins 1, 2, and 3 (NLGN1-3miR) and NLGN3miR have been previously characterized (Shipman and Nicoll, 2012b; Shipman et al., 2011). Targeting sequence for the NLGN2miR construct was TTGCTGTTGAACTTGCTCCAT. Gephyrin-miR targeting sequence was AACAGGGAATGAGCTACTAAA. All targeting sequences were cloned using BLOCK-iT miR RNAi kit (Invitrogen). All constructs used for biolistic

transfection and lentiviral production co-expressed either a GFP or mCherry fluorophore for visualization.

Human pCAG-NLGN4X (WT, R704C, T707A, or T707D)-IRES-mCherry, pCAG-eGFP, pCAG-NLmiRs-GFP, and pRK5-FLAG-GluA1 plasmids were used for biochemical, electrophysiological, and imaging (synaptic markers) experiments. Human pCAG-HA-NLGN4X (WT, R704C, T707A, or T707D) were used in surface expression imaging experiments. pGEX-GST-NLGN c-tail constructs were made as previously described (Bemben et al., 2014). Point mutations were introduced using QuikChange Site-Directed mutagenesis. The primers used to construct NLGN4X R704C were Forward (FOR) 5' - ACAAAAAGGACAAGAGGTGCCATGAGACTCACAGG - 3' and Reverse (REV) 5' - CCTGTGAGTCTCATGGCACCTCTTGTCCTTTTTGT - 3', NLGN4X T707A were FOR 5' - AGGCGCCATGAGGCTCACAGGCGCC - 3' and REV 5' - GGCGCCTGTGAGCCTCATGGCGCCT - 3', and NLGN4X T707D were FOR 5'- GAGGCGCCATGAGGATCACAGGCGCCCC - 3' and REV 5' - GGGGCGCCTGTGACCTCATGGCGCCTC - 3'. The primers used to insert the HA-tag in pCAG-NLGN4X were FOR 5'- TATCCATACGACGTTCCGGACTACGCTCCAGT TGTCAACACAAATTATGGC -3' and REV 5'- AGCGTAGTCCGGAACGTCGTATG GATAATACTGTGCTTGGCTGTCAATGAG -3'.

The human codon-optimized Cas9 and chimeric gRNA expression plasmid (pX458) and lentiviral plasmid for expression of Cas9 (lentiCRISPR) were developed by the Zhang lab and obtained from Addgene (plasmid #48138 and #52961) (Ran et al., 2013; Sanjana et al., 2014). Design of gRNAs for CRISPR/Cas9 was followed as previously described (Incontro et al., 2014). Primers used to generate gRNA oligos were: β1 FOR 5' - CACC

GTTGATCCAAAACGACACCC - 3' and REV 5' - AAAC GGGTGTCGTTTTGGATCAAC - 3'; β2 FOR 5' - CACC GGATGAACAAAACTGCACGT - 3' and REV 5' - AAAC ACGTGCAGTTTTGTTCATCC - 3'; β3 FOR 5' - CACC GTAAAATTCAATGTCATCCG - 3' and REV 5' - AAAC CGGATGACATTGAATTTTAC -3'. gRNA oligos were initially cloned into px458 and then subcloned into pFUGW-mCherry. For subcloning and generation of chained gRNAs the following primers were used: insertion of first gRNA cassette FOR 5' - TTAATCGTACGAATTCGAGGGCCTATTTCCC - 3' and REV 5' - GGGTTAATTAATTCGAATGGCGTTACTATTGA - 3'; insertion of second and third gRNA cassette FOR 5' - TAGTAACGCCATTGCAAGAGGGCCTATTTCCC - 3' and REV 5' - GGGTTAATTAATTCGAATGGCGTTACTATTGA - 3'. The first gRNA cassette was inserted into pFUGW-mCherry digested with BstBI and EcoRI HF. The resulting oligo was cut with BstBI for each subsequent cassette insertion. gRNAs for β1 and β3 were optimized to recognize both rat and mouse genomic sequences whereas the gRNA for β2 only recognizes the rat genomic sequence due to high disparity between the rat and mouse genome for this gene.

For rescue experiments cDNA was obtained from GE Dharmacon for GABRB3 (CloneId: 3871111) and cloned into NheI and XmaI sites of pCAGGS-ires-GFP using the following primers: FOR 5' - ATTCGCGGCCGCTAGCGCCACC ATGTGGGGCCTTGCGGGAGG - 3' and REV 5' - AGGGGCGGATCCCGGG TCAGTTAACATAGTACAGCCAGTAAACTAAGTTGAAAAGAGA - 3'. Editing to prevent recognition of the cDNA by the CRISPR gRNA was done using the following

primers: FOR 5’ - CACCA CGGACGATATCGAGTTCTAT TGGCG - 3’ and REV 5’ - CGCCAATAGAACTCGATATCGTCCGTGGTG - 3’.

Lentivirus production

HEK293T cells were co-transfected with psPAX2, pVSV-G, and either NL2miR, Gephyrin-miR, lenti-CRISPR or β123-CRISPR-gRNAs, using FuGENE HD (Promega). Supernatant was collected 40 hours later, filtered, and concentrated using PEG-it Virus Precipitation Solution (System Biosciences). Resulting pellet was resuspended in Opti-mem, flash-frozen, and stored at -80°C.

qRT-PCR

Primary rat hippocampal dissociated neurons were prepared at E18.5 and infected with lentivirus expressing a Gephyrin-miR, NLGN2miR, or control GFP construct at DIV 4-7. Neurons were harvested at DIV17-18 by lysis and reverse transcribed to synthesize cDNA using a Power SYBR Green Cells-to-CT kit (Life Technologies). Amplification of cDNA by real-time PCR was quantified using SYBR Green with the following sequence specific primers: Neuroligin 2 FOR 5’ - CATTCAGAAGGGCTGTTCCA - 3’ and REV 5’ - GTCTTCCCGGGAGCTAGTAG - 3’; Gephryin FOR 5’ - GGGAATGAGCTACTAAATCCTG - 3’ and REV 5’ - TGATACCCTCATTCAAGGCA - 3’.

Immunoblotting

Primary rat hippocampal dissociated neurons were prepared at E18.5 and infected with lentivirus expressing constructs of interest at DIV 4-7. Neurons were harvested at DIV17-18 in Tris-buffered saline (25mM Tris pH 7.4, 150 mM NaCl) plus 0.5% Triton-X and protease inhibitor mix (Roche Applied Sciences, cOmplete Protease Inhibitor Cocktail Tablets). After incubation at 4°C for 30 minutes, cell lysates were centrifuged for 15 minutes at 12000g. Proteins were resolved by SDS-PAGE and analyzed by western blot using antibodies against gephyrin (1:5000, Synaptic Systems), actin (1:5000, Millipore C4), β1 (1:1000, NeuroMab), and β2/3 (1:500, NeuroMab).

To generate the rabbit NLGN4X pT707-Ab (against residues 703-712 in NLGN4X), animals were immunized with synthetic phosphopeptide Ac-CKRRHE(pT)HRRP-amide (New England Peptide). All Immunoblotting with the NLGN4X T707-Ab began with blocking in 5% PhosphoBLOCKER (CELL BIOLABS, INC) at room temperature, followed by 1% PhosphoBLOCKER in the primary and secondary Ab incubations. Antibodies used in the NLGN4X study were anti-NLGN4X (Sigma), anti-NLGN4X (abcam), anti-pan NLGN 4F9 (Synaptic Systems), anti-GST (Bethyl Laboratories), anti-FLAG (Sigma), anti-HA rat (Roche), anti-HA rabbit (Abcam), anti GluA1 pS831 (Covance), anti-PSD-95 (Neuromab), anti-VGLUT1 (Millipore), anti-MAP2 (Cell Signaling), and anti-actin (ABM) and were used at a concentration of 1 μg/μL.

For immunoblotting in HEK cells, HEK293T cells were maintained, transfected, and proteins were isolated as previously described (Bemben et al., 2014). Treatment with 200

ng/μL PMA (Tocris) or DMSO (Sigma) began 30-60 minutes before protein isolation. For IPs, cell lysates were incubated with 6 μg of NLGN4X pT707-Ab and protein A-Sepharose beads (GE Healthcare) at 4°C overnight. The following day the IPs were washed in TBS buffer containing 150 mM NaCl, 50 mM Tris-HCl, 1 mM EDTA, protease (Roche), and phosphatase (Sigma) inhibitors. The antibody conjugated beads were resuspended in SDS-PAGE sample buffer and subjected to Western blotting.

GST-Fusion Protein Production, *In Vitro* Phosphorylation, and Mass Spectrometry

Reagents were prepared and assays were performed and analyzed as previous described (Bemben et al., 2014).

Immunostaining and Imaging

Primary rat hippocampal dissociated neurons were prepared at E18.5 and transfected using Lipofectamine 2000 with pCaggs NLmiRs-GFP and either pCaggs-NLGN2, pCaggs-NLGN2Δ133 or NLGN4X constructs without the HA tag. 7 days later cells were prepped for immunostaining for surface and intracellular markers. Cells were first washed with cold HEPES external buffer (115 mM NaCl, 3.5 mM KCl, 10mM HEPES, 20mM Glucose, 1mM $MgCl_2$, 1.5mM $CaCl_2$, adjusted to pH 7.3 with NaOH) then incubated with anti-HA antibody (Y-11, 1:250, Santa Cruz Biotech) for 20 mins in the cold. Cells were then washed with HEPES external buffer and fixed in 4% paraformaldehyde in 4% PBS for 15 minutes room temperature. Cells were then washed with PBS and blocked in 10% goat serum in PBS with 0.1% Triton X-100. Cells were then washed with PBS with 0.1% Triton X-100

and labeled with Alexa 546- conjugated anti-rabbit secondary antibody (1:250, Thermo-Fisher Scientific) in PBS with 0.1% Triton X-100 with 2.5% goat serum and mounted with SlowFade Gold Antifade Mountant (Molecular Probes). Neurons were imaged with a 100x objective on a Zeiss LSM 510 confocal microscope. For analysis, images were collected and quantified by normalizing the fluorescence intensity of surface-expressed NLGN2 (or NLGN2Δ133) with the fluorescence intensity of GFP in each cell using ImageJ (NIH). All data analysis was done blinded to experimental conditions. Spine number was counted using the GFP signal from the NLmiRs construct from 3-4 regions of 30 μm/cell. Methods, reagents, and analysis for imaging were done as previously described (Bemben et al., 2014).

Human Neuron Cultures

Human fetal neural cells were cultured as previously reported (Wang et al., 2006). Total NLGN4X protein was quantified using the anti-NLGN4X Ab (Sigma).

Slice culture and biolistic transfection

Rat and mouse slice cultures were prepared on P6–8 as previously described (Stoppini et al., 1991). All experiments were performed in accordance with established protocols approved by the University of California San Francisco Institutional Animal Care and Use Committee.

Sparse biolistic transfections of organotypic slice cultures were performed 1 day after culturing as previously described (Schnell et al., 2002). Briefly, 100 μg total of mixed plasmid DNA was coated on 1μm-diameter gold particles in 0.5 mM spermidine, precipitated with 0.1 mM $CaCl_2$, and washed four times in pure ethanol. The gold particles were coated onto PVC tubing, dried using ultra-pure N_2 gas, and stored at 4°C in desiccant. DNA-coated gold particles were delivered with a Helios Gene Gun (BioRad). When biolistically expressing two plasmids, gold particles were coated with equal amounts of each plasmid and plasmids always expressed different fluorescent markers. Observed frequency of coexpression was nearly 100%. Slices were maintained at 34 °C with media changes every other day.

Electrophysiological recording

Recordings were performed at 7-10 DIV after 6-9 days of expression or for CRISPR experiments at DIV 22-36 after 3-5 weeks of expression. Dual whole-cell recordings of CA1 pyramidal neurons were done by simultaneously recording responses from a fluorescent transfected neuron and a neighboring untransfected control neuron. Synaptic responses were evoked by stimulating with a monopolar glass electrode filled with aCSF in stratum radiatum of CA1. Typically each pair of neurons is from a separate slice, whereas on rare occasions two pairs may come from one slice. For all paired recordings, the number of experiments (*n*) reported in the figure legends refer to the number of pairs. Pyramidal neurons were identified by morphology and location. To ensure stable recording, membrane holding current, input resistance, and pipette series resistance were monitored throughout recording. All recordings were made at 20–25 °C using glass patch

electrodes filled with an internal solution consisting of 135 mM $CsMeSO_4$, 8 mM NaCl, 10 mM HEPES, 0.3 mM EGTA, 4 mM Mg-ATP, 0.3 mM Na-GTP, 5 mM QX-314, and 0.1 mM spermine and an external solution containing 119 mM NaCl, 2.5 mM KCl, 4 mM $MgSO_4$, 4 mM $CaCl_2$, 1 mM NaH_2PO_4, 26.2 mM $NaHCO_3$ and 11 mM glucose bubbled continuously with 95% O_2 and 5% CO_2. Recordings of IPSCs were made in the presence of APV (100 μM) and NBQX (10 μM) to block NMDA and AMPA-mediated currents respectively. Recordings of excitatory current were made in the presence of picrotoxin (100 μM) to block inhibitory currents and a small (50 nM) amount of NBQX to reduce epileptiform activity at −70 mV (AMPA). AMPAR-mediated currents were measured at the peak of the current at -70 mV whereas NMDA currents were measured at +40 mV and 100 ms after the stimulation. Stimulation was delivered using 8 sec interstimulus intervals. Data were acquired using a Multiclamp 700B amplifier (Axon Instruments) controlled by a Master 8 stimulator (A.M.P.I.).

GABA puff experiments were performed using a Picospritzer II (General Valve Corporation). 100μM final concentration of GABA was dissolved in 140 mM NaCl, 5 mM KCl, 5 mM EGTA, 1.4 mM MgSO4, 1 mM NaH2PO4, 10 mM glucose, and 10 mM Hepes, pH 7.2. Agonist was applied using 100 ms pulses at a pressure of 100-300 kPa.

For optogenetic experiments, a TLED+ transmitted light source (Sutter Instruments) was used to deliver blue light through the 40x objective. Light pulse duration and onset were controlled by the Master 8 stimulator. Duration of light pulses ranged from 0.5-2 ms and intensity ranged from 0.5-2.5 mW/mm^2. Optogenetic stimulation was delivered at 15 sec interstimulus intervals.

Statistical analysis

All paired whole-cell data were analyzed using a two-tailed Wilcoxon matched-pairs signed rank test. For comparisons between different experimental groups, a Mann Whitney test was used on the ratios of the transfected cell to the control cell. Data analysis was carried out in Igor Pro (Wavemetrics), GraphPad Prism (GraphPad Software) and Excel (Microsoft). Statistical significance of immunoblots was tested using a t-test, immunocytochemistry with a one-way ANOVA.

CHAPTER 3:

Distinct roles for extracellular and intracellular domains in neuroligin function at inhibitory synapses

Introduction

Proper balance between inhibitory and excitatory connections is important for proper functioning of neuronal circuits (Bang and Owczarek, 2013; Mackowiak et al., 2014). Cell adhesion molecules have a critical role in coordinating the apposition of presynaptic terminals with postsynaptic sites of differentiation (Washbourne et al., 2004; Yamagata et al., 2003). While much work has been done to determine the molecular organization of cell adhesion molecules at excitatory synapses, less is known about how these components are organized at inhibitory synapses.

Neuroligins are a family of postsynaptic cell adhesion molecules that interact trans-synaptically with their corresponding presynaptic neurexin binding partners to mediate proper synaptic function (Chih et al., 2005; Sudhof, 2008). Rats express three neuroligins (NLGN1-3): NLGN1 is expressed exclusively at excitatory synapses, NLGN2 is selectively present at inhibitory synapses, while NLGN3 is found at both excitatory and inhibitory synapses (Budreck and Scheiffele, 2007; Song et al., 1999; Varoqueaux et al., 2004). NLGN2 and 3 share many previously identified domains both in their extracellular and intracellular regions. Despite the similarities between the two proteins, it is currently unknown whether they perform the same function at inhibitory synapses. One notable difference between NLGN2 and 3 resides in the extracellular region at splice site A which has previously been proposed to affect NLGN binding to its presynaptic neurexin partner (Chih et al., 2006; Ichtchenko et al., 1996).

It has been suggested that NLGN2 functions through a direct interaction on its cytoplasmic tail with gephyrin, a scaffold protein thought to be essential for stabilizing glycine and $GABA_A$ receptors at inhibitory synapses (Choii and Ko, 2015; Tyagarajan and Fritschy,

2014). In addition, it has been proposed that collybistin, a brain-specific guanine nucleotide exchange factor (GEF), helps regulate the localization of gephyrin, and that NLGN2 is a specific activator of collybistin via a direct interaction at the proline rich region in its cytoplasmic tail (Kins et al., 2000; Poulopoulos et al., 2009; Soykan et al., 2014). While previous studies have been able to link these interactions to NLGN2, there has been no direct study of whether these interactions are necessary for proper functioning of NLGNs at inhibitory synapses.

To investigate the importance of NLGN2 and 3 at inhibitory synapses, we used microRNAs targeted to NLGN2 or 3 individually. We found that NLGN2 is a critical component of inhibitory synapses while NLGN3 function at inhibitory synapses depends on the presence of NLGN2. Further investigation expressing chimeric constructs of NLGN2 and 3 in isolation, using a microRNA targeting all three endogenously expressed NLGNs 1, 2, and 3, identified a previously uncharacterized domain in the extracellular region that accounted for this functional difference between NLGN2 and 3. Using a similar technique to study the importance of the intracellular region in NLGN function at inhibitory synapses, we found a critical requirement for the cytoplasmic tail and identified two key residues that are separately involved in gephyrin-dependent and gephyrin-independent mechanisms of NLGN function at inhibitory synapses. We further show that an autism-associated mutation inhibits the gephyrin-dependent pathway while a phosphorylation site is responsible for modulating the gephyrin-independent pathway. These findings identify new mechanisms for NLGN function, particularly at inhibitory synapses, and provide new avenues of study for elucidating the molecular mechanisms present at inhibitory synapses.

Results

NLGN2 is the critical NLGN at inhibitory synapses

To determine the relative contributions of NLGN2 and 3 to inhibitory synaptic transmission, we utilized targeted miRNA constructs to knockdown either NLGN2 or 3 (validated in Figure 2a and (Shipman and Nicoll, 2012b)). We biolistically transfected organotypic hippocampal slices with our constructs of interest and performed dual-whole cell recordings from CA1 neurons 7-10 days after transfection. Compared to a previously validated knockdown construct of NLGNs 1-3 (Shipman et al., 2011) which reduces inhibitory synaptic transmission to about 50% (Figure 1a) we found that while NLGN2 knockdown alone recapitulated the 50% decrease in inhibitory synaptic transmission (Figure 1b and 1d), NLGN3 knockdown alone had no effect on inhibitory synaptic transmission (Figure 1c and 1d). Furthermore, while overexpression of NLGN3 alone does enhance inhibitory synaptic transmission (Figure 1e and 1g), overexpression of NLGN3 with a NLGN2 knockdown construct fails to enhance inhibitory responses (Figure 1f and 1g), suggesting that NLGN3 requires the presence of NLGN2 to function at inhibitory synapses. This is consistent with previous results showing no enhancement of inhibitory responses when NLGN3 was overexpressed on a NLGN1-3 knockdown background (Shipman et al., 2011). Notably, NLGN3 overexpression on a NLGN2 knockdown background still enhanced excitatory responses similar to NLGN3 overexpression alone (Figure 2b, 2c, and 2d), suggesting our effects are specific for inhibitory synapses.

Difference between NLGN 2 and 3 function at inhibitory synapses resides in distinct domain in the extracellular region

To determine where this functional difference between NLGN2 and 3 at inhibitory synapses resides, we made chimeric constructs and expressed them on the reduced endogenous NLGN (NLGN1-3miR) background to study the effects of our constructs in isolation (Figure 3a). Expression of the full-length NLGN2 resulted in a large enhancement of inhibitory currents (Figure 3b and 3e). Expression of a construct containing the NLGN2 extracellular region and NLGN3 cytoplasmic tail enhanced inhibitory currents (Figure 3c and 3e) similar to full-length NLGN2 (Figure 3e). However, expression of a construct containing the NLGN3 extracellular region and NLGN2 intracellular region failed to enhance inhibitory currents (Figure 3d and 3e), suggesting that the functional difference between NLGN2 and 3 at inhibitory synapses resides in the extracellular region. Importantly, while the NLGN3 extracellular-NLGN2 intracellular chimeric construct failed to enhance inhibitory responses, it was still able to potentiate excitatory responses (Figure 4), indicating that this construct is expressed and functional. It further shows that there are differential requirements for NLGN3 function at inhibitory versus excitatory synapses, and that the NLGN2 c-tail is capable of functioning at excitatory synapses.

We constructed further chimeric constructs to determine where in the extracellular region this difference between NLGN2 and 3 resides and if we could effectively confer NLGN2 function onto NLGN3 by transplanting a critical domain. There are various components located in the extracellular region which have previously been suggested to be important for NLGN function (Figure 5a and Figure 6a). One key component of the extracellular region, the critical dimerization residues, are conserved between NLGN2 and

3, suggesting that differences between NLGN2 and 3 may not be due to differences in ability to dimerize (Dean et al., 2003; Ko et al., 2009; Shipman and Nicoll, 2012a). One notable domain of interest resides in splice site A, which is important for neurexin binding (Chih et al., 2006; Ichtchenko et al., 1996). Interestingly, there are many differences between NLGN2 and 3 at this splice site, and these might account for the functional differences between the two.

Starting from the proximal region closest to the transmembrane region, we progressively added back regions of NLGN2 onto the NLGN3 extracellular region while keeping the NLGN2 c-tail intact. We first inserted a region of NLGN2 up to the 623rd amino acid that contains substantial differences between it and NLGN3 (Figure 5a and Figure 6a). Neither this chimeric construct (Figure 5b and 5h) nor one adding back NLGN2 right before splice site A at the 180th amino acid (Figure 5c and 5h) was able to enhance inhibitory currents. However, adding back NLGN2 up to the 52nd amino acid was able to potentiate inhibitory currents (Figure 5d and 5h). Further refinement showed that transplanting just the domain between the 52nd and 180th amino acid of NLGN2 was able to fully confer NLGN2 ability to potentiate inhibitory currents onto NLGN3 (Figure 5e and 5h). Since this domain encompassed the splice site A and a previously uncharacterized domain of the extracellular region, we wanted to know whether the splice site A or the uncharacterized domain alone was sufficient to confer NLGN2 function onto NLGN3. While expression of a chimeric construct containing the uncharacterized extracellular domain of NLGN2 between amino acids 52-164 showed a modest enhancement of inhibitory currents (Figure 5f and 5h), it was far less than the effect of the full length NLGN2 (Figure 5h). A chimera containing only the splice site A domain of NLGN2

(Figure 5g and 5h) failed to enhance inhibitory responses. Importantly, all chimeric constructs, except NLGN3-180-NLGN2 which appears non-functional, that failed to potentiate inhibitory responses were still able to potentiate excitatory responses, indicating that they were functional (Figure 6b). Together, this suggests that the splice site A domain alone does not account for the differences between NLGN2 and 3 function but that a previously uncharacterized adjacent domain is also required.

A c-tail is required for NLGN function

Since the c-tails of the NLGNs share many similar domains (Figure 7a), and our previous results showed that the c-tails of NLGN2 and 3 were interchangeable (Figure 3c and 3d), we wanted to know whether the c-tail of NLGN1, a NLGN that is selectively present at excitatory synapses, was also capable of functioning at inhibitory synapses. In experiments done on a reduced endogenous NLGN background, full-length NLGN1 was unable to enhance inhibitory responses (Figure 7b and 7d), while a chimeric construct containing the NLGN2 extracellular region with a NLGN1 intracellular region was able to enhance inhibitory currents (Figure 7c and 7d). To determine whether a c-tail is required at all, we created a truncation mutant lacking most of the c-tail except for a few amino acids closest to the transmembrane domain which might be necessary for proper trafficking of the protein (Δ133, Figure 7a). While overexpression of this truncation mutant on a wild-type background (Figure 8b and 8c) enhanced inhibitory currents to a similar extent as full-length NLGN2 (Figure 8a and 8c), expression on a reduced endogenous NLGN background showed no potentiation (Figure 7e and 7f), indicating that a c-tail is required for proper NLGN function and further underlies the need to observe the effects of our

mutant NLGNs on a reduced endogenous background due to the possibility of heterodimerization with endogenous NLGN. Importantly, the effect of the c-tail truncation was not due to impaired surface trafficking as shown by surface immunostaining of the HA-tagged NLGN2 constructs (Figure 8d and 8e).

Previously identified domains not critical for NLGN function at inhibitory synapses

To determine what domain(s) in the c-tail are necessary for NLGN function at inhibitory synapses, we made a series of truncations to the c-tail of NLGN2, deleting previously identified domains proposed to be important for its function (full diagram of relevant sites in Figure 10). First, it has previously been suggested that PSD-95 binds NLGN2, since it contains a PDZ domain (Irie et al., 1997). Second, in addition to PSD-95, which is localized to excitatory synapses, S-SCAM is another protein that is localized to both excitatory and inhibitory synapses and can also interact via the NLGN2 PDZ domain (Woo et al., 2013). To determine whether any of these interactions via the PDZ domain are important for NLGN2 function, we made a truncation mutant lacking the entire PDZ domain (NLGN2Δ4). We found that deleting the PDZ domain did not alter the function of NLGN2 (Figure 9a and 9d). Proximal to the PDZ domain is the proline-rich region, which has been shown to be important for collybistin binding and enabling the recruitment of gephyrin (Kins et al., 2000; Poulopoulos et al., 2009; Soykan et al., 2014). However, excision of this domain (NLGN2Δ32-39) or truncation of this domain and everything downstream of it including the PDZ domain (NLGN2Δ39) still significantly potentiates inhibitory currents (Figure 9b and 9d).

Another key domain suggested to be critical for NLGN function is the gephyrin-binding domain (Poulopoulos et al., 2009). The reigning model of NLGN function at inhibitory synapses purports that the interaction of gephyrin with NLGN2 via its gephyrin-binding domain enables the recruitment of $GABA_A$ receptors to the synapse (Choii and Ko, 2015; Tyagarajan and Fritschy, 2014). However, there have also been reports of gephyrin-independent mechanisms of $GABA_A$ receptor enrichment at inhibitory synapses (Kneussel et al., 2001; Levi et al., 2004). To determine whether the gephyrin-binding domain is critical for NLGN2 function, we employed a variety of methods to either disrupt or excise this region of interest. Surprisingly, we found that expression of NLGN2 with a phospho-mimic mutation previously shown to disrupt gephyrin binding (NLGN2 Y770A) (Giannone et al., 2013; Poulopoulos et al., 2009), excision of the whole gephyrin-binding domain (NLGN2Δ55-69), or, most dramatically, truncation of the gephyrin-binding domain and everything downstream of it, including all known functional domains of the NLGN2 c-tail (NLGN2Δ69), all still displayed significant potentiation of inhibitory currents (Figure 9c and 9d).

While our results suggest that the gephyrin-binding domain is not critical for NLGN2 function, we wondered whether gephyrin, itself, is required. To address this, we created a targeted knockdown construct for gephyrin that effectively knocks down more than 90% of gephyrin expression (Figure 12a and 12b). Expression of this construct reduced inhibitory currents to about 50%, similar to knockdown of all endogenous NLGNs (Figure 11a and 11c). Surprisingly, a NLGN2 truncation mutant lacking all known functional domains of the c-tail (NLGN2Δ69) coexpressed with our gephyrin and endogenous NLGN knockdown constructs was fully capable of enhancing inhibitory

currents (Figure 11b and 11c). These results indicate that NLGN2 can function, not only without previously known domains, but entirely independently of gephyrin as well.

NLGN function at inhibitory synapses requires two distinct regions in the c-tail

Our results suggested that there might be a previously uncharacterized region of the NLGN c-tail that is critical for its function at inhibitory synapses. We made further truncations starting at the region closest to our most terminal c-tail truncation (NLGN2Δ133) and found that deletion of a 35 amino acid stretch from that point (NLGN2Δ98-133) resulted in the loss of enhancement of inhibitory responses (Figure 13a and 13e). Further refinement identified a domain of 16 amino acids that, when deleted (NLGN2Δ117-133), also showed no enhancement (Figure 13b and 13e).

We next sought to identify any candidate residues that could be important within this domain. We were informed by our previous results that any NLGN c-tail would be able to function at inhibitory synapses and thus looked for residues that were shared among all the NLGNs. We focused on two sites, a residue at R705 linked to an autism mutation previously found in NLGN4 that inhibited its function at excitatory synapses (Bemben et al., 2015a), and a putative phosphorylation site at S714 previously shown to affect gephyrin binding to NLGN2 (Antonelli et al., 2014).

Individual mutations at these sites, either by expressing the phospho-null (NLGN2-S714A) (Figure 14a and 14d), phospho-mimic (NLGN2-S714D) (Figure 14b and 14d), or the analogous autism point mutation (NLGN2-R705C) (Figure 14c and 14d), still enhanced inhibitory responses comparable to full-length NLGN2. However, when we expressed the

double point mutant of the autism-associated mutation with the phospho-null mutation (NLGN2-R705C-S714A) (Figure 13c and 13e) the enhancement was dramatically reduced, suggesting that together these residues are critical for NLGN function at inhibitory synapses. Notably, when we tested another double point mutant with a phospho-mimic mutation at S714 instead, (NLGN2-R705C-S714D) (Figure 13d and 13e), we still saw robust enhancement of inhibitory currents, showing that our effect is phosphorylation-dependent.

Gephyrin-dependent and gephyrin-independent mechanisms

Our finding that there are two distinct requirements for NLGN function at inhibitory synapses could explain why we were unable to see an effect earlier with our gephyrin mutants if there are both gephyrin-dependent and gephyrin-independent mechanisms for NLGN function at inhibitory synapses. To determine whether this was the case, we made two more double mutants, combining either the autism mutation or phospho-null mutation with the point mutation in the gephyrin-binding domain that inhibits gephyrin binding (NLGN2-R705C-Y770A or NLGN2-S714A-Y770A). Since the Y770A mutation inherently blocks the gephyrin-dependent pathway, we wanted to know which of our mutations when combined with this manipulation would reveal the presence of a gephyrin-independent pathway. We expect that if either the R705C or S714A point mutations were in a gephyrin-independent pathway, we would observe reduced enhancement of inhibitory currents when combined with the Y770A point mutation that blocks gephyrin binding.

The combined autism mutation and gephyrin-binding double point mutant (NLGN2-R705C-Y770A) exhibited enhancement comparable to full-length NLGN2 (Figure 13f and 13h), while the combined phospho-null mutation and gephyrin-binding double point mutant (NLGN2-S714A-Y770A) showed significantly reduced enhancement (Figure 13g and 13h). Thus, while the three individual point mutations on their own still exhibited enhancement of inhibitory currents, it was only when we mutated both S714 and R705 or S714 and Y770A did we see impairment, suggesting these mutations to be involved in separate pathways. Also, mutation of both R705 and Y770 still exhibited enhancement of inhibitory currents similar to full-length NLGN2, suggesting that they function in the same pathway. Together, we propose the existence of two pathways: a gephyrin-independent pathway modulated at S714 and a gephyrin-dependent pathway modulated at both R705 and Y770 (Figure 15).

Discussion

Our results have uncovered the critical features of NLGN2 for proper inhibitory synaptic function and reveal domains in both the extracellular and intracellular regions of the NLGNs that are necessary for their function specifically at inhibitory synapses. Our systematic dissection of the relative contributions of NLGN2 and 3 to inhibitory synaptic function through targeted knockdown of one or the other revealed that while NLGN3 appears to be a dispensable component, NLGN2 is not and that, in fact, NLGN3 function depends on the presence of NLGN2. Further analysis via expression of chimeric NLGN2/3 constructs on a reduced endogenous NLGN background revealed that this difference between NLGN2 and 3 function at inhibitory synapses is due to differences within a domain in the extracellular region corresponding to a site important for neurexin binding, as well as a proximal uncharacterized region.

While this result seemed to suggest that the intracellular region is not important, our results clearly show that, although the intracellular region of any NLGN is sufficient for function at inhibitory synapses, if paired with the extracellular region of NLGN2, a c-tail is very much required. Thus, a NLGN2 truncation lacking most of the intracellular region failed to enhance inhibitory responses while maintaining a normal ability to traffic to the surface. Further refinement identified two distinct regions of the NLGN c-tail corresponding to gephyrin-dependent and gephyrin-independent mechanisms that enable proper function at inhibitory synapses. These results suggest that while the extracellular region is important for specifying function at an inhibitory or excitatory synapse, the intracellular region is critical for carrying out that function at both an inhibitory or excitatory synapse.

Due to the heterogeneous nature of inhibitory synapses, one question that arises is whether our observations are relevant only for particular subsets of inhibitory synapses. Previous work using simultaneous recording from connected neurons showed that NLGN2 knockout animals specifically displayed a deficit in PV but not SOM inputs onto hippocampal pyramidal neurons (Gibson et al., 2009). A similar set of studies in NLGN3 knockout animals showed an enhancement of CCK inputs but no change in PV inputs (Foldy et al., 2013). In our experimental system, we find that while knockdown of NLGN2 critically affects inhibitory transmission, knockdown of NLGN3 does not. Our results are consistent with the observations at PV synapses, suggesting either that our stimulation placement preferentially recruits responses from these types of synapses or that in our system PV inputs are responsible for a large proportion of inhibitory responses.

One limitation of our study is that the results we observe may not occur universally among all brain regions. Indeed, recent work has shown that within the cerebellum the basket/stellate cell synapses onto Purkinje cells exhibit a decrease in mIPSC frequency but not amplitude with knock-out of just NLGN2 while the double knockout of NLGN2 and 3 exhibit a much more dramatic impairment in both mIPSC frequency and amplitude (Zhang et al., 2015). In addition, there are inherent limitations with the organotypic slice preparation we have utilized in our experiments including but not limited to the presence of sprouting and rewiring of circuits and the high level of expression imparted by biolistic transfection.

The role of NLGN3 at inhibitory synapses

What might be the role of NLGN3 at inhibitory synapses since our results show that its absence does not affect inhibitory transmission, and that NLGN3 requires the presence of NLGN2 to function at inhibitory synapses? One possible explanation is that NLGN3 functions as an available mechanism to quickly enhance existing inhibitory synapses. Previous work looking at overexpression of NLGN2 or 3 in cerebral cortical neurons noticed that the majority of NLGN3 was not localized synaptically while the majority of NLGN2 was synaptically located (Fekete et al., 2015). From this, we can surmise the presence of a readily available pool of NLGN3 located outside the synapse that could be recruited and associate with NLGN2 in response to induction of plasticity.

This hypothesis is further strengthened by our result showing that transplanting a domain of the NLGN2 extracellular region corresponding to a key area associated with neurexin binding fully enabled NLGN3 to function at inhibitory synapses by itself. It suggests that NLGN3 is unable to bind to the corresponding neurexin partner at inhibitory synapses alone and that it needs to heterodimerize with NLGN2 in order to function. Previous work has already shown that different neurexin isoforms are expressed at different types of synapses, and that the neurexin isoform expressed at inhibitory synapses can bind to NLGN2 but not NLGN1 (Fuccillo et al., 2015; Futai et al., 2013). Thus, it is possible that NLGN3, which seems to be able to bind to the neurexins at excitatory synapses by itself, needs to associate with NLGN2 in order to bind to the neurexins at an inhibitory synapse, and this special property of NLGN2 resides in a unique domain in its extracellular region that we have now identified. An alternative hypothesis, and one that does not necessarily require the presence of NLGN2/3 heteromers, is that there is another molecule

in addition to neurexin that interacts within that domain of NLGN2 to stabilize the synapse and enable recruitment of NLGN3.

Extracellular region confers specificity

Our results showing that a chimeric NLGN3 extracellular region with a NLGN2 intracellular region was unable to potentiate inhibitory responses but could still enhance excitatory responses indicates that there are differential requirements for NLGN function at excitatory versus inhibitory synapses and that the extracellular region is critical for mediating this specificity. This is not surprising given that neurexin binding occurs at the extracellular region and that different neurexin isoforms are present preferentially at particular synapses. However, there could be other possible interactors that help define this functional specificity. Previous work has shown that NMDA receptors are able to bind to the extracellular region of NLGN1 but not NLGN2 or 3 (Budreck et al., 2013). In addition, the presence of the B splice site insertion in NLGN1 enables it to enhance NMDA currents and promote LTP, and this site is notably absent in NLGN3 (Shipman and Nicoll, 2012b). For inhibitory synapses, previous work has shown that MAM domain-containing glycosylphosphatidylinositol anchor proteins (MDGAs) are able to negatively regulate the function of NLGN2 through an interaction within their extracellular region (Lee et al., 2013; Pettem et al., 2013). Also, there are multiple glycosylation sites in the extracellular region of the NLGNs and previous work has shown that glycosylation state can affect neurexin binding (Comoletti et al., 2003; Hoffman et al., 2004). However, the analogous glycosylation sites initially found in NLGN1 are conserved among both NLGN2 and 3 within our critical domain, suggesting that they may not explain the difference we see in

function. Previously identified cysteine residues that form disulfide bonds within the extracellular region are also conserved between NLGN2 and 3 within our critical domain (Hoffman et al., 2004). Thus, it would be of interest to determine what molecular interactions are occurring at our critical extracellular domain to mediate NLGN function at inhibitory synapses both in baseline conditions and in response to plasticity.

Intracellular region contains the toolbox for NLGN function at both excitatory and inhibitory synapses

Our results with chimeric constructs show that any NLGN c-tail is able to function at inhibitory synapses if linked with a NLGN2 extracellular region, and that the NLGN2 c-tail is able to function at excitatory synapses when linked with the NLGN3 extracellular region. This suggests that there is no specificity within the c-tail itself to determine NLGN function at either an excitatory or inhibitory synapse. These results are consistent with previous work showing that overexpression on a wild-type background of chimeric constructs containing NLGN1 extracellular linked to NLGN2 intracellular, or NLGN2 extracellular linked to NLGN1 intracellular, is fully capable of enhancing excitatory and inhibitory currents respectively (Futai et al., 2013). Our work eliminates the possibility that previous observations might be due to heterodimerization of chimeric constructs with endogenous NLGNs by expressing all of our chimera on a reduced endogenous NLGN background.

While the c-tail is the toolbox that contains all the functional residues necessary to perform at either an excitatory or inhibitory synapse, it is important to note that the

particular type of synapse determines which residues will be utilized. Indeed, prior work has shown that phosphorylation at the gephyrin binding domain enables preferential recruitment of PSD-95 versus gephyrin to the intracellular region of NLGN1 (Giannone et al., 2013). In addition, while it has been shown that there is a critical residue in the NLGN3 c-tail that is important for its function at excitatory synapses, mutation of the analogous residue in NLGN2 does not affect its function at inhibitory synapses (Shipman et al., 2011). Therefore, the mechanisms we describe are specific for NLGN function at inhibitory synapses.

Gephyrin-dependent and gephyrin-independent mechanisms for NLGN function at inhibitory synapses

We were surprised to find that not only the PDZ and collybistin domain are dispensable for NLGN function at inhibitory synapses but also the gephyrin-binding domain as well. There have been previous reports of gephyrin-independent function at inhibitory synapses, either in development or during plasticity (Danglot et al., 2003; Niwa et al., 2012). In addition, previous work done in mice lacking the cytoplasmic protein dystrophin showed selective reduction in clustering of α2 containing $GABA_A$ receptors but no change in gephyrin clustering, suggesting there might be dystrophin-dependent and gephyrin-independent mechanisms for clustering of specific $GABA_A$ receptor subtypes (Knuesel et al., 1999). Thus, it would be of interest to determine whether phosphorylation of the S714 site affects dystrophin function.

Phosphorylation at the S714 residue of NLGN2 has been found to negatively regulate the interaction between NLGN2 and gephyrin (Antonelli et al., 2014). However, our results indicate that phosphorylation at this site positively regulates NLGN2 function through a gephyrin-independent mechanism, since only the phospho-null form is able to block enhancement of inhibitory currents when paired with a mutation that blocks the gephyrin-dependent pathway (Figure 15). This discrepancy might be explained by the previous study's use of non-neuronal cells for characterization of the interaction between gephryin and the phosphorylation state at that site. It remains to be determined what kinase phosphorylates this particular site and what molecules are recruited in response to phosphorylation to mediate gephyrin-independent NLGN2 function.

The R705C point mutation is the only autism-associated mutation in the NLGNs identified to date that resides in the intracellular region. Previous characterization of this autism mutation at the analogous residue in NLGN3 showed no effect at inhibitory synapses (Etherton et al., 2011). This is consistent with our results showing that NLGN2 with the R705C point mutation alone is fully capable of enhancing inhibitory transmission (Figure 14c and 14d). However, by combining the R705C mutation with the S714A mutation, we were able to uncover a deficit in NLGN function (Figure 15). Similarly, it was only by combining the Y770A mutation with the S714A mutation, not the R705C mutation, that we were able to prevent NLGN2 from enhancing inhibitory currents, suggesting that the R705C mutation operates via a gephyrin-dependent pathway (Figure 15). These results underscore the additive effects of multiple point mutations, and highlight how disease phenotypes can be due to the interaction of a number of different factors. While the R705C mutation was shown to inhibit PKC-mediated interaction with NLGN4X

at excitatory synapses, there is no analogous PKC phosphorylation site in NLGN2 (Bemben et al., 2015a). Thus, it remains to be determined what molecules interact at this site and how this autism-associated mutation results in disruption of gephyrin binding to NLGN2.

Our findings have highlighted the separate roles of the NLGN extracellular and intracellular regions. The extracellular region is important for specifying function at a particular synapse while the intracellular region is important for carrying out the molecular mechanisms at either an excitatory or inhibitory synapse. We identify a domain in the extracellular region that is necessary and sufficient for specifying NLGN function at inhibitory synapses and elucidate both a gephyrin-dependent and gephyrin-independent mechanism for NLGN function at inhibitory synapses operating via intracellular interactions modulated by a phosphorylation site and an autism-associated mutation. These results advance our fundamental understanding of NLGN function at inhibitory synapses and provide multiple new avenues of study for further dissection of the various molecular interactors of the NLGNs, both extracellularly and intracellularly, and in normal and disease conditions.

Figure 1: Neuroligin 2 is the critical neuroligin at inhibitory synapses

a) Knockdown of endogenous neuroligins 1-3 reduces inhibitory responses compared to untransfected control cells (*p = 0.0391, n = 9). b) Scatter plot showing reduction in IPSCs in NLGN2 miRNA-transfected neurons compared to untransfected controls (***p = 0.0002, n = 15). c) Scatter plot showing no reduction in IPSCs in NLGN3 miRNA-transfected neurons compared to untransfected controls (p = 0.3013, n = 12). d) Summary graph of b and c. e) Scatter plot showing overexpression of NLGN3 enhances IPSCs compared to untransfected controls (**p = 0.0084, n = 15). f) Scatter plot showing overexpression of NLGN3 combined with NLGN2 knockdown fails to enhance IPSCs (p = 0.2661, n = 12). g) Summary graph of e and f. For panels a-c and e-f, open circles are individual pairs, filled circle is mean ± s.e.m. Black sample traces are control, green are transfected. Scale bars represent 100 pA and 50 ms. For panels a, d, and g summary graph plots mean transfected amplitude ± s.e.m, expressed as a percentage of control amplitude. Significance above each column represents pairwise comparison between transfected and untransfected cells.

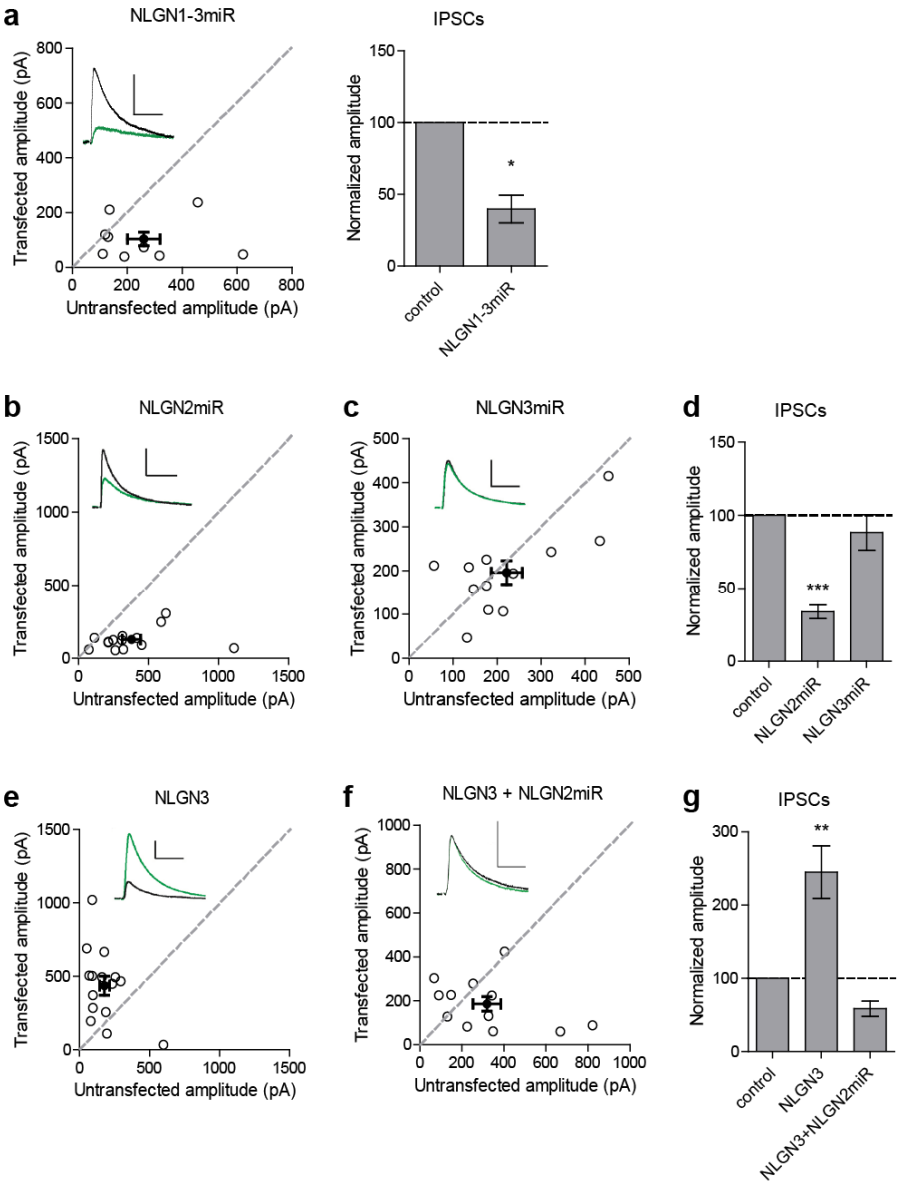
a
NLGN1-3miR
Transfected amplitude (pA)
Untransfected amplitude (pA)
IPSCs
Normalized amplitude
control
NLGN1-3miR
b
NLGN2miR
c
NLGN3miR
d
IPSCs
control
NLGN2miR
NLGN3miR
e
NLGN3
f
NLGN3 + NLGN2miR
g
IPSCs
control
NLGN3
NLGN3+NLGN2miR

Figure 2: Validation of NLGN2 knockdown construct and EPSCs for NLGN3 overexpression

a) qRT-PCR bar graph shows mean ± s.e.m. of NLGN2 mRNA remaining following NLGN2miR transduction normalized to control GFP transduction (n = 2 technical replicates). b) Scatter plot showing overexpression of NLGN3 enhances EPSCs compared to untransfected controls (***p = 0.0002, n = 15). c) Scatter plot showing overexpression of NLGN3 combined with NLGN2 knockdown enhances EPSCs (**p = 0.0078, n = 9). d) Summary graph of b and c. For panels b and c, open circles are individual pairs, filled circle is mean ± s.e.m. Black sample traces are control, green are transfected. Scale bars represent 100 pA and 50 ms. For panel d, summary graph plots mean transfected amplitude ± s.e.m, expressed as a percentage of control amplitude. Significance above each column represents pairwise comparison between transfected and untransfected cells.

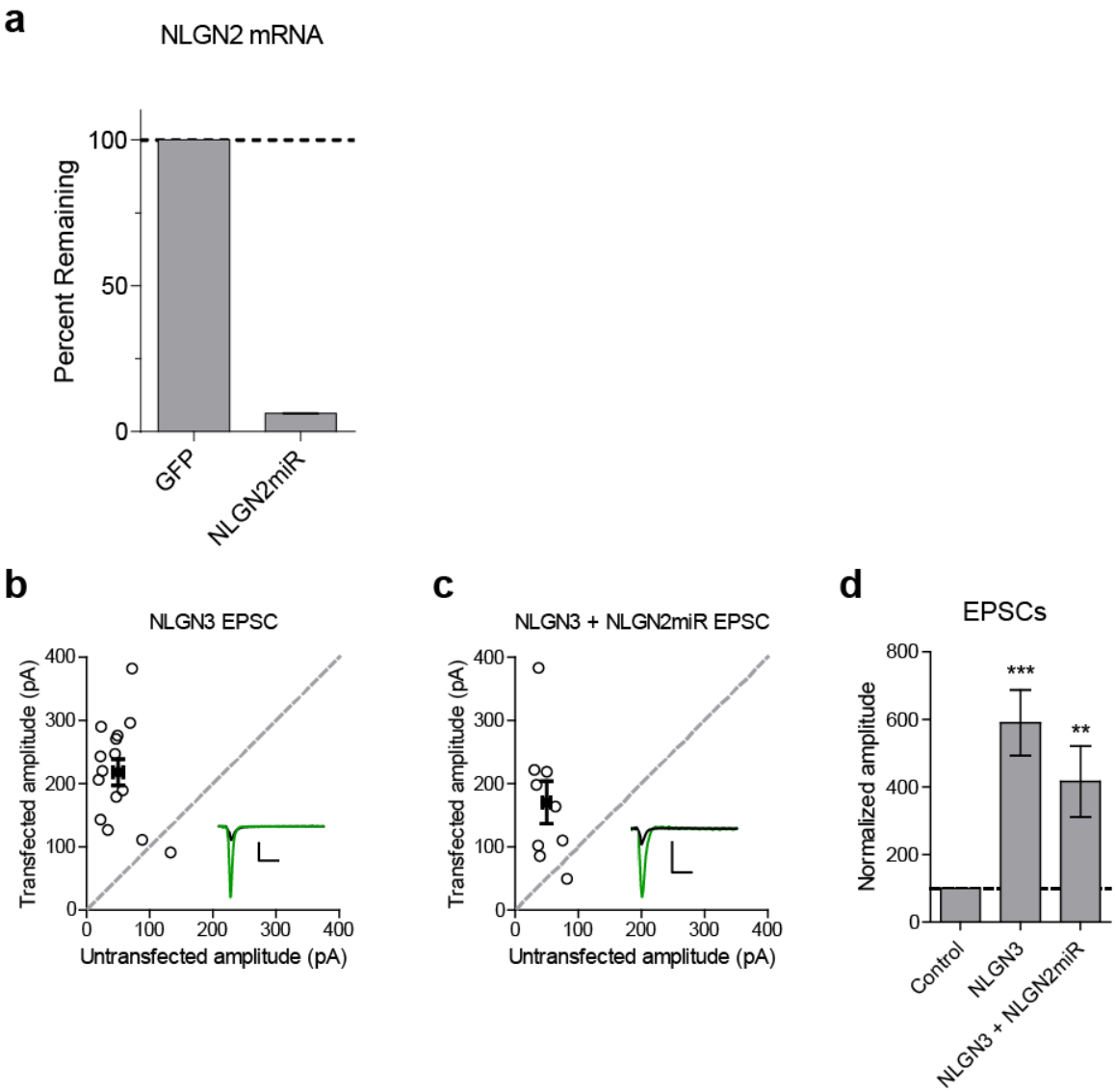
a
NLGN2 mRNA
Percent Remaining
100
50
0
GFP
NLGN2miR
b
NLGN3 EPSC
Transfected amplitude (pA)
Untransfected amplitude (pA)
c
NLGN3 + NLGN2miR EPSC
Transfected amplitude (pA)
Untransfected amplitude (pA)
d
EPSCs
Normalized amplitude
***
**
Control
NLGN3
NLGN3 + NLGN2miR

Figure 3: Difference between NLGN2 and 3 function at inhibitory synapses resides in the extracellular region

a) To determine where this functional difference between NLGN2 and 3 resides, we made chimeric constructs and expressed them on a reduced endogenous neuroligin background. Black TM is transmembrane domain. b) Scatter plot showing expression of NLGN2 on a NLGN1-3miR knockdown background enhances IPSCs compared to untransfected controls (****$p < 0.0001$, $n = 25$). c) Scatter plot showing expression of a construct containing the NLGN2 extracellular region and NLGN3 cytoplasmic tail (NLGN2e-3ctail) on a NLGN1-3miR knockdown background enhanced IPSCs (**$p = 0.002$, $n = 10$). d) Scatter plot showing expression of a construct containing the NLGN3 extracellular region and NLGN2 cytoplasmic tail (NLGN3e-2ctail) on a NLGN1-3miR knockdown background failed to enhance IPSCs ($p = 0.5771$, $n = 11$). e) Summary graph of b-d. Effect of expressing NLGN3e-2ctail is significantly less than expression of NLGN2e-3ctail (*$p = 0.0124$) or NLGN2 (**$p = 0.0067$). For panels b-d, open circles are individual pairs, filled circle is mean ± s.e.m. Black sample traces are control, green are transfected. Scale bars represent 100 pA and 50 ms. For panel e, graph plots mean transfected amplitude ± s.e.m, expressed as a percentage of control amplitude. Significance above each column represents pairwise comparison between transfected and untransfected cells.

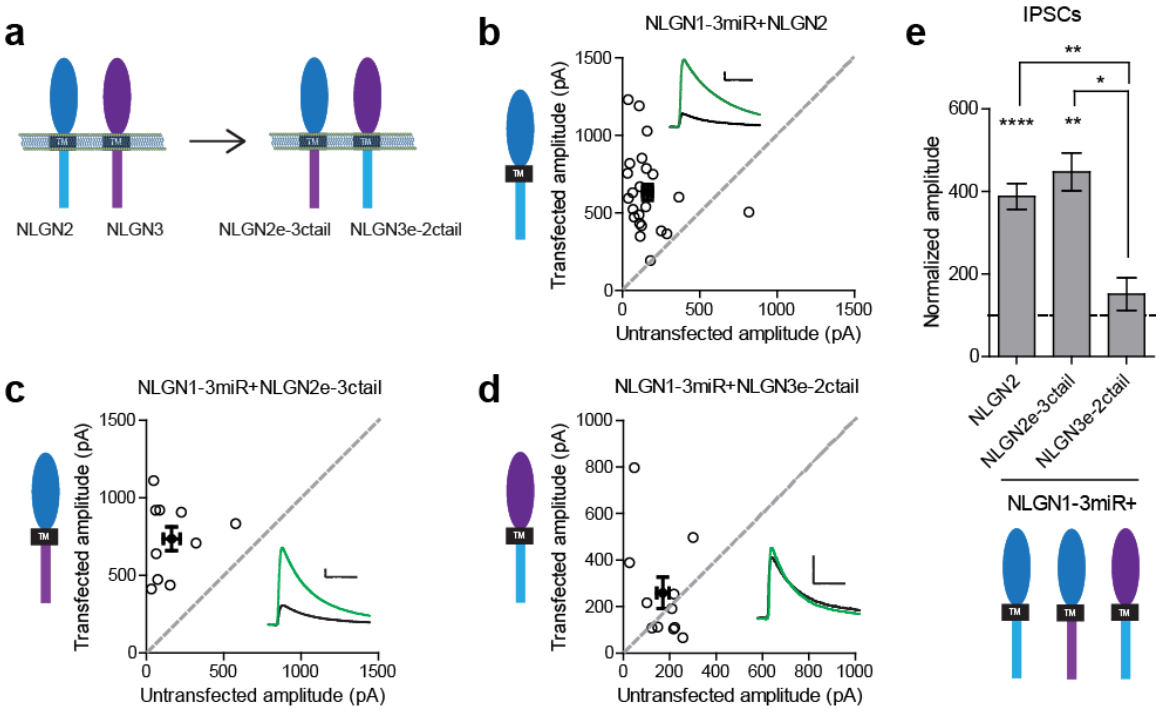
a
NLGN2
NLGN3
NLGN2e-3ctail
NLGN3e-2ctail
b
NLGN1-3miR+NLGN2
Transfected amplitude (pA)
Untransfected amplitude (pA)
c
NLGN1-3miR+NLGN2e-3ctail
Transfected amplitude (pA)
Untransfected amplitude (pA)
d
NLGN1-3miR+NLGN3e-2ctail
Transfected amplitude (pA)
Untransfected amplitude (pA)
e
IPSCs
Normalized amplitude
NLGN2
NLGN2e-3ctail
NLGN3e-2ctail
NLGN1-3miR+

Figure 4: Distinct requirements for NLGN function between inhibitory and excitatory synapses

While expression of a construct containing the NLGN3 extracellular region and NLGN2 cytoplasmic tail failed to rescue IPSCs, it was still able to enhance excitatory synaptic transmission (**p = 0.0098, n = 10). Open circles are individual pairs, filled circle is mean ± s.e.m. Black sample traces are control, green are transfected. Scale bars represent 100 pA and 50 ms. Summary graph plots transfected amplitude normalized to control ± s.e.m. Significance represents pairwise comparison between transfected and untransfected cells.

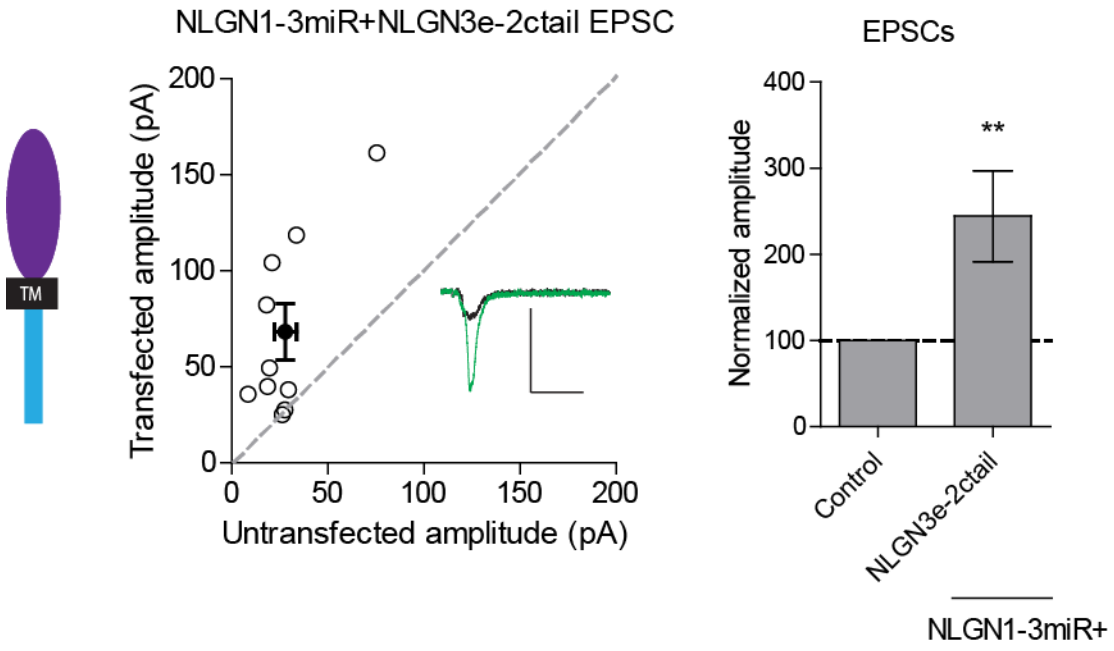
TM
NLGN1-3miR+NLGN3e-2ctail EPSC
Transfected amplitude (pA)
Untransfected amplitude (pA)
0
50
100
150
200
EPSCs
Normalized amplitude
400
300
200
100
0
**
Control
NLGN3e-2ctail
NLGN1-3miR+

Figure 5: Identification of critical domain to confer NLGN function at inhibitory synapses

a) Schematic of NLGN2 and 3 showing positions of chimera. Yellow are critical dimerization residues, pink is splice site A, grey SP is signal peptide, and black TM is transmembrane domain. b) Scatter plot showing that adding NLGN2 onto the NLGN3 extracellular region up to the 623rd residue fails to enhance IPSCs ($p = 0.4229$, $n = 16$). c) Scatter plot showing that adding up to the 180th residue also fails to enhance IPSCs ($p = 0.2754$, $n = 10$). d) Scatter plot showing that adding up to the 52nd residue is successful at conferring NLGN function at inhibitory synapses and enhancing IPSCs (**$p = 0.002$, $n = 10$) e) Expression of further chimeric constructs identifies a domain between residue 52-180 on NLGN2 that is sufficient to confer the ability to enhance IPSCs to NLGN3 (**$p = 0.0039$, $n = 9$). Within this region, we also expressed only f) the region between 52-164 (**$p = 0.0098$, $n = 10$) or g) residues corresponding to differences in splice site A (164-180) ($p = 0.0522$, $n = 12$). h) Summary graph. While the chimeric construct NLGN2-52-164-NLGN3 showed enhancement of IPSCs compared to untransfected control cells, the level of potentiation was significantly less than what we see with full-length NLGN2 (*$p = 0.0152$). For panels b-g, open circles are individual pairs, filled circle is mean ± s.e.m. Black sample traces are control, green are transfected. Scale bars represent 100 pA and 50 ms. For panel h, graph plots mean transfected amplitude ± s.e.m, expressed as a percentage of control amplitude. Significance above each column represents pairwise comparison between transfected and untransfected cells.

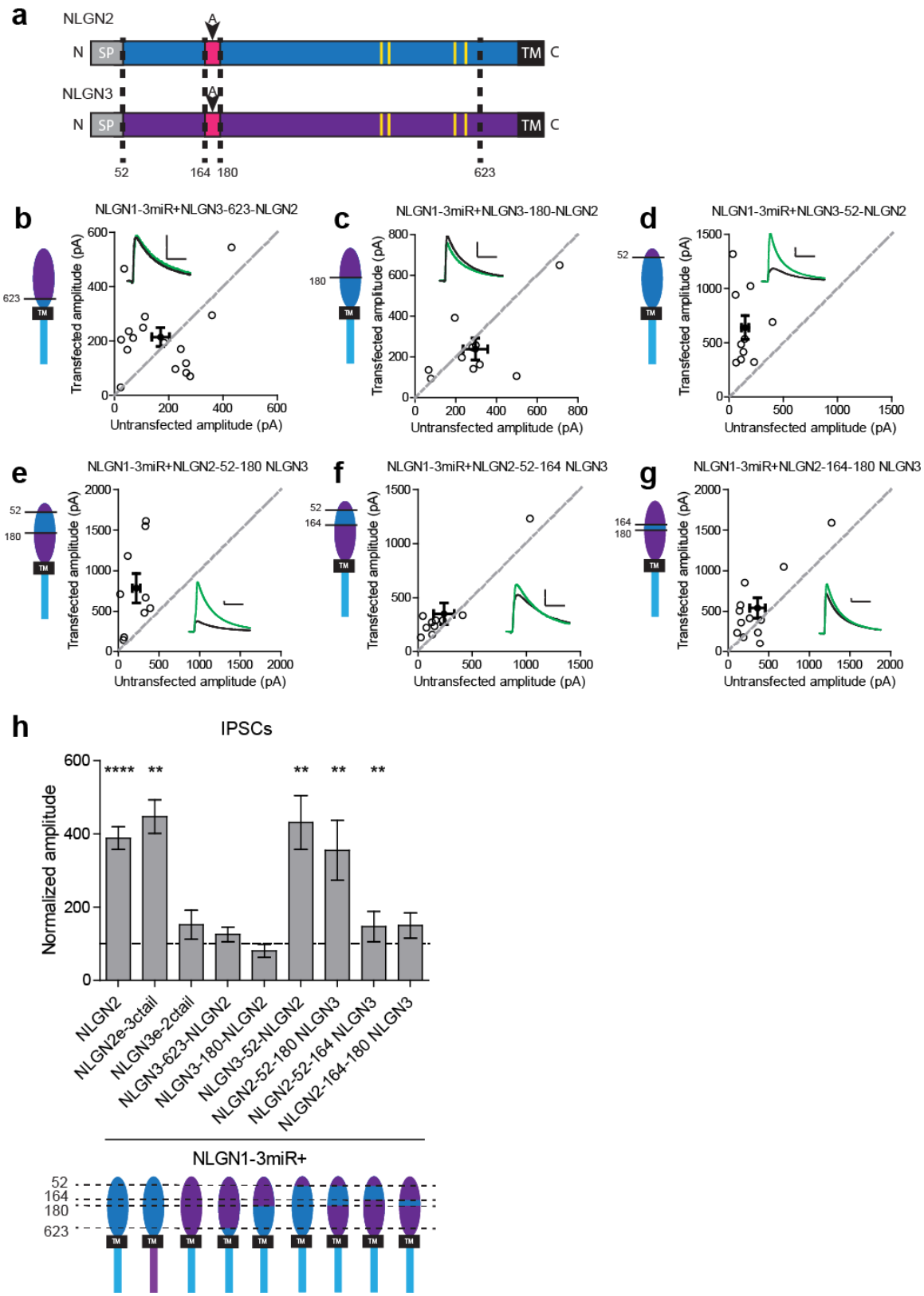
a
NLGN2
A
N
SP
TM
C
NLGN3
52
164
180
623
b
NLGN1-3miR+NLGN3-623-NLGN2
Transfected amplitude (pA)
Untransfected amplitude (pA)
c
NLGN1-3miR+NLGN3-180-NLGN2
d
NLGN1-3miR+NLGN3-52-NLGN2
e
NLGN1-3miR+NLGN2-52-180 NLGN3
f
NLGN1-3miR+NLGN2-52-164 NLGN3
g
NLGN1-3miR+NLGN2-164-180 NLGN3
h
IPSCs
Normalized amplitude
****
**
NLGN2
NLGN2e-3ctail
NLGN3e-2ctail
NLGN3-623-NLGN2
NLGN3-180-NLGN2
NLGN3-52-NLGN2
NLGN2-52-180 NLGN3
NLGN2-52-164 NLGN3
NLGN2-164-180 NLGN3
NLGN1-3miR+

Figure 6: Chimeric extracellular mutants and effect on excitatory transmission

a) Alignment of the NLGN2 and NLGN3 extracellular regions. Sequence before residue 52 encompasses the highly dissimilar signal sequence and was not included in alignment. Highlighted in magenta is splice site A while key dimerization residues are highlighted in yellow. Relevant sites where chimeric constructs were made are identified in alignment. The first amino acid at the beginning of splice site A at residue 163 is conserved between NLGN2 and 3, therefore our chimera was made after this residue. b) Excitatory responses of chimera that did not potentiate IPSCs. Constructs that did not potentiate IPSCs could still enhance EPSCs including: NLGN3e-2ctail (**p = 0.0098, n = 10), NLGN3-623-NLGN2 (**p = 0.0039, n = 9), NLGN2-52-164-NLGN3 (*p = 0.0353, n = 14), NLGN2-164-180-NLGN3 (***p = 0.0005, n = 13). The chimeric construct NLGN3-180-NLGN2 did not enhance EPSCs (p = 0.3804, n = 12) and was significantly impaired compared to NLGN3e-2ctail (*p = 0.0111). Summary graph plots transfected amplitude normalized to control ± s.e.m. Significance above each column represents pairwise comparison between transfected and untransfected cells.

a

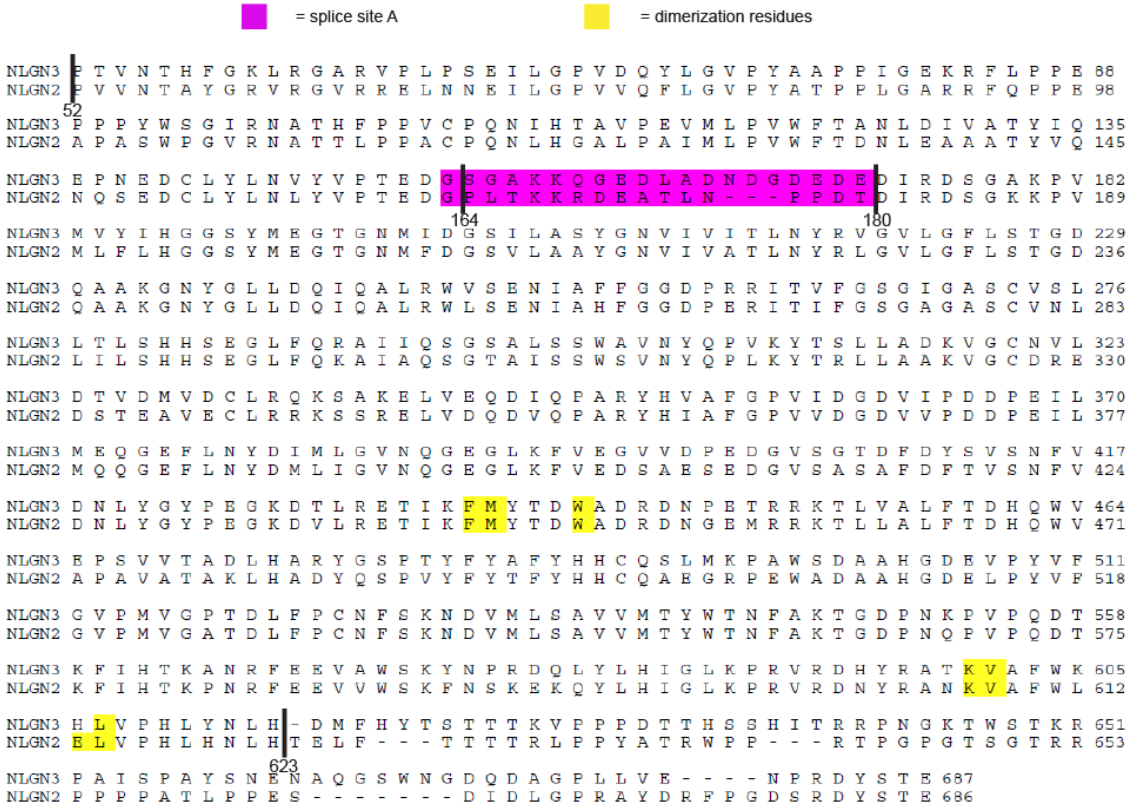
= splice site A
= dimerization residues
52
164
180
623

b

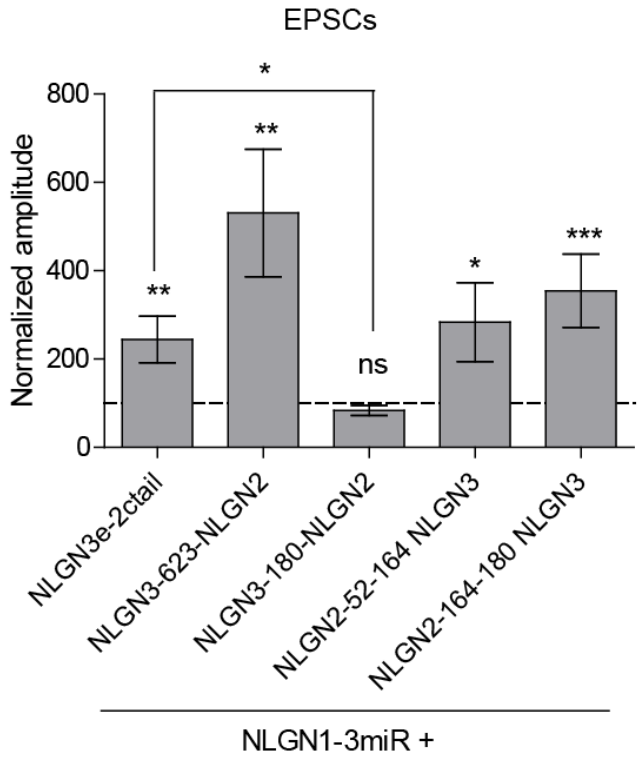
EPSCs
Normalized amplitude
800
600
400
200
0
*
**
**
ns
*
***
NLGN3e-2ctail
NLGN3-623-NLGN2
NLGN3-180-NLGN2
NLGN2-52-164 NLGN3
NLGN2-164-180 NLGN3
NLGN1-3miR +

Figure 7: While NLGN c-tails do not confer specialization to inhibitory synapses, a c-tail is required for NLGN function

a) Alignment of NLGN1-4. Sequences correspond to mouse NLGN1, rat NLGN2, and human NLGN3 and NLGN4. Indicated at residue 133 is where most proximal c-tail truncation was performed. Highlighted in gray is the transmembrane domain. In light red is a conserved residue that is the site of an autism-associated mutation in NLGN4. Highlighted in light purple is the critical region, previously shown to be important for NLGN function at excitatory synapses but not inhibitory synapses18. Highlighted in brown is the gephyrin-binding domain. In green is the proline-rich region, and in light orange is the PDZ domain. Phosphorylation sites are highlighted in yellow. b) Scatter plot showing expression of full-length NLGN1 on a NLGN1-3miR knockdown background failed to enhance inhibitory responses ($p = 0.6726$, $n = 19$), c) Scatter plot showing expression of a chimeric NLGN2 extracellular region with NLGN1 c-tail on a NLGN1-3miR knockdown background is able to enhance inhibitory responses ($*p = 0.0244$, $n = 11$). d) Summary graph. Effect of expressing NLGN2e-1ctail is significantly greater than with full-length NLGN1 ($*p = 0.0314$). e) Scatter plot showing expression of the c-tail truncation mutant NLGN2Δ133 on a reduced endogenous neuroligin background is unable to enhance inhibitory synaptic responses, indicating that a c-tail is required for NLGN function ($p = 0.6387$, $n = 15$). f) Summary graph of e. Effect of expressing NLGN2Δ133 is significantly less than with full-length NLGN2 ($***p = 0.0002$). For panels b-c and e, open circles are individual pairs, filled circle is mean ± s.e.m. Black sample traces are control, green are transfected. Scale bars represent 100 pA and 50 ms. For panels d and f, graph plots

transfected amplitude normalized to control ± s.e.m. Significance above each column represents pairwise comparison between transfected and untransfected cells.

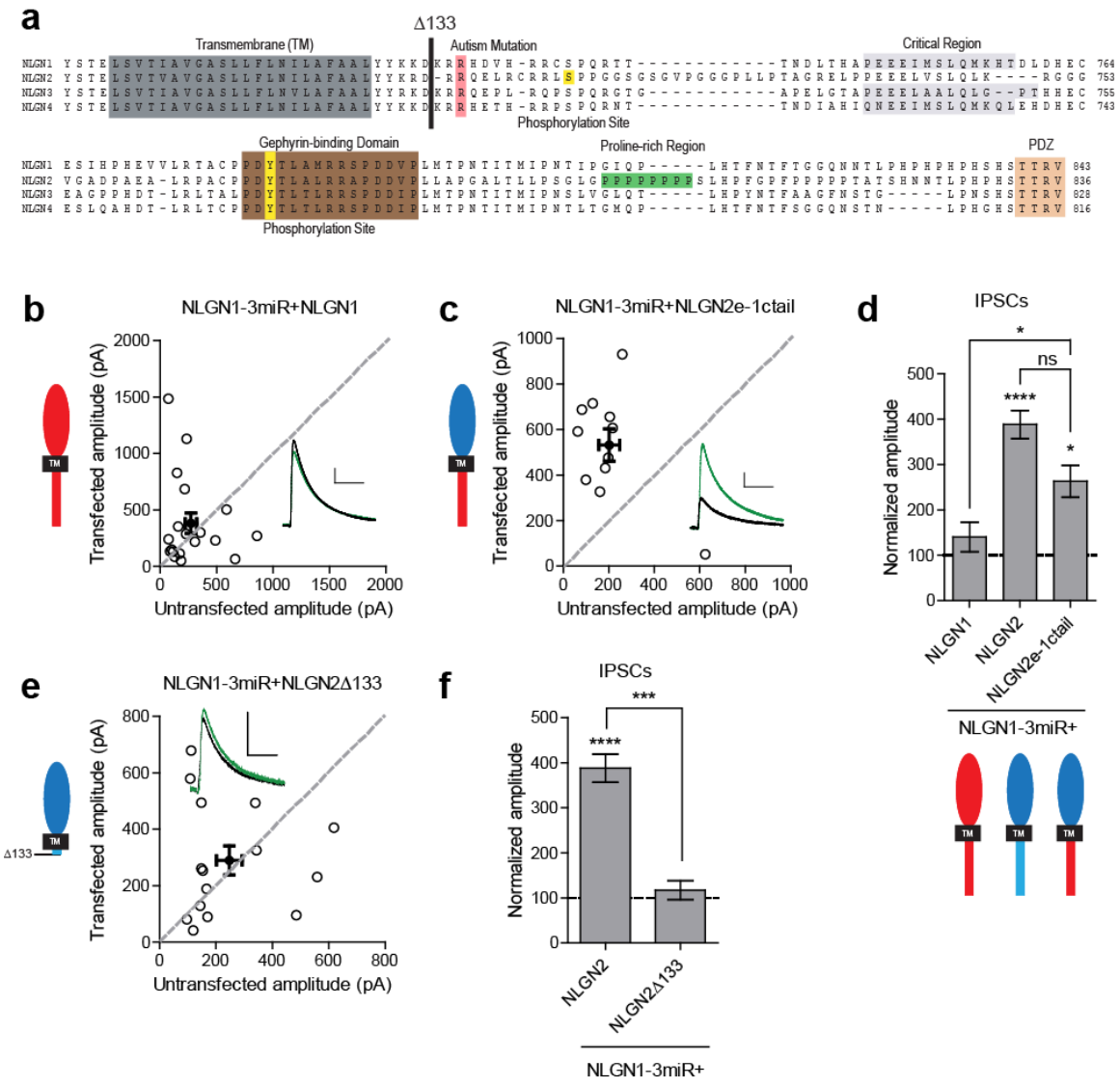
a
Δ133
Transmembrane (TM)
Autism Mutation
Critical Region
Phosphorylation Site
Gephyrin-binding Domain
Proline-rich Region
PDZ
Phosphorylation Site
b
NLGN1-3miR+NLGN1
Transfected amplitude (pA)
Untransfected amplitude (pA)
c
NLGN1-3miR+NLGN2e-1ctail
Transfected amplitude (pA)
Untransfected amplitude (pA)
d
IPSCs
Normalized amplitude
ns
NLGN1
NLGN2
NLGN2e-1ctail
NLGN1-3miR+
e
NLGN1-3miR+NLGN2Δ133
Δ133
Transfected amplitude (pA)
Untransfected amplitude (pA)
f
IPSCs
Normalized amplitude
NLGN2
NLGN2Δ133
NLGN1-3miR+

Figure 8: Further characterization of c-tail deletion mutant

a-b) Scatter plots showing overexpression on a wild-type background of a) NLGN2 (**p = 0.0039, n = 9) and b) NLGN2Δ133 (*p = 0.042, n = 11), both potentiate inhibitory responses. c) Summary of a-b. d) Immunostaining of dissociated hippocampal cultures transfected with NLGNmiRs-GFP alone or with either HA-tagged NLGN2 or HA-tagged NLGN2Δ133 and surface stained for HA. Scale bar represents 20 μm. e) Summary of d. Graph plots intensity of HA signal normalized to GFP (p = 0.189, n = 11 cells per group). Error bars are mean ± s.e.m. For panels a and b, open circles are individual pairs, filled circle is mean ± s.e.m. Black sample traces are control, green are transfected. Scale bars represent 100 pA and 50 ms. For panel c, graph plots transfected amplitude normalized to control ± s.e.m. Significance above each column represents pairwise comparison between transfected and untransfected cells.

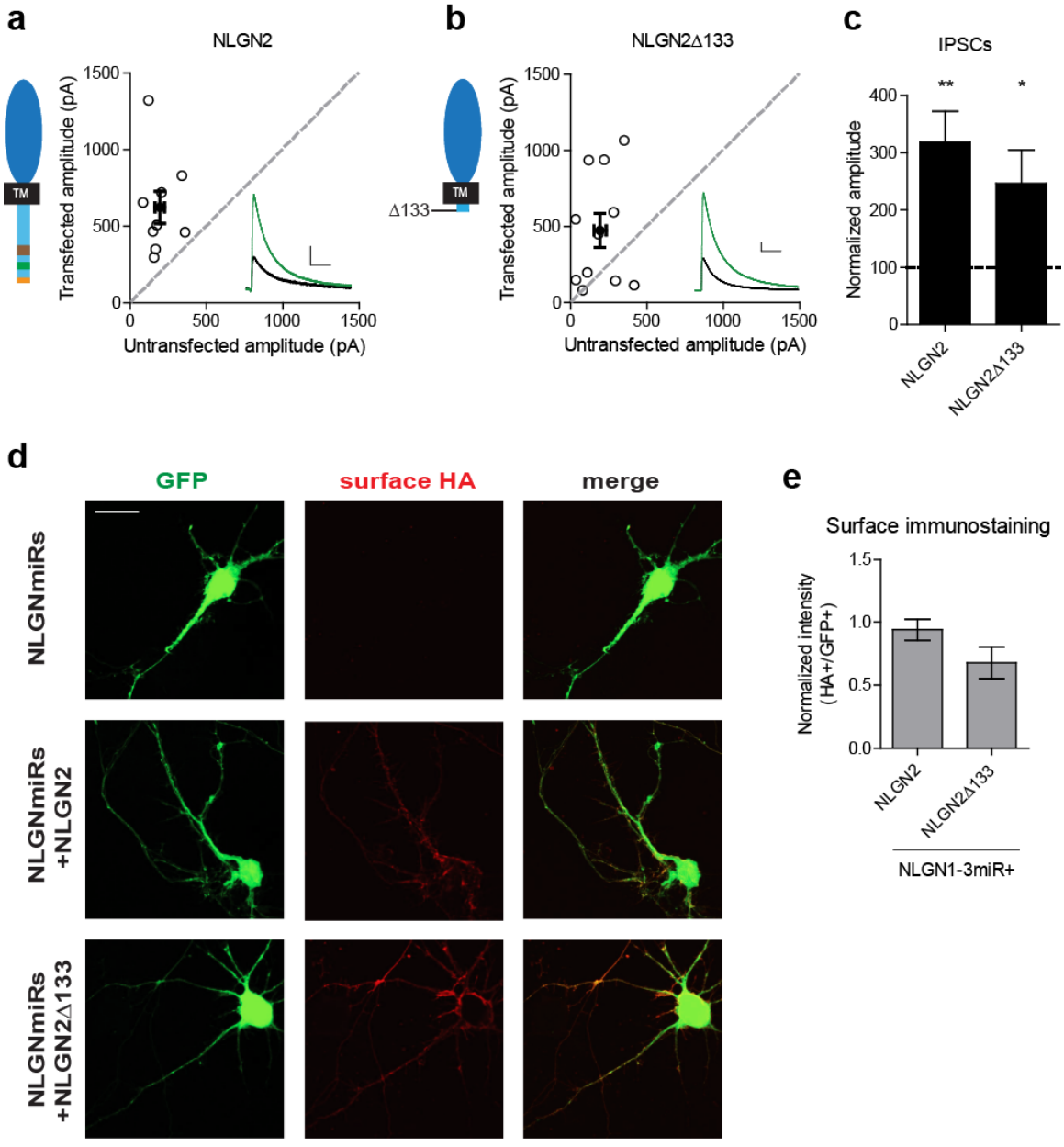
a
NLGN2
TM
Transfected amplitude (pA)
Untransfected amplitude (pA)
0
500
1000
1500
b
NLGN2Δ133
TM
Δ133
c
IPSCs
Normalized amplitude
**
*
NLGN2
NLGN2Δ133
d
GFP
surface HA
merge
NLGNmiRs
NLGNmiRs +NLGN2
NLGNmiRs +NLGN2Δ133
e
Surface immunostaining
Normalized intensity (HA+/GFP+)
0.0
0.5
1.0
1.5
NLGN2
NLGN2Δ133
NLGN1-3miR+

Figure 9: Previously identified domains not required for NLGN2 function

a-c) Scatter plots showing replacement of endogenous neuroligin with truncation mutants a) lacking the PDZ domain (NLGN2Δ4) (**p = 0.0098, n = 11), b) truncation of all regions downstream of the proline rich region (NLGN2Δ39) (**p = 0.0017, n = 14), or c) truncation of all regions downstream of the gephyrin binding domain (NLGN2Δ69) (**p = 0.0017, n = 18), is still able to potentiate inhibitory synaptic responses compared to paired neighboring control cells. d) Summary graph. Shown are further mutants including deletion of only the proline rich region (NLGN2Δ32-39) (**p = 0.002, n = 10), deletion of only the gephyrin binding domain (NLGN2Δ55-69) (*p = 0.0273, n = 10) or expression of a phospho-mimic point mutant that has been shown to disrupt gephyrin binding (NLGN2 Y770A) (***p = 0.0005, n = 17), which all still potentiate inhibitory responses. For panels a-c, open circles are individual pairs, filled circle is mean ± s.e.m. Black sample traces are control, green are transfected. Scale bars represent 100 pA and 50 ms. For panel d, graph plots transfected amplitude normalized to control ± s.e.m. Significance above each column represents pairwise comparison between transfected and untransfected cells.

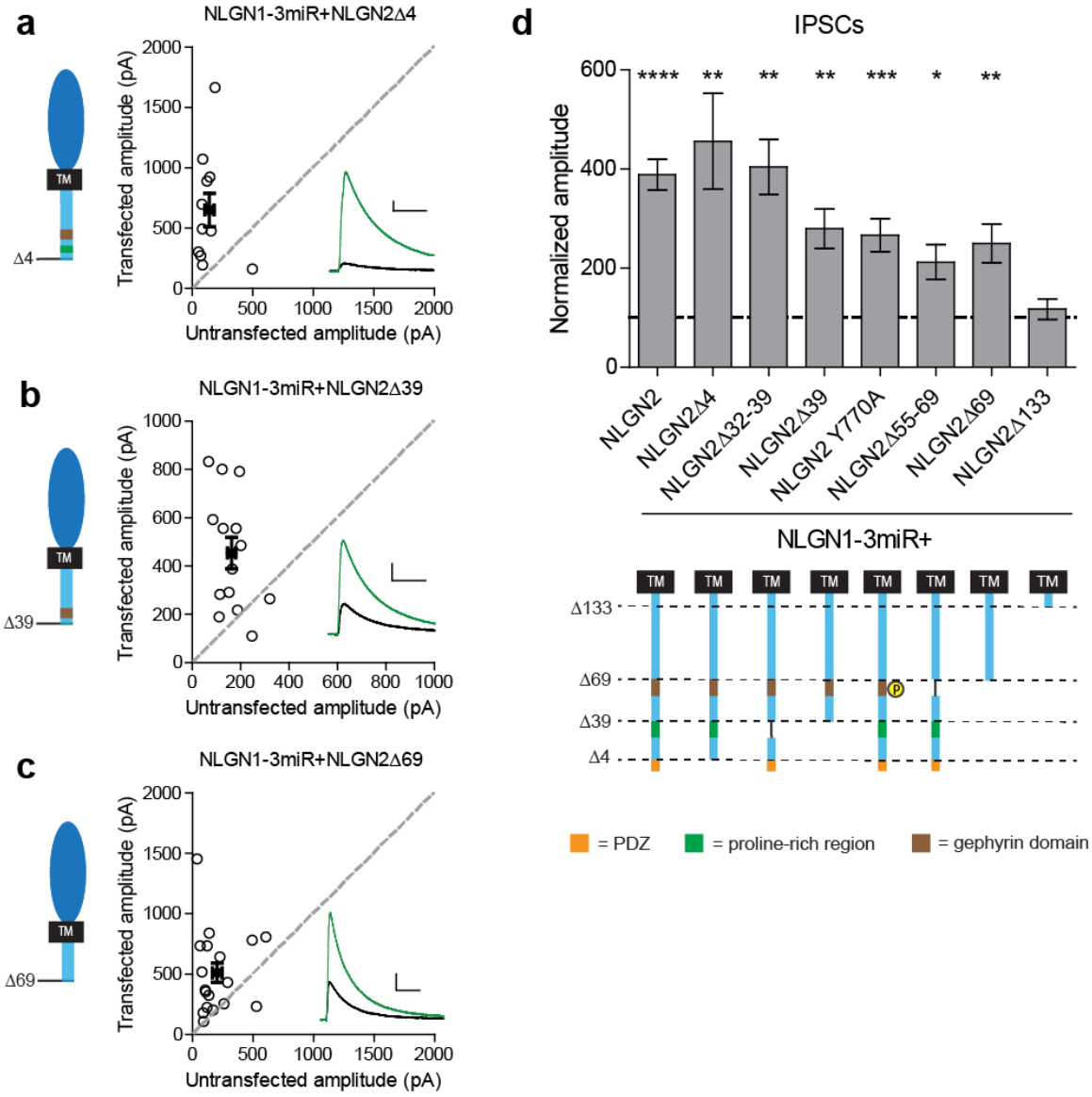
a
NLGN1-3miR+NLGN2Δ4
TM
Δ4
Transfected amplitude (pA)
Untransfected amplitude (pA)
b
NLGN1-3miR+NLGN2Δ39
Δ39
c
NLGN1-3miR+NLGN2Δ69
Δ69
d
IPSCs
Normalized amplitude
NLGN2
NLGN2Δ4
NLGN2Δ32-39
NLGN2Δ39
NLGN2 Y770A
NLGN2Δ55-69
NLGN2Δ69
NLGN2Δ133
NLGN1-3miR+
Δ133
Δ69
Δ39
Δ4
= PDZ
= proline-rich region
= gephyrin domain

Figure 10: More detailed NLGN alignment

Alignment showing where all truncations and point mutations were made. Highlighted in gray is the transmembrane domain. In light red is a conserved residue that is a site of an autism-associated mutation in NLGN4. Highlighted in light purple is the critical region, previously shown to be important for NLGN function at excitatory synapses but not inhibitory synapses (Shipman et al., 2011). Highlighted in brown is the gephyrin-binding domain. In green is the proline-rich region, and in light orange is the PDZ domain. Phosphorylation sites are highlighted in yellow.

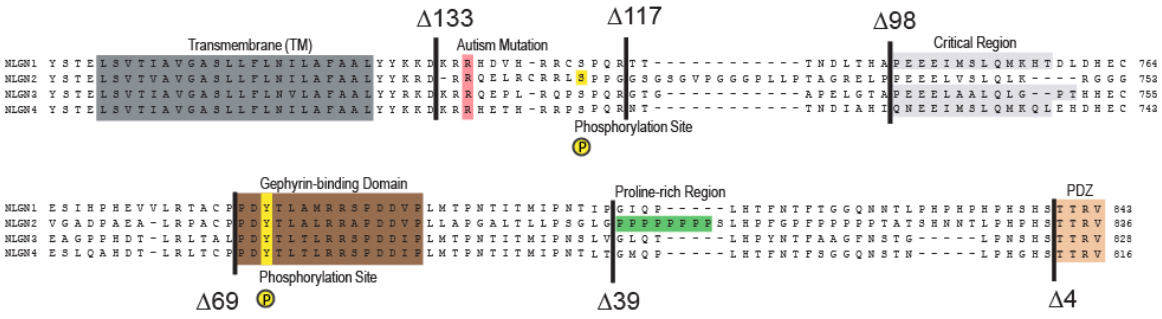
Δ133
Δ117
Δ98
Transmembrane (TM)
Autism Mutation
Critical Region
Phosphorylation Site
Gephyrin-binding Domain
Proline-rich Region
PDZ
Phosphorylation Site
Δ69
Δ39
Δ4

Figure 11: Gephyrin-independent NLGN2 function

a) Scatter plot showing overexpression of a Gephyrin-miR construct to knockdown gephyrin expression significantly reduces inhibitory synaptic responses (#p = 0.0156, n = 8). b) Scatter plot showing replacement of endogenous neuroligin with a truncation mutant lacking all known domains of neuroligin 2 (NLGN2Δ69) on a gephyrin knockdown background is still able to potentiate inhibitory synaptic responses, indicating that neuroligin 2 is able to function independently of gephyrin (**p = 0.0039, n = 9). c) Summary graph. Asterisks indicate significant enhancement compared to control cells where ** = $p < 0.01$ and *** = $p < 0.001$, while hash sign indicates significant depression compared to control cells where # = $p < 0.05$. For panels a and b, open circles are individual pairs, filled circle is mean ± s.e.m. Black sample traces are control, green are transfected. Scale bars represent 100 pA and 50 ms. For panel c, graph plots transfected amplitude normalized to control ± s.e.m. Significance above each column represents pairwise comparison between transfected and untransfected cells.

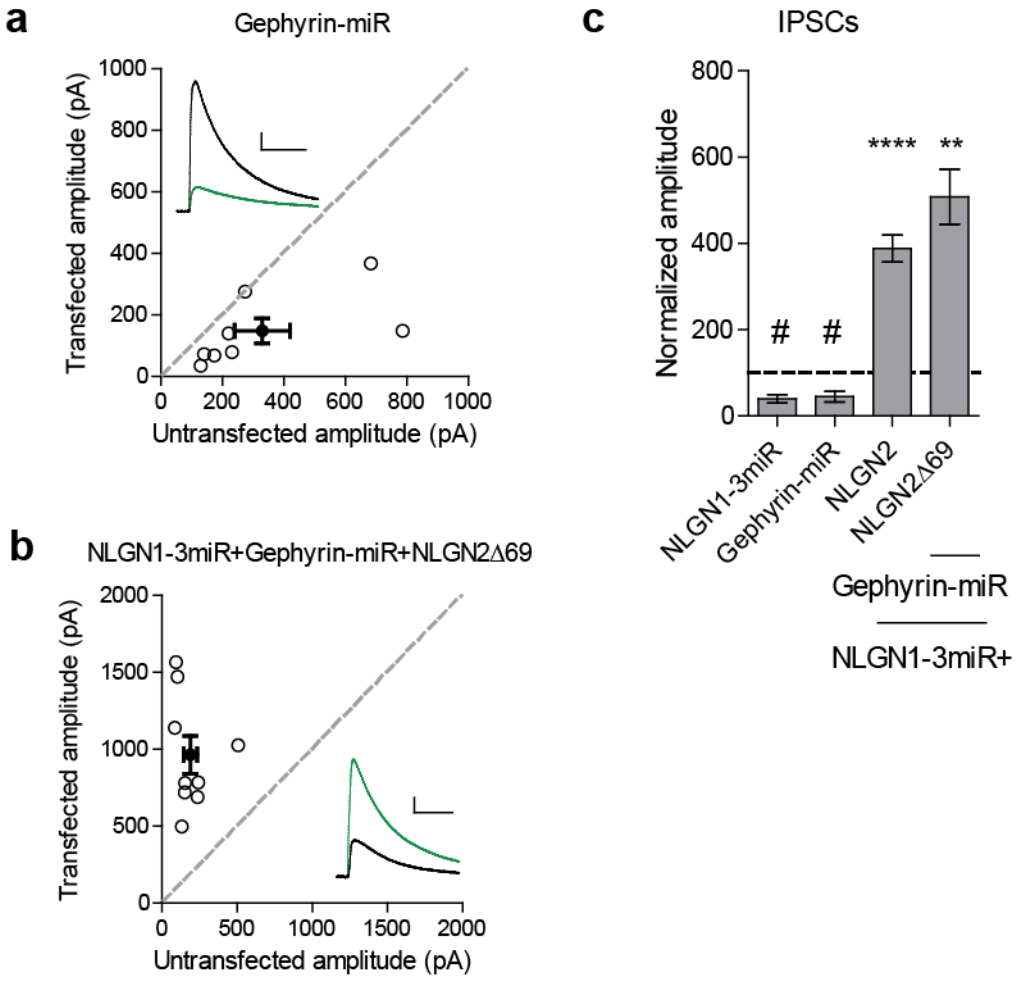
a
Gephyrin-miR
Transfected amplitude (pA)
Untransfected amplitude (pA)
0
200
400
600
800
1000
b
NLGN1-3miR+Gephyrin-miR+NLGN2Δ69
Transfected amplitude (pA)
Untransfected amplitude (pA)
0
500
1000
1500
2000
c
IPSCs
Normalized amplitude
0
200
400
600
800
#
#
****
**
NLGN1-3miR
Gephyrin-miR
NLGN2
NLGN2Δ69
Gephyrin-miR
NLGN1-3miR+

Figure 12: Characterization of Gephyrin knockdown construct

a) Graph shows mean ± s.e.m. of gephyrin mRNA remaining following Gephyrin-miR transduction normalized to control (n = 3 technical replicates). b) Western blot of lysates taken from dissociated hippocampal cultures following Gephyrin-miR transduction compared to control uninfected neurons. Shown is representative image of 6 technical replicates. Top band is gephyrin, lower band is actin. Size in kDa.

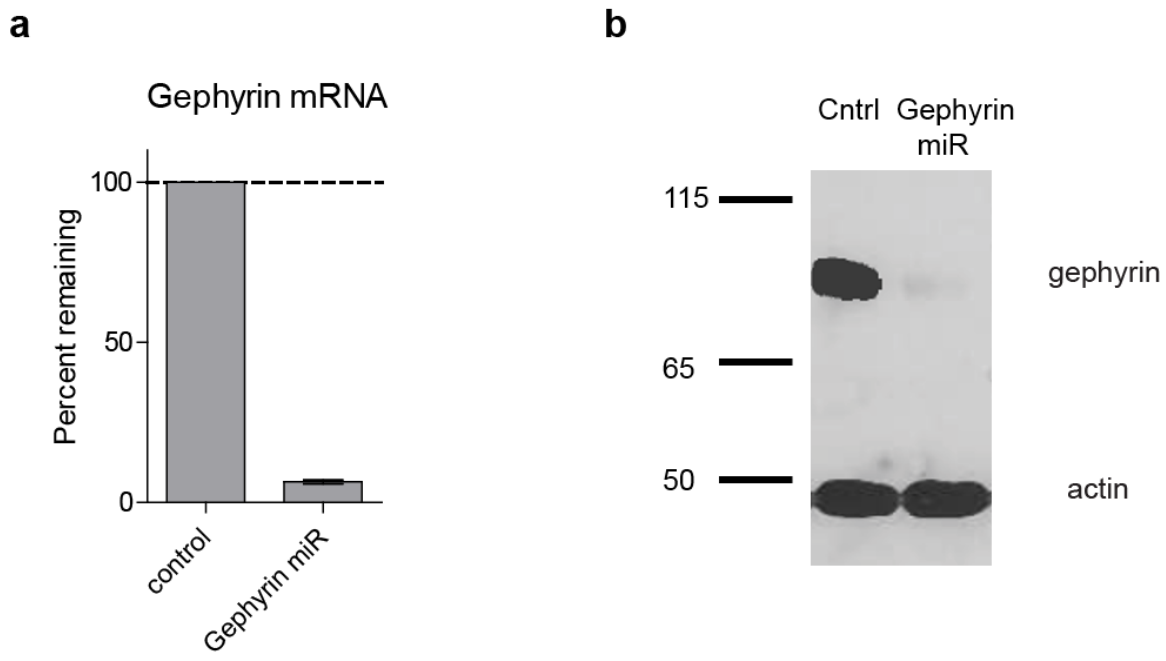
a
Gephyrin mRNA
Percent remaining
100
50
0
control
Gephyrin miR
b
Cntrl
Gephyrin miR
115
65
50
gephyrin
actin

Figure 13: Identification of critical residues in NLGN2 c-tail

a) Scatter plot showing deletion of a region from the most proximal c-tail truncation (NLGN2Δ98-133) failed to enhance inhibitory responses ($p = 0.1698$, $n = 17$). b) Further refining this area of interest, NLGN2Δ117-133 still failed to enhance inhibitory responses ($p = 0.6953$, $n = 10$). c) Scatter plot showing double point mutant with autism-associated mutation at R705 and phospho-null mutation at S714 (NLGN2-R705C-S714A) also showed deficits in inhibitory transmission ($p = 0.0522$, $n = 12$). d) Scatter plot showing double point mutant with autism-associated mutation at R705 and phospho-mimic mutation at S714 (NLGN2-R705C-S714D) displayed normal enhancement of IPSCs (***$p = 0.0002$, $n = 15$). e) Summary graph. Expression of full-length NLGN2 results in greater enhancement of IPSCs compared to NLGN2Δ98-133 (***$p = 0.0001$), NLGN2Δ117-133 (****$p < 0.0001$), and NLGN2-R705C-S714A (**$p = 0.0061$). Expression of NLGN2-R705C-S714D results in greater enhancement of IPSCs compared to NLGN2-R705C-S714A (*$p = 0.0429$). f) Scatter plot showing double point mutant with autism-associated mutation at R705 and a phospho-mimic point mutant shown to disrupt gephyrin binding at Y770 is still able to enhance inhibitory responses (***$p = 0.0005$, $n = 17$). g) Scatter plot showing double point mutant with phospho-null mutation at S714 and a phospho-mimic point mutant shown to disrupt gephyrin binding at Y770 exhibited modest enhancement of IPSCs (*$p = 0.0274$, $n = 13$). h) Summary graph. While the double mutant NLGN2-S714A-Y770A showed enhancement of IPSCs compared to untransfected control cells, the level of potentiation was far less than what we see with full-length NLGN2 (**$p = 0.0089$). For panels a-d, and f-g open circles are individual pairs, filled circle is mean ± s.e.m. Black sample traces are control, green are transfected. Scale bars represent 100 pA and 50 ms.

For panel e and h, bar graph plots transfected amplitude normalized to control ± s.e.m. Significance above each column represents pairwise comparison between transfected and untransfected cells.

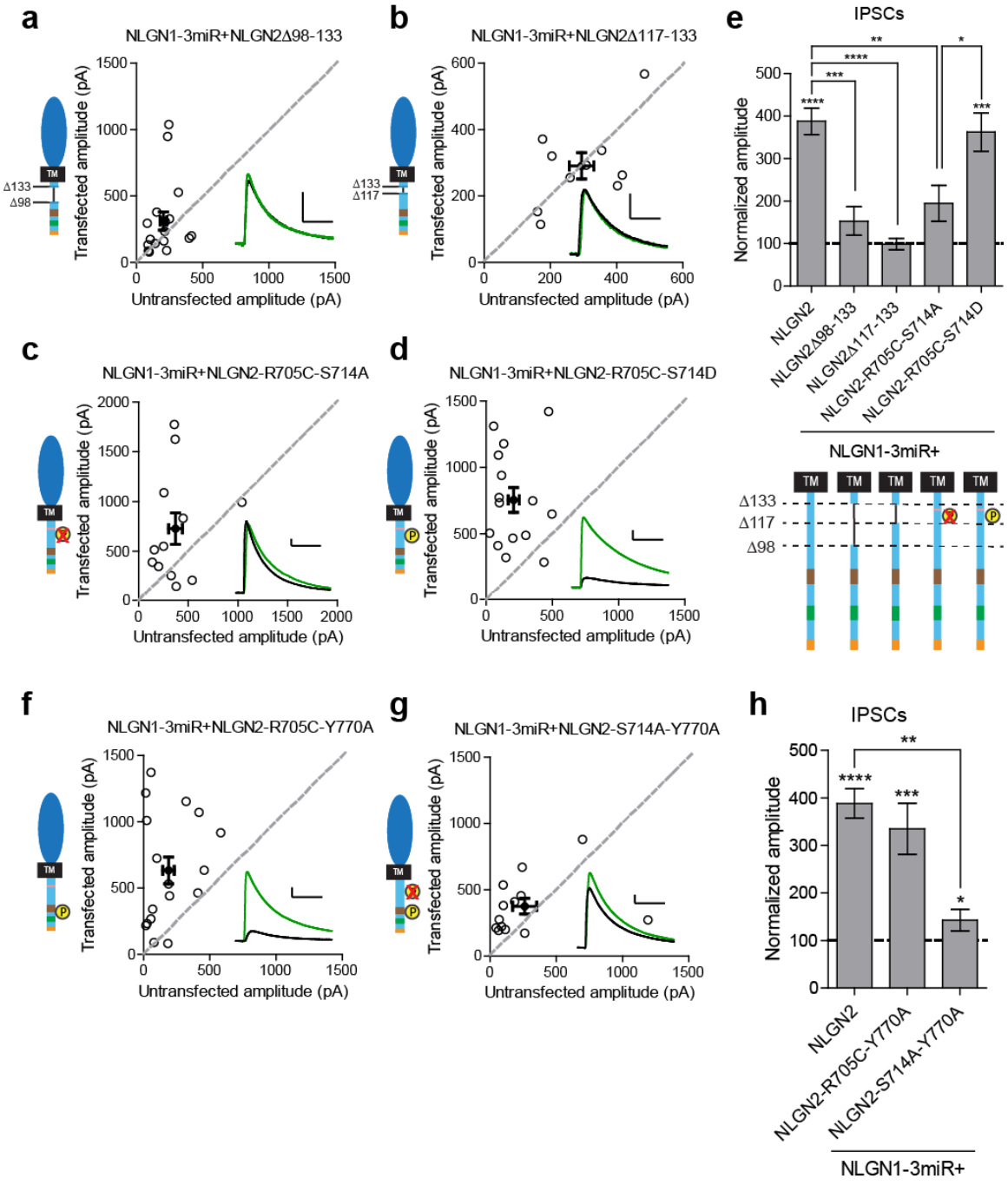
a
NLGN1-3miR+NLGN2Δ98-133
Transfected amplitude (pA)
Untransfected amplitude (pA)
Δ133
Δ98
TM
b
NLGN1-3miR+NLGN2Δ117-133
Δ133
Δ117
c
NLGN1-3miR+NLGN2-R705C-S714A
d
NLGN1-3miR+NLGN2-R705C-S714D
e
IPSCs
Normalized amplitude
NLGN2
NLGN2Δ98-133
NLGN2Δ117-133
NLGN2-R705C-S714A
NLGN2-R705C-S714D
NLGN1-3miR+
f
NLGN1-3miR+NLGN2-R705C-Y770A
g
NLGN1-3miR+NLGN2-S714A-Y770A
h
IPSCs
NLGN2
NLGN2-R705C-Y770A
NLGN2-S714A-Y770A
NLGN1-3miR+

Figure 14: Individual c-tail point mutations do not affect NLGN2 function

a-c) Scatter plots showing replacement of endogenous neuroligin with individual mutants of either a) phospho-null mutation (*p = 0.0195, n = 9), b) phospho-mimic mutation (***p = 0.0007, n = 13), or c) autism-associated mutation (*p = 0.0391, n = 9) still potentiates IPSCs. d) Summary graph. For panels a-c, open circles are individual pairs, filled circle is mean ± s.e.m. Black sample traces are control, green are transfected. Scale bars represent 100 pA and 50 ms. For panel d, bar graph plots transfected amplitude normalized to control ± s.e.m. Significance above each column represents pairwise comparison between transfected and untransfected cells.

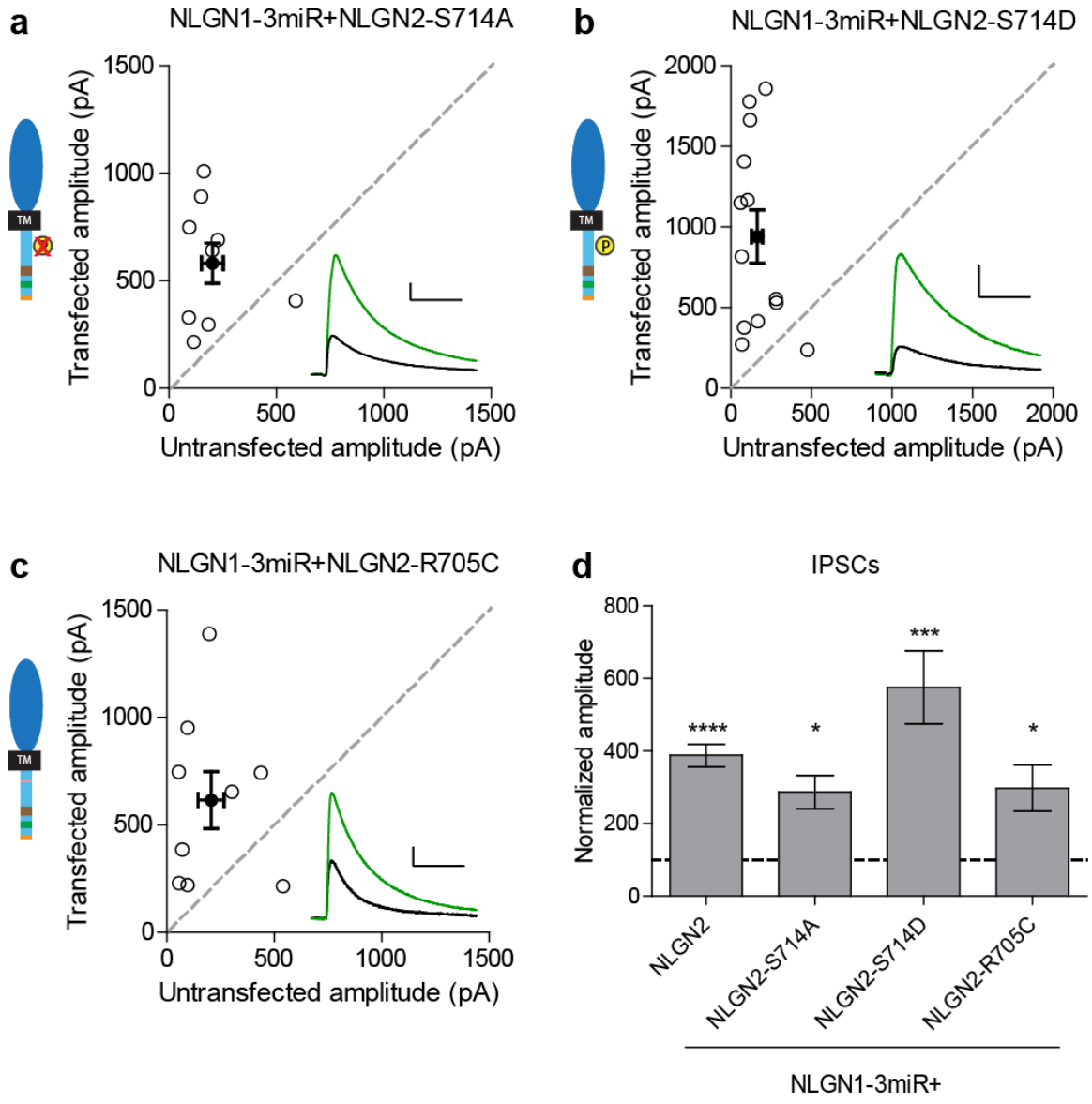
a
NLGN1-3miR+NLGN2-S714A
TM
Transfected amplitude (pA)
Untransfected amplitude (pA)
0
500
1000
1500
b
NLGN1-3miR+NLGN2-S714D
TM
P
Transfected amplitude (pA)
Untransfected amplitude (pA)
0
500
1000
1500
2000
c
NLGN1-3miR+NLGN2-R705C
TM
Transfected amplitude (pA)
Untransfected amplitude (pA)
0
500
1000
1500
d
IPSCs
Normalized amplitude
0
200
400
600
800
****
*
***
*
NLGN2
NLGN2-S714A
NLGN2-S714D
NLGN2-R705C
NLGN1-3miR+

Figure 15: Separate gephyrin-dependent and gephyrin-independent mechanisms for neuroligin function at inhibitory synapses

We propose separate gephyrin-dependent and gephyrin-independent mechanisms for NLGN function at inhibitory synapses. In our NLGN2-R705C-S714A manipulation, we block the gephyrin-independent pathway by preventing phosphorylation at the S714 residue, and also block the gephyrin-dependent pathway by the autism-associated mutation at R705. Therefore, the resulting effect we see is impaired function at inhibitory synapses. In our NLGN2-R705C-S714D manipulation, we facilitate the gephyrin-independent pathway by mimicking phosphorylation at the S714 residue, while the gephyrin-dependent pathway is blocked by the autism-associated mutation at R705. The resulting effect we see is intact function at inhibitory synapses. In our NLGN2-R705C-Y770A manipulation, we only block the gephyrin-dependent pathway with the autism-associated mutation at R705 and a mutation at Y770 that blocks gephyrin-binding. The resulting effect we see is intact function at inhibitory synapses. In our NLGN2-S714A-Y770A manipulation, we block the gephyrin-independent pathway by preventing phosphorylation at the S714 residue, and also block the gephyrin-dependent pathway with the mutation at Y770 that blocks gephyrin-binding. Therefore, the resulting effect we see is impaired function at inhibitory synapses. Green is gephyrin. Yellow residues are phosphorylation sites. The Y770A point mutant has been previously characterized and shown to function as a phospho-mimic mutation that blocks gephyrin binding (Giannone et al., 2013).

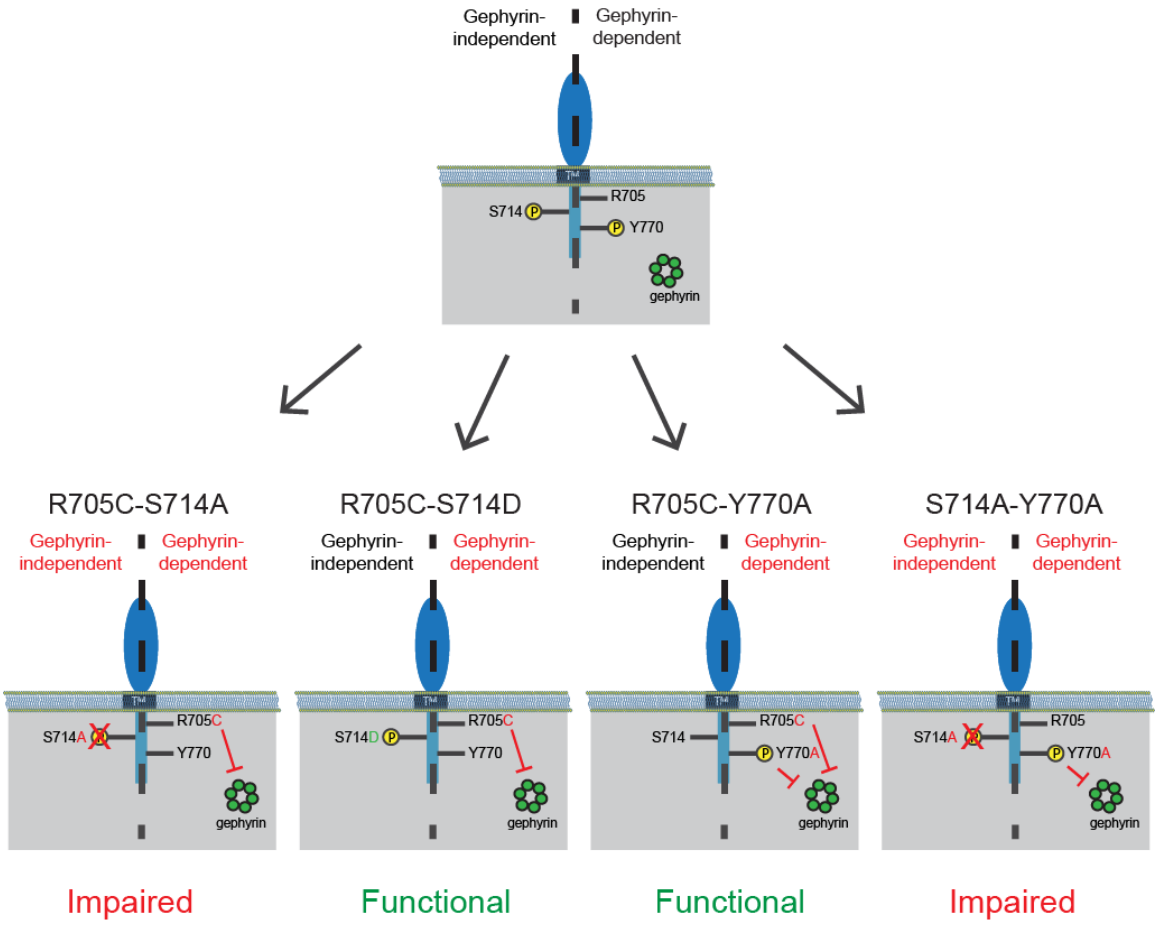
Gephyrin-independent
Gephyrin-dependent
TM
S714
P
R705
Y770
gephyrin
R705C-S714A
S714A
R705C
Y770
R705C-S714D
S714D
R705C-Y770A
S714
Y770A
S714A-Y770A
R705
Impaired
Functional
Functional
Impaired

CHAPTER 4:

Autism-associated mutation inhibits protein kinase C-mediated neuroligin-4X enhancement of excitatory synapses

Introduction

In a 2014 report published by the Centers for Disease Control and Prevention (CDC), it was estimated that 1 in 68 children in the United States have an ASD (Developmental Disabilities Monitoring Network Surveillance Year Principal et al., 2014). These neuropsychiatric disorders have a strong genetic component consistent with high recurrence rates between siblings and a higher concordance frequency seen in monozygotic than dizygotic twins. Furthermore, deletions, insertions, and substitutions have been identified within the genome that increase the risk of these disorders (Abrahams and Geschwind, 2008; Zoghbi and Bear, 2012). These cytogenetic and genome sequencing studies have revealed that NLGNs are one of a subset of genes encoding synaptic proteins associated with ASDs (Jamain et al., 2003; Sudhof, 2008).

The NLGN gene family consists of five members (*Nlgn1, 2, 3, 4X,* and *4Y*) within the human genome that encode transsynaptic cell adhesion molecules that are critical for synapse assembly, maintenance, and plasticity (Craig and Kang, 2007; Dean and Dresbach, 2006; Sudhof, 2008). Numerous studies have identified a variety of mutations in X-linked NLGN3 and 4X genes that range from copy number variants (Levy et al., 2011; Marshall et al., 2008; Sanders et al., 2011; Thomas et al., 1999) to protein truncations and amino acid substitutions in patients with ASDs (Jamain et al., 2003; Laumonnier et al., 2004; Lawson-Yuen et al., 2008). Interestingly, all of the point mutations in NLGN3 and NLGN4X reside in their extracellular domains except for a single point mutation in the cytoplasmic domain (c-tail) of NLGN4X at arginine (R) 704, which is modified to a cysteine (C) (Yan et al., 2005). How this mutation or other NLGN disease mutations contribute to the pathophysiology is unknown.

Protein phosphorylation is a critical modulator of NLGN function (Bemben et al., 2014; Giannone et al., 2013). Recently, we showed that Ca^{2+}/CaM Kinase II (CaMKII) phosphorylates the c-tail of NLGN1 in an isoform-specific and activity-dependent manner, which regulates its ability to enhance excitatory synapses (Bemben et al., 2014). Next, we wondered if different kinases might regulate the function of other NLGN isoforms?

In the present study, we show *in vitro* and *in vivo* that NLGN4X is robustly phosphorylated by PKC. We identified the dominant phosphorylation site as T707, a residue not conserved in NLGNs 1, 2, and 3. Intriguingly, PKC phosphorylation is eliminated with the autism-associated mutation R704C. Most dramatically, we found that the phospho-mimetic mutation at T707 profoundly enhances anatomical markers for synapses and potentiates NLGN4X-mediated excitatory synaptic transmission. This study establishes compelling evidence that NLGN4X can act at and regulate excitatory synapses. Furthermore, it demonstrates, strikingly, how a single point mutation in NLGNs can acutely adjust synaptic properties.

Results

PKC Phosphorylates NLGN4X at T707

To test if NLGNs are substrates for kinases other than CaMKII, we conducted an *in vitro* kinase assay with GST-fusion constructs with the c-tails of NLGNs 1, 2, 3, and 4X (Figure 16A and Figure 17), and found that NLGN4X was robustly phosphorylated by PKC as evaluated by radiography (Figure 16B). Weak phosphorylation of NLGN1 and NLGN3 was observed when compared to NLGN4X (Figure 16B, see longer exposure), indicating NLGN4X to be the best NLGN substrate for PKC. To identify the individual PKC phosphorylation site(s), we subjected NLGN4X to the same *in vitro* kinase assay and evaluated phosphorylation using liquid chromatography coupled to tandem mass spectrometry (LC-MS/MS) and identified the major phosphorylation site as T707 (Figure 16C), a residue that is not conserved in NLGNs 1, 2, and 3 (Figure 16A and Figure 17 for complete alignment).

Autism-Associated Mutation Eliminates PKC Phosphorylation of NLGN4X

Interestingly, T707 resides only a few amino acids away from the only known autism-associated mutation (R704C) in the c-tail of any NLGN protein (Figure 16A). This substitution replaces a positive charge for a polar amino acid, and occupies a critical residue in a potential PKC consensus sequence (RXXS/T, where X denotes any amino acid). Might the autism-related R704C mutation abolish PKC phosphorylation of NLGN4X at T707? To independently verify the mass spectrometry results, we performed the same *in vitro* kinase assay with a non-phosphorylatable point mutation, T707A, and showed that T707

was the dominant NLGN4X PKC phosphorylation site, which resulted in an approximately 75% reduction in NLGN4X phosphorylation. Likewise, NLGN4X R704C eliminated T707 phosphorylation (Figure 16D and 16E). Importantly, CaMKII phosphorylation of NLGN4X T718, the only other known phosphorylation site near T707, was not reduced by the R704C mutation demonstrating that this mutation did not result in a generalized problem rendering the protein unphosphorylated (Figure 18A and 18B). Taken together, these results indicate that NLGN4X is a robust substrate for PKC, and the only autism-associated NLGN4X c-tail mutation abolishes T707 phosphorylation.

To detect NLGN4X T707 phosphorylation *in vivo*, we produced a phosphorylation state-specific antibody (Ab), pT707-Ab, against residues 703-712 in NLGN4X (Figure 16A). The pT707-Ab only detected NLGN4X that was phosphorylated on T707 as detected by a PKC *in vitro* kinase assay that was resolved by SDS-PAGE and subsequent immunoblotting (Figure 16F). Critically, the pT707-Ab did not show any immunoreactivity with the non-phosphorylated NLGN4X, the non-phosphorylatable mutants (R704C or T707A), or any of the other NLGN isoforms that were tested.

The *in vitro* experiments were performed with fusion proteins of NLGN c-tail isoforms. To test whether full-length NLGN4X can be phosphorylated in mammalian cells and modulated by PKC activity, we transfected wild-type (WT) NLGN4X or various NLGN4X mutants (R704C, T707A, or T707D) in COS-7 cells and immunoblotted cell lysates with the pT707-Ab. Under basal conditions, NLGN4X was not phosphorylated at T707, but transient activation of PKC by phorbol 12-myristate 13-acetate (PMA) triggered a robust increase in pT707 phosphorylation (Figure 16G). NLGN4X R704C resulted in an approximately 95% reduction in pT707 phosphorylation, whereas NLGN4X T707A or the

phospho-mimetic mutation, T707D, were not detected by the pT707-Ab (Figure 16G and 16H). Phosphorylation of serine (S) 831 on GluA1 was used as a positive control for PMA activation of PKC (Roche et al., 1996) (Figure 16G and 16I). Additionally, the pT707-Ab had astonishing specificity for immunoprecipitating (IP) only NLGN4X phosphorylated on T707 as validated by Western blotting with two independent NLGN4X Abs and a pan NLGN-Ab (Figure 19). Collectively, these data demonstrate that NLGN4X T707 is phosphorylated in heterologous cells, and the pT707-Ab is a dynamic and isoform- specific reagent that faithfully distinguishes the phosphorylated form of NLGN4X on T707.

Phosphorylation of NLGN4X at T707 Induces Synaptogenesis

Previously, two autism-associated mutations in NLGN3 (R451C) and NLGN4X (R87W) were shown to disrupt surface expression (Poulopoulos et al., 2009; Tabuchi et al., 2007). Moreover, phosphorylation of the NLGN1 c-tail regulates its forward trafficking (Bemben et al., 2014). Does T707 regulate NLGN4X surface expression? To test this possibility, cultured rat hippocampal neurons were transfected with NLGN4X (WT, R704C, T707A, or T707D) and visualized with immunofluorescence confocal microscopy. To prevent potential heterodimerization, we performed these experiments on a reduced endogenous NLGN background using an exogenous chained microRNA against NLGNs 1, 2, and 3 (NLmiRs) as previously described (Shipman et al., 2011). Human NLGN4X and NLGN4Y are absent in rats (Bolliger et al., 2008). Consequently, rat neurons were used in all imaging and physiology experiments to ensure a NLGN4 null background to avoid any complications that might occur between dimerization of WT and mutant NLGN4 receptors. Phosphorylation at T707 did not affect the trafficking of NLGN4X to the cell

surface (Figure 20A and 20B). However, we noticed that expression of a phospho-mimetic mutation of NLGN4X T707 (T707D) resulted in a robust increase in dendritic protrusions when compared to NLGN4X WT and the non-phosphorylatable mutants, R704C and T707A (Figure 20A and 20C). To examine if the increase in spines resulted in new excitatory synapses, we co-expressed NLmiRs with NLGN4X (WT, R704C, T707A, or T707D) in rat hippocampal cultures and assayed for anatomical measures of functional synapses, namely increases in presynaptic VGLUT1 and postsynaptic PSD-95. Using immunofluorescence confocal microscopy, we found that the NLGN4X phospho-mimetic (T707D) mutation resulted in an increase in both VGLUT1 and PSD-95 staining, an enhancement that was absent in non-phosphorylated NLGN4X protein (Figure 20D, 20E, and 20F). These results indicate that T707 phosphorylation promotes NLGN4X-induced synaptogenesis independent of regulating its surface expression.

To test whether these new synapses were functional, we biolistically co-expressed NLmiRs with NLGN4X (WT, R704C, T707A, or T707D) in rat organotypic hippocampal slice cultures and used a dual whole cell recording configuration to simultaneously record evoked excitatory postsynaptic currents in both transfected and neighboring control, untransfected cells. Expression of NLGN4X T707D resulted in a profound increase in both AMPA receptor (AMPAR) and NMDA receptor (NMDAR) mediated currents when compared to a control cell or NLGN4X (WT, R704C, or T707A) (Figure 21A, 21B, 21C, and 21D). Previously, we, as well as others, have reported that NLGN4X expression on a WT background decreased postsynaptic excitatory currents (Poulopoulos et al., 2009; Shipman et al., 2011). However, on a reduced NLGN background, which alone reduces AMPAR and NMDAR mediated currents by about 50% (Figure 22), NLGN4X expression

induced a modest, but significant, increase in AMPAR transmission, an enhancement that was absent in R704C and T707A (Figure 21A, 21B, 21C, and 21D). Together, these results show that phosphorylation at T707 dynamically regulates NLGN4X's ability to robustly induce the genesis of functional excitatory synapses.

Endogenous NLGN4X is Phosphorylated by PKC in Human Neurons

Because our NLGN4X pT707-Ab was so specific, we were able to investigate endogenous NLGN4X T707 phosphorylation in cultured human embryonic neurons. These cultures consisted primarily of MAP2 positive neurons (Figure 23A) and transient activation of PKC with PMA resulted in approximately an 8-fold increase in NLGN4X pT707 phosphorylation (Figure 23B and 23C). Consistent with previous reports, NLGN4X was expressed in human embryonic neurons, as detected with two independent NLGN4X Abs and a pan NLGN-Ab (Marei et al., 2012). Taken together, these results show that endogenous NLGN4X is phosphorylated in human neurons by PKC.

Discussion

We set out to examine whether other NLGN isoforms, like NLGN1, were regulated by phosphorylation. We identified a PKC phosphorylation site on human NLGN4X at T707, which establishes a novel interplay between two critical constituents of the synapse. It was to our surprise, R704, a residue mutated in a familial case of autism (Yan et al., 2005), resided within the PKC consensus sequence in the c-tail of NLGN4X. However, after identification, it was not unexpected that the autism mutation (R704C) abolished the kinase's ability to chemically modify NLGN4X at T707. Using a diverse combination of techniques, we show that phosphorylated NLGN4X can dynamically enhance excitatory synapses.

Prior to this report, the importance of protein phosphorylation on NLGN1 was established (Bemben et al., 2014; Giannone et al., 2013). CaMKII phosphorylation of T739 regulates NLGN1's ability to potentiate excitatory synaptic transmission by regulating its surface expression. This current study demonstrates that PKC phosphorylation of T707 dramatically enhances NLGN4X's ability to potentiate excitatory currents independent of modulating its surface expression. Therefore phosphorylation is a key regulatory modification modulating both NLGN1 and NLGN4X's function but by different kinases, at different sites, and likely by different molecular mechanisms. Collectively, these studies raise two exciting questions: Might other kinases phosphorylate NLGN2 and NLGN3 and regulate their synaptic functions similarly to NLGN1 and NLGN4X? Secondly, what is the molecular mechanism by which T707 phosphorylation induces the genesis of functional synapses independent of surface expression? These answers remain to be elucidated but are currently an area of future investigation.

Interestingly, human NLGN4X is not well conserved in rodents, unlike NLGNs 1, 2, and 3. NLGN4 is absent in *Rattus norvegicus* and highly divergent and on an autosome in *Mus musculus* (Bolliger et al., 2008). This has made the investigation of human autism mutations in NLGN4X challenging and led some researchers to study the R704C point mutation in NLGN3. Although R704 is conserved in all human NLGNs, the residue analogous to NLGN4X T707 is not conserved. A knock-in mutation in NLGN3 resulted in minor synaptic phenotypes (Etherton et al., 2011). Therefore we believe it is imperative to study the R704C mutation in NLGN4X, and more generally for all disease mutations to be studied in their respective isoforms independent of residue(s) conservation.

Canonically, NLGN1 is known as a critical component of the excitatory synapse based on its cellular localization (Chih et al., 2005; Song et al., 1999), regulation by CaMKII (Bemben et al., 2014), and its ability to robustly potentiate AMPAR and NMDAR postsynaptic currents (Chubykin et al., 2007; Shipman et al., 2011). Conversely, mouse NLGN4 is known to localize to and modulate inhibitory transmission (Hoon et al., 2011). However, the human and mouse isoforms are not well conserved. This raises the possibility that these proteins might perform distinct functions in different species. Here, we show that like NLGN1, human NLGN4X can enhance excitatory synapses, suggesting that NLGN4X may associate with excitatory synapses in humans. At a minimum, this underscores the reservations of studying human NLGN4X and rodent NLGN4 interchangeably. However, it is important to note our study does not preclude the possibility that human NLGN4X may act or be expressed at inhibitory synapses in humans.

Notably, all the NLGN-associated autism point mutations reported thus far reside in their extracellular or transmembrane domains, except for NLGN4X R704C. This may

be a result of chance or may highlight the critical importance of T707 phosphorylation in regulating NLGN4X's synaptic properties. It is tempting to speculate whether this phosphorylation occurs at a critical developmental period to shape synaptic properties or whether it is a global switch that happens continually at excitatory synapses. The profound effect the phospho-mimetic mutation (T707D) has on excitatory synapses may suggest the prior.

Mouse models of autism have increasingly revealed underlying imbalances of excitatory/inhibitory transmission, which are believed to play a central role in the etiology of ASDs (Foldy et al., 2013; Rothwell et al., 2014; Tabuchi et al., 2007). Our results are consistent with this hypothesis, which support a pathophysiological model by which NLGN4X R704C decreases excitatory transmission by abolishing PKC-mediated NLGN4X potentiation of excitatory transmission. Furthermore, we believe given the overlap of synaptic proteins found to be candidate genes in ASDs that by understanding the biology of specific mutations such as R704C has implications for clinical, as well as future therapeutic treatment for ASDs.

Figure 16: Autism-associated mutation eliminates PKC phosphorylation of NLGN4X

(A) Alignment of the transmembrane domains and partial c-tails of human NLGNs 1, 2, 3, 4X, and 4Y. The PKC phosphorylation site, T707, is boxed in orange; autism mutation, R704, boxed in blue; and pT707-Ab epitope boxed in yellow. The CaMKII phosphorylation site on NLGN1 is boxed in gray. (B and D) Purified PKC and [γ-P-32]ATP were incubated with GST-fusion proteins and analyzed by autoradiography. CBB protein staining was used to visualize total protein, and GST (negative) and GST-GluA1 c-tail (positive) functioned as phosphorylation controls. (C) ETD MS/MS spectrum of chymotrypsin digested phosphorylated NLGN4X peptide 704-RHETHRRPSPQ-714 found in GST-NLGN4X fusion proteins that were incubated with ATP and purified PKC. Samples were analyzed using the LC/MS/MS method. (E) Means ± SEM of phosphorylated NLGN4X by PKC normalized to WT (n = 4) for NLGN4X R704C (P = 0.0013, n = 4) and NLGN4X T707A (P = 0.0030, n = 4). (F) GST, GST-NLGNs 1, 2, 3, and 4X (WT, R704C, and T707A) were incubated with PKC, and phosphorylation was evaluated by immunoblotting with pT707-Ab. Total protein was evaluated with a GSTAb. (G) GFP, FLAG-GluA1, or NLGN4X (WT, R704C, T707A, or T707D) were transfected in COS cells and treated with DMSO or PMA, a PKC activator. GluA1 pS831 served as control for PKC activation and the arrow denotes the NLGN4X specific band. (H) Means ± SEM of phosphorylated NLGN4X pT707 achieved by PMA activation normalized to WT (n = 3) and NLGN4X R704C (P = 0.0310, n = 3). (I) Means ± SEM of phosphorylated GluA1 S831 achieved by PMA activation (P = 0.0187, n = 3) normalized to no treatment (n = 3). Immunoblots (WB) were probed with indicated antibodies in F and G. *P < 0.05 **P < 0.01.

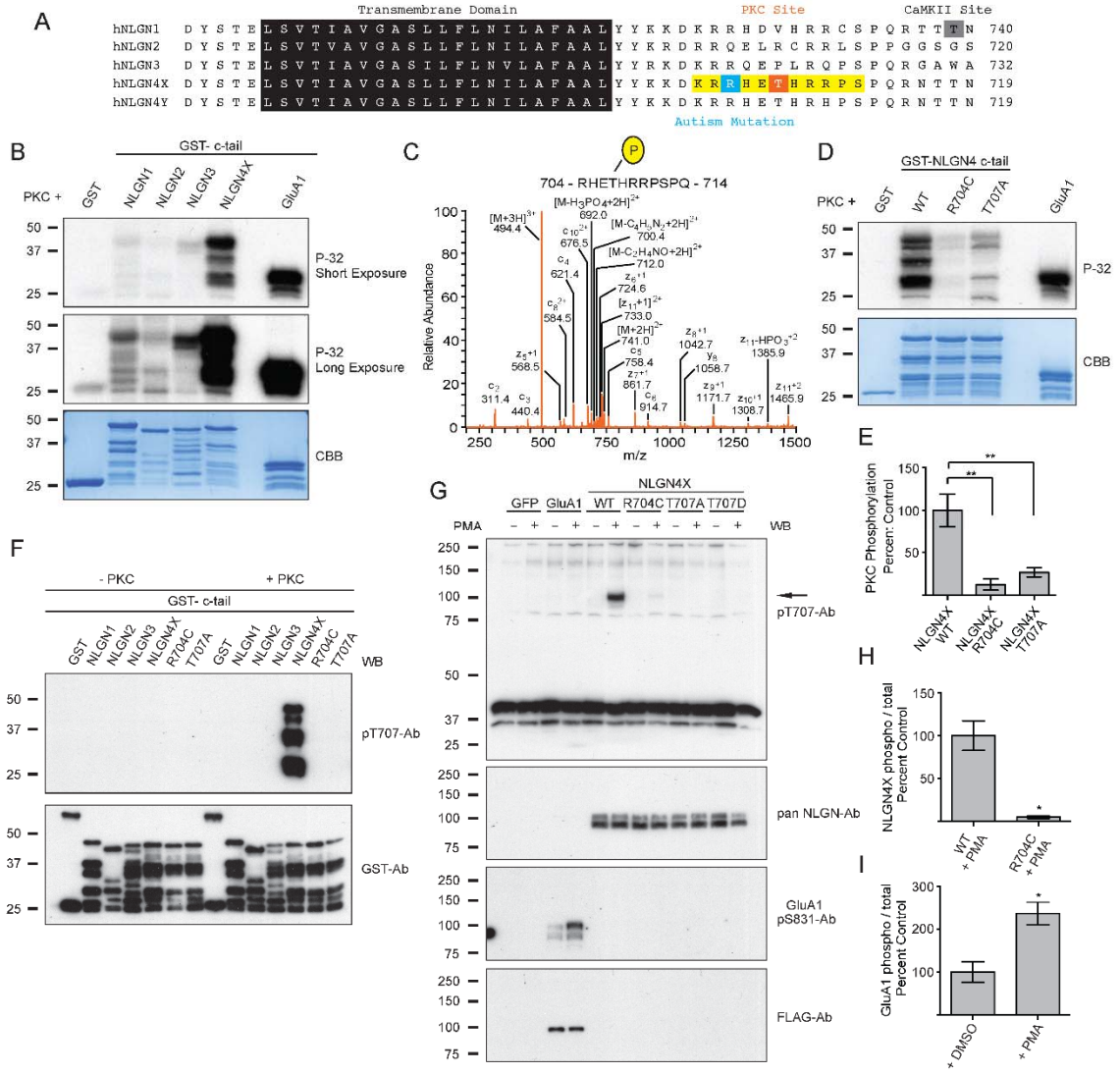
A
Transmembrane Domain
PKC Site
CaMKII Site
hNLGN1 D Y S T E L S V T I A V G A S L L F L N I L A F A A L Y Y K K D K R R H D V H R R C S P Q R T T T N 740
hNLGN2 D Y S T E L S V T V A V G A S L L F L N I L A F A A L Y Y K R D R R Q E L R C R R L S P P G G S G S 720
hNLGN3 D Y S T E L S V T I A V G A S I L F L N V L A F A A L Y Y R K D K R R Q E P L R Q P S P Q R G A W A 732
hNLGN4X D Y S T E L S V T I A V G A S L L F L N I L A F A A L Y Y K K D K R R H E T H R R P S P Q R N T T N 719
hNLGN4Y D Y S T E L S V T I A V G A S L L F L N I L A F A A L Y Y K K D K R R H E T H R H P S P Q R N T T N 719
Autism Mutation
B
GST- c-tail
PKC +
GST
NLGN1
NLGN2
NLGN3
NLGN4X
GluA1
P-32 Short Exposure
P-32 Long Exposure
CBB
C
704 - RHETHRRPSPQ - 714
Relative Abundance
m/z
D
GST-NLGN4 c-tail
PKC +
GST
WT
R704C
T707A
GluA1
P-32
CBB
E
PKC Phosphorylation Percent: Control
NLGN4X WT
NLGN4X R704C
NLGN4X T707A
F
- PKC
+ PKC
GST- c-tail
WB
pT707-Ab
GST-Ab
G
NLGN4X
GFP
GluA1
WT
R704C
T707A
T707D
PMA
WB
pT707-Ab
pan NLGN-Ab
GluA1 pS831-Ab
FLAG-Ab
H
NLGN4X phospho / total Percent Control
WT + PMA
R704C + PMA
I
GluA1 phospho / total Percent Control
+ DMSO
+ PMA

Figure 17: Alignment of the transmembrane domains and complete c-tails of human NLGNs 1, 2, 3, 4X, and 4Y

The PKC phosphorylation site boxed in orange; key autism residue boxed in blue, and pT707-Ab epitope boxed in yellow. All other known NLGN phosphorylation sites boxed in gray.

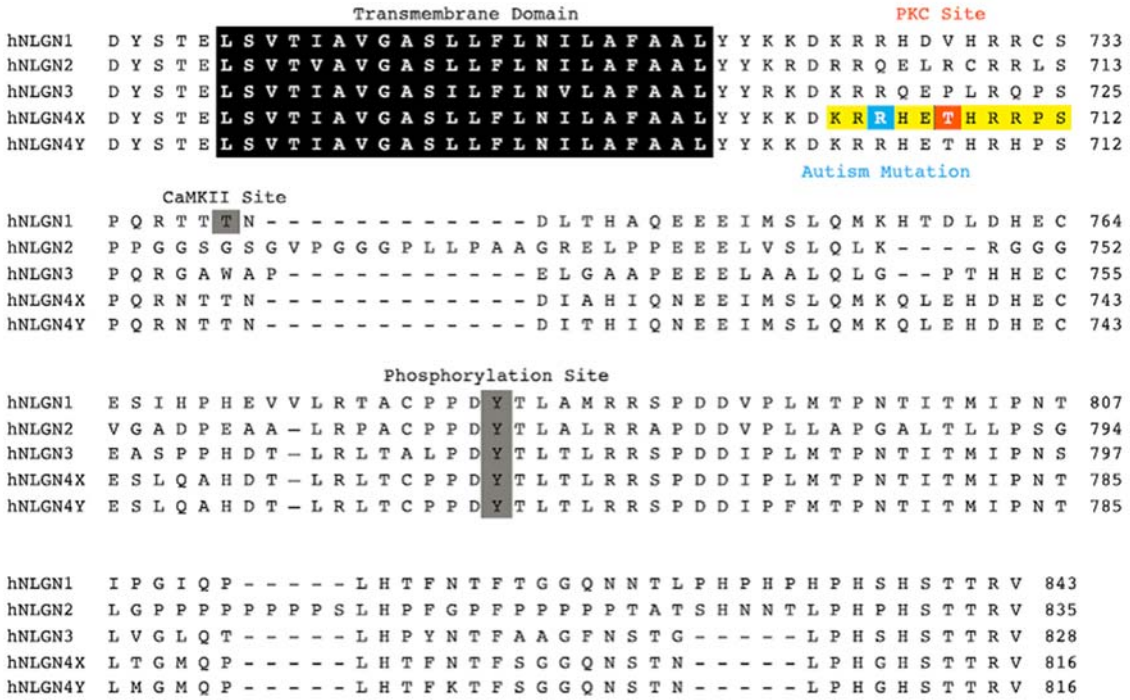
Transmembrane Domain
PKC Site
Autism Mutation
CaMKII Site
Phosphorylation Site
hNLGN1 D Y S T E L S V T I A V G A S L L F L N I L A F A A L Y Y K K D K R R H D V H R R C S 733
hNLGN2 D Y S T E L S V T V A V G A S L L F L N I L A F A A L Y Y K R D R R Q E L R C R R L S 713
hNLGN3 D Y S T E L S V T I A V G A S I L F L N V L A F A A L Y Y R K D K R R Q E P L R Q P S 725
hNLGN4X D Y S T E L S V T I A V G A S L L F L N I L A F A A L Y Y K K D K R R H E T H R R P S 712
hNLGN4Y D Y S T E L S V T I A V G A S L L F L N I L A F A A L Y Y K K D K R R H E T H R H P S 712
hNLGN1 P Q R T T T N - - - - - - - - - - - - - - D L T H A Q E E E I M S L Q M K H T D L D H E C 764
hNLGN2 P P G G S G S G V P G G G P L L P A A G R E L P P E E E L V S L Q L K - - - - R G G G 752
hNLGN3 P Q R G A W A P - - - - - - - - - - - - E L G A A P E E E L A A L Q L G - - P T H H E C 755
hNLGN4X P Q R N T T N - - - - - - - - - - - - - D I A H I Q N E E I M S L Q M K Q L E H D H E C 743
hNLGN4Y P Q R N T T N - - - - - - - - - - - - - D I T H I Q N E E I M S L Q M K Q L E H D H E C 743
hNLGN1 E S I H P H E V V L R T A C P P D Y T L A M R R S P D D V P L M T P N T I T M I P N T 807
hNLGN2 V G A D P E A A - L R P A C P P D Y T L A L R R A P D D V P L L A P G A L T L L P S G 794
hNLGN3 E A S P P H D T - L R L T A L P D Y T L T L R R S P D D I P L M T P N T I T M I P N S 797
hNLGN4X E S L Q A H D T - L R L T C P P D Y T L T L R R S P D D I P L M T P N T I T M I P N T 785
hNLGN4Y E S L Q A H D T - L R L T C P P D Y T L T L R R S P D D I P F M T P N T I T M I P N T 785
hNLGN1 I P G I Q P - - - - - L H T F N T F T G G Q N N T L P H P H P H P H S H S T T R V 843
hNLGN2 L G P P P P P P P P S L H P F G P F P P P P P T A T S H N N T L P H P H S T T R V 835
hNLGN3 L V G L Q T - - - - - L H P Y N T F A A G F N S T G - - - - - L P H S H S T T R V 828
hNLGN4X L T G M Q P - - - - - L H T F N T F S G G Q N S T N - - - - - L P H G H S T T R V 816
hNLGN4Y L M G M Q P - - - - - L H T F K T F S G G Q N S T N - - - - - L P H G H S T T R V 816

Figure 18: Autism-associated mutation does not reduce CaMKII phosphorylation of NLGN4X

(A) Purified CaMKII and [γ-P-32]ATP were incubated with GSTfusion proteins and analyzed by autoradiography. CBB protein staining was used to visualize total protein, and GST (negative) and GST-NLGN1 c-tail (positive) functioned as phosphorylation controls. (B) Means ± SEM of phosphorylated NLGN4X by CaMKII normalized to WT (n = 4) for NLGN4X R704C ($P > 0.05$, n = 4) and NLGN4X T707A ($P > 0.05$, n = 4).

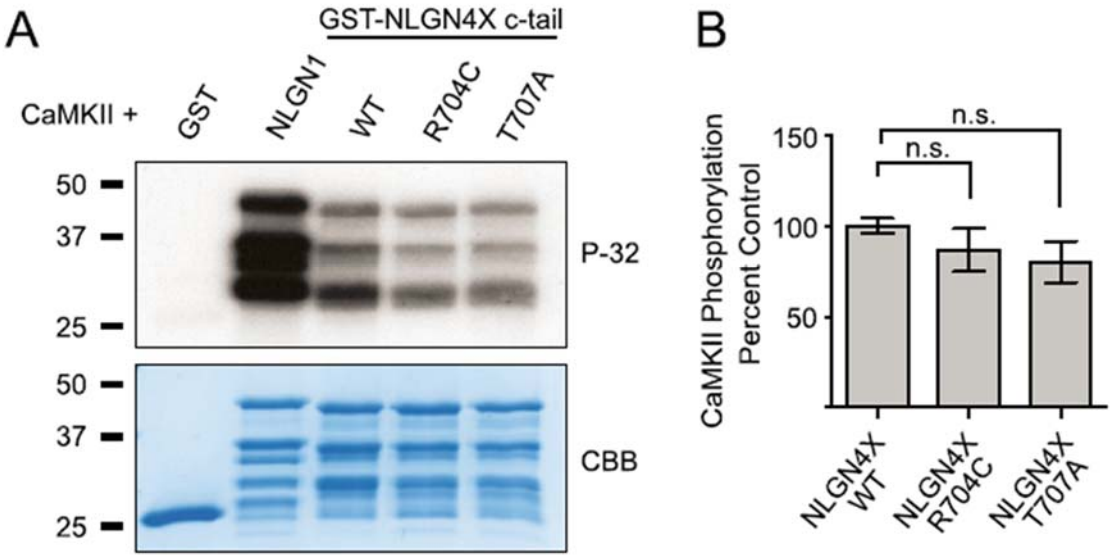
A
GST-NLGN4X c-tail
CaMKII +
GST
NLGN1
WT
R704C
T707A
50
37
25
P-32
50
37
25
CBB
B
CaMKII Phosphorylation
Percent Control
150
100
50
n.s.
n.s.
NLGN4X WT
NLGN4X R704C
NLGN4X T707A

Figure 19: NLGN4X pT707-Ab specifically immunoprecipitates phosphorylated NLGN4X

GFP or NLGN4X were transfected in COS cells and treated with DMSO (−) or PMA (+) and immunoprecipitated with pT707-Ab. Immunoblots (WB) were probed with indicated antibodies.

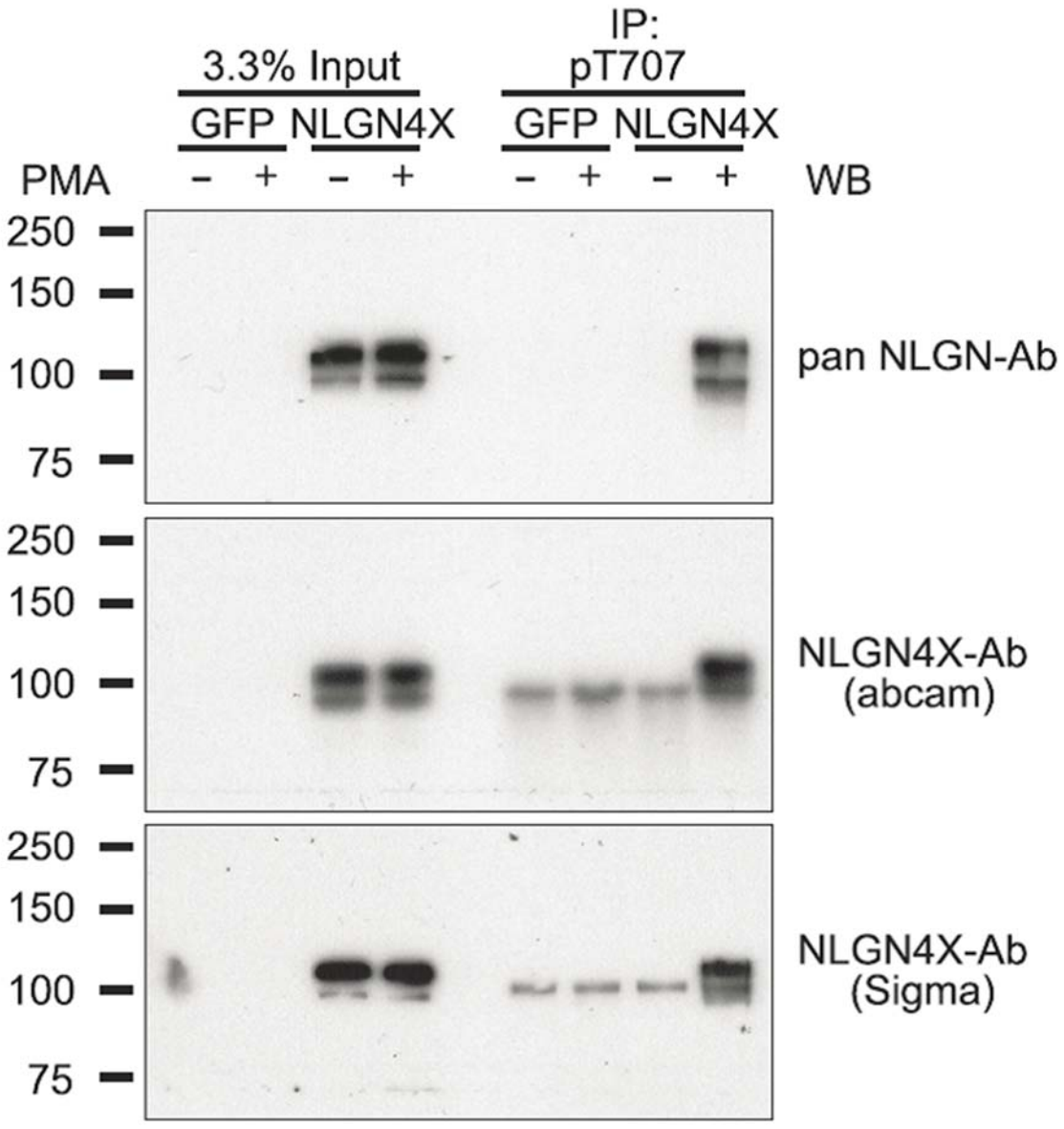
3.3% Input
IP:
pT707
GFP
NLGN4X
GFP
NLGN4X
PMA
– + – + – + – +
WB
250
150
100
75
pan NLGN-Ab
250
150
100
75
NLGN4X-Ab
(abcam)
250
150
100
75
NLGN4X-Ab
(Sigma)

Figure 20: NLGN4X phosphorylation at T707 induces synaptogenesis

(A) Coexpression of NLmiRs and NLGN4X (WT, R704C, T707A, or T707D) in rat hippocampal neurons. Surface and intracellular receptors were labeled with an anti-hemagglutinin (HA) antibody, which recognized a tag inserted downstream of the signal peptide. (Scale bar, 20 μm.) (B) Means ± SEM normalized to NLGN4X (n = 27), NLGN4X R704C ($P > 0.05$, n = 29), NLGN4X T707A ($P > 0.05$, n = 30), and NLGN4X T707D ($P > 0.05$, n = 29). (C) Means of spine number ± SEM normalized to NLGN4X (n = 30), NLGN4X R704C ($P > 0.05$, n = 30), NLGN4X T707A ($P > 0.05$, n = 30), and NLGN4X T707D ($P = 0.001$, n = 30). (D) Same transfections as in A except NLGN4X constructs did not contain an HA tag. Endogenous VGLUT1 and PSD-95 were stained and visualized as described in Experimental Procedures. (E) Means ± SEM of VGLUT1 normalized to NLGN4X (n = 30) for NLGN4X R704C ($P > 0.05$, n = 30), NLGN4X T707A ($P > 0.05$, n = 30), and NLGN4X T707D ($P = 0.0466$, n = 30). (F) Means ± SEM of PSD-95 normalized to NLGN4X (n = 30) for NLGN4X R704C ($P > 0.05$, n = 27), NLGN4X T707A ($P > 0.05$, n = 28), and NLGN4X T707D ($P = 0.0049$, n = 30). *$P < 0.05$ **$P < 0.01$, ***$P < 0.001$.

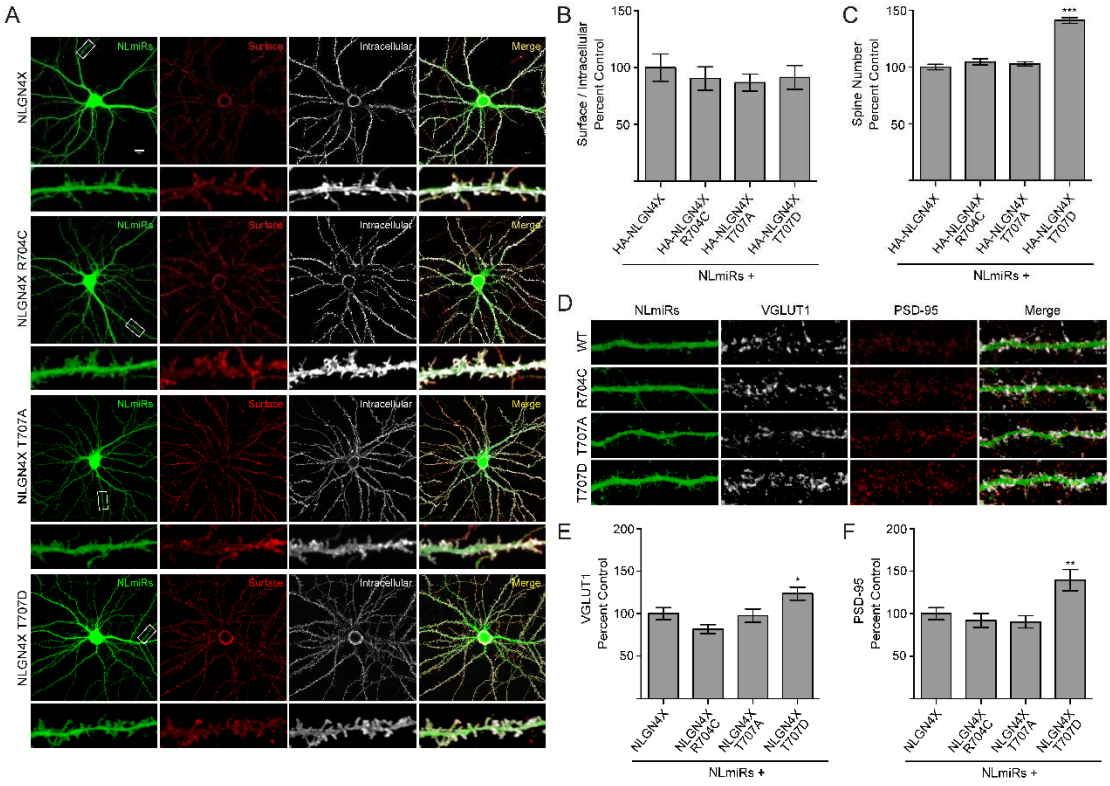
A
NLGN4X
NLGN4X R704C
NLGN4X T707A
NLGN4X T707D
NLmiRs
Surface
Intracellular
Merge
B
Surface / intracellular
Percent Control
150
100
50
HA-NLGN4X
HA-NLGN4X R704C
HA-NLGN4X T707A
HA-NLGN4X T707D
NLmiRs +
C
Spine Number
Percent Control
***
D
NLmiRs
VGLUT1
PSD-95
Merge
WT
R704C
T707A
T707D
E
VGLUT1
Percent Control
200
150
100
50
*
NLGN4X
NLGN4X R704C
NLGN4X T707A
NLGN4X T707D
NLmiRs +
F
PSD-95
Percent Control
**

Figure 21: NLGN4X T707D dramatically enhances excitatory postsynaptic currents

(A) AMPAR-mediated EPSC scatter plots. Expression of either NLGN4X or NLGN4X T707D results in a potentiation of AMPARmediated currents compared with control, untransfected cells ($P = 0.0023$, $n = 18$; $P = 0.0010$, $n = 11$). The enhancement was absent in NLGN4X R704C ($P > 0.05$, $n = 13$) and NLGN4X T707A ($P > 0.05$, $n = 11$) expressing cells. Experiments were performed in rat organotypic slice cultures on a reduced NLGN background (NLmiRs). Open circles are individual pairs; filled (in red) are mean ± SEM. Black sample traces are control; green are transfected. (Scale bars, 15 pA and 10 ms.) (B) Summary graph of data in A. Expression of NLGN4X T707D resulted in a greater enhancement of AMPAR-mediated currents compared with NLGN4X ($P = 0.0143$), NLGN4X R704C ($P = 0.0025$), or NLGN4X T707A ($P = 0.0066$). (C) NMDARmediated EPSC scatter plots. Expression of NLGN4X ($n = 12$) or phosphodeficient mutants, NLGN4X R704C ($n = 11$), or NLGN4X T707A ($n = 13$), did not enhance NMDAR-mediated currents compared with control untransfected cells ($P > 0.05$), whereas expression of NLGN4X T707D significantly potentiated NMDA-mediated currents ($P = 0.0117$, $n = 9$). Open circles are individual pairs, filled (in red) are mean ± SEM. Black sample traces are control; green are transfected. (Scale bars, 30 pA and 20 ms.) (D) Summary graph of data in C. Expression of NLGN4X T707D resulted in an enhancement of NMDAR-mediated currents compared with NLGN4X ($P = 0.0409$), NLGN4X R704C ($P = 0.0250$), and NLGN4X T707A ($P = 0.0138$). *$P < 0.05$ **$P < 0.01$, ***$P < 0.001$.

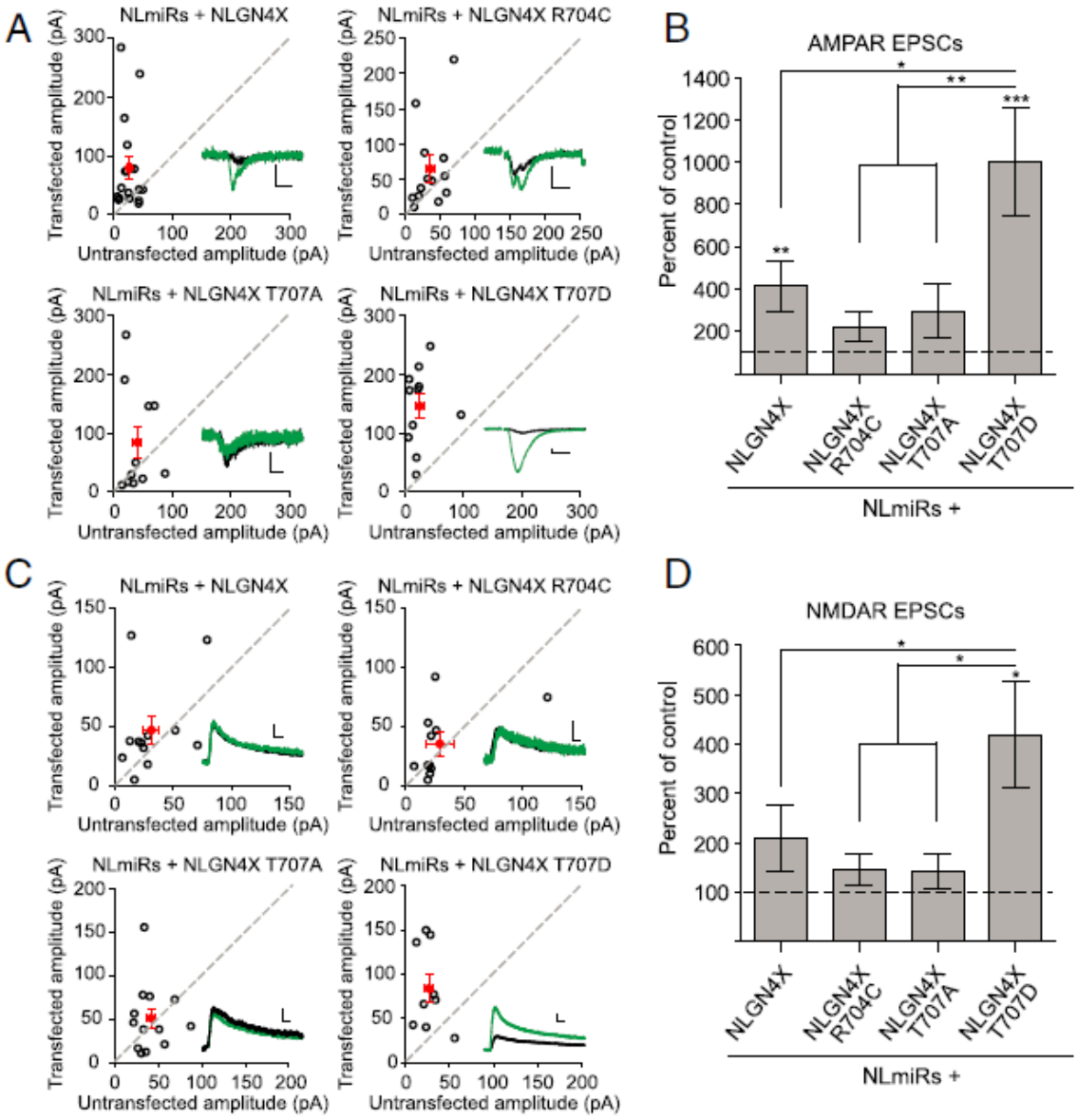
A
NLmiRs + NLGN4X
NLmiRs + NLGN4X R704C
NLmiRs + NLGN4X T707A
NLmiRs + NLGN4X T707D
Transfected amplitude (pA)
Untransfected amplitude (pA)
B
AMPAR EPSCs
Percent of control
NLGN4X
NLGN4X R704C
NLGN4X T707A
NLGN4X T707D
NLmiRs +
C
NLmiRs + NLGN4X
NLmiRs + NLGN4X R704C
NLmiRs + NLGN4X T707A
NLmiRs + NLGN4X T707D
Transfected amplitude (pA)
Untransfected amplitude (pA)
D
NMDAR EPSCs
Percent of control
NLGN4X
NLGN4X R704C
NLGN4X T707A
NLGN4X T707D
NLmiRs +

Figure 22: NLmiRs reduces AMPA and NMDA currents

(A) AMPAR-mediated EPSC scatter plot. Expression of NLmiRs (3–4 d) results in a reduction of AMPARmediated currents compared with control, untransfected cells ($P = 0.0078$, $n = 8$). Open circles are individual pairs, filled (in red) are mean ± SEM. Black sample traces are control; green are transfected. (Scale bar, 15 pA and 10 ms.) Bar graph of data is transfected amplitude (NLmiRs) normalized to neighboring, nontransfected cell (control). (B) NMDAR-mediated EPSC scatter plot, showing similar reductions in NMDAR-mediated currents ($P = 0.0098$, $n = 10$) as seen in A. (Scale bar, 30 pA and 20 ms.) $^{**}P < 0.01$.

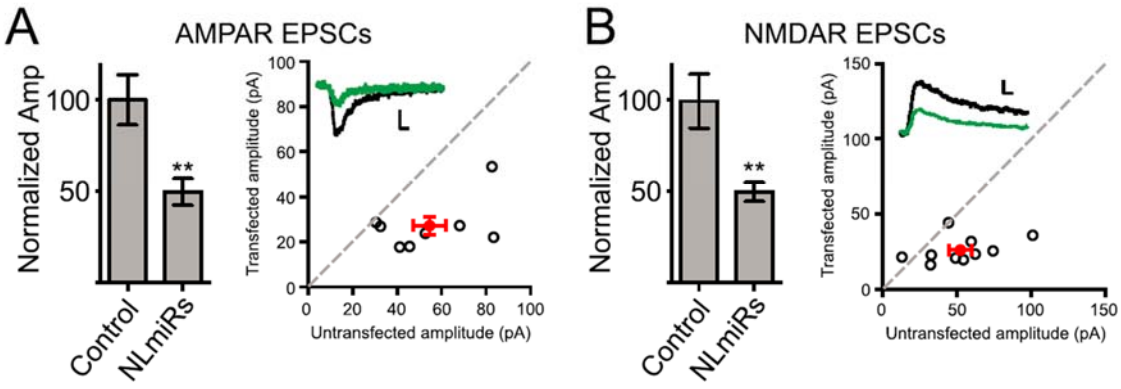
A
AMPAR EPSCs
Normalized Amp
100
50
**
Control
NLmiRs
Transfected amplitude (pA)
Untransfected amplitude (pA)
L
B
NMDAR EPSCs
Normalized Amp
100
50
**
Control
NLmiRs
Transfected amplitude (pA)
Untransfected amplitude (pA)
L

Figure 23: PKC phosphorylates endogenous NLGN4X in human neurons

(A) Immunofluorescence image of human embryonic neurons stained with the neuronal marker MAP2. (B) Regulation of NLGN4X phosphorylation at T707 in human embryonic neurons ± PMA treatment. Arrow denotes the NLGN4X pT707-specific band. Immunoblots (WB) were probed with indicated antibodies. (C) Means ± SEM of phosphorylated NLGN4X T707 achieved by PMA activation normalized to no treatment (n = 4) and + PMA treatment (P = 0.0148, n = 4).

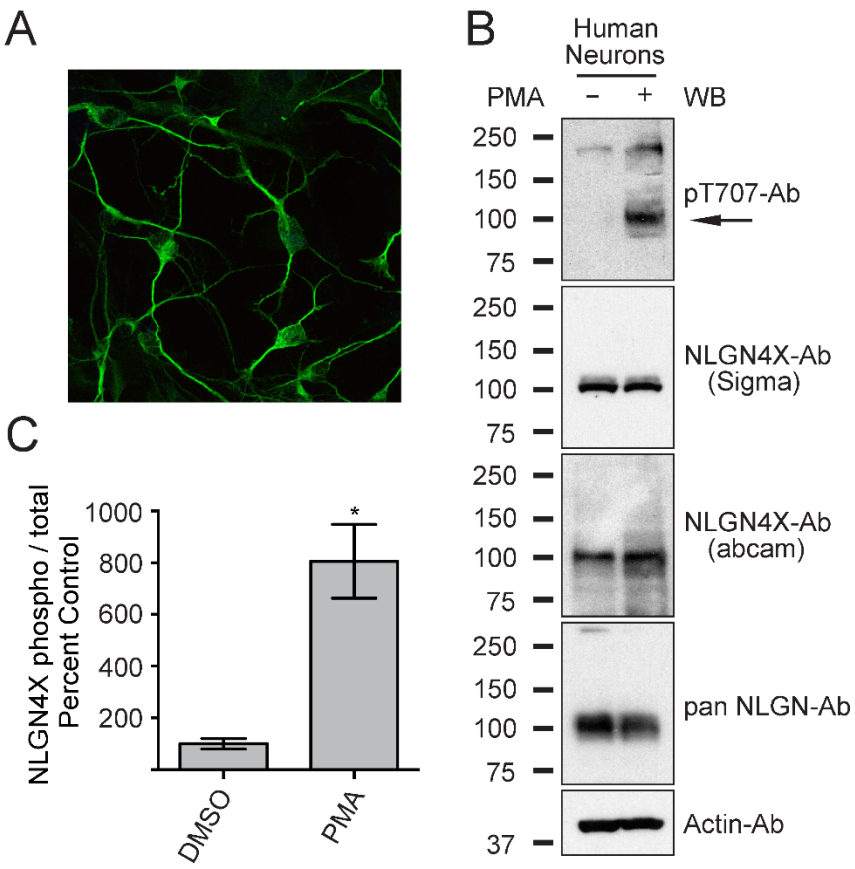
A
B
Human
Neurons
PMA
–
+
WB
250
150
100
75
pT707-Ab
NLGN4X-Ab
(Sigma)
NLGN4X-Ab
(abcam)
pan NLGN-Ab
Actin-Ab
37
C
NLGN4X phospho / total
Percent Control
1000
800
600
400
200
*
DMSO
PMA

CHAPTER 5:

The $GABA_A$ receptor β subunit is critical for inhibitory transmission

Introduction

$GABA_A$ receptors are heteropentameric ionotropic receptors which mediate the majority of fast inhibitory neurotransmission in the brain (Olsen and Sieghart, 2008; Sieghart, 2006). These receptors are comprised of a multitude of different subunit families each with their own number of different isoforms, including α1-6, β1-3, γ1-3, δ, ε, θ, π, and ρ1-3 (Simon et al., 2004). The vast diversity of subunits makes studying this particular receptor especially daunting. However, previous work has established that the canonical assembly of the $GABA_A$ receptor contains the presence of two α subunits, two β subunits, and a fifth subunit (Chang et al., 1996; Sieghart and Sperk, 2002).

Much of the work on assembly and function of $GABA_A$ receptors has been done using heterologous expression systems to observe functional assembly of discrete sets of overexpressed subunits. A key criticism of this approach is the potential assembly of subunit combinations that normally would not occur in the native mammalian system (Olsen and Sieghart, 2008). In addition, the different $GABA_A$ receptor subunits vary in their expression profiles temporally and spatially within the brain, suggesting that particular receptor subunit profiles may exist within specific brain regions and in particular neuronal circuits (Fritschy and Panzanelli, 2014; Laurie et al., 1992). This insight however has not translated into much progress in understanding the role of native receptor subunits since only a handful of genetic knockouts exist for particular subunits (Rudolph and Mohler, 2004).

CRISPR/Cas9 technology enables efficient gene editing without the time and expense necessary to generate knockout mice. This approach has previously been shown to enable complete deletion of synaptic proteins in post-mitotic neurons (Incontro et al.,

2014; Straub et al., 2014). We utilize this technology to probe the function of the β subunits of the $GABA_A$ receptor in inhibitory synaptic transmission onto CA1 hippocampal pyramidal cells. We find that, indeed, the β subunit is required for assembly of functional $GABA_A$ receptors and that expression of the β3 subunit in particular is important for proper inhibitory transmission. We show that knockout of β3 affects inputs from parvalbumin (PV) but not somatostatin (SOM) expressing interneurons onto pyramidal cells. Furthermore, we show that expression of β3 alone is sufficient to rescue inhibitory currents in the context of a β1-3 subunit knockout. Our findings identify a key requirement for the β subunit and highlight the unique importance of the β3 subunit in regulating $GABA_A$ receptor function, showcasing an approach that can be used for the study of native receptor composition and function at inhibitory synapses.

Results

Functional $GABA_A$ receptors require the β subunit

To determine the importance of the β subunits to inhibitory transmission, we utilized CRISPR-Cas9 technology to develop a knockout construct containing individual single guide RNA (sgRNA) sequences for β1, β2, and β3 chained together (Figure 24a). Lentiviral-mediated expression of these guides along with Cas9 in dissociated hippocampal cultures resulted in a dramatic reduction in protein levels of all three subunits (Figure 24b). The remaining signal we see is most likely due to incomplete co-infection of both constructs in all neurons. We then biolistically transfected rat organotypic hippocampal slices with these constructs to enable sparse transfection. Since our constructs co-express a fluorophore, we are able to specifically record from cells expressing both constructs. We measured inhibitory currents induced with a stimulus electrode placed in CA1. Simultaneous recording of a transfected and untransfected, neighboring CA1 pyramidal cell revealed complete loss of inhibitory currents (IPSCs) in transfected cells, showing that functional $GABA_A$ receptors require the inclusion of the β subunit (Figure 24c, 24d, and 24e). Regardless of the size of the current elicited in the control cell, we consistently failed to see a significant response in the transfected cell (Figure 24d). The time course for the full effect is about 3 weeks and, therefore, all recordings were made after 3 weeks.

The β3 subunit is most important for inhibitory transmission

While transgenic knockout animals exist for the β2 and β3 subunit, there is no knockout for β1. Previous work looking at the effects of β2 knockout on synaptic

transmission in dentate gyrus granule cells found no effect on miniature IPSCs (Herd et al., 2008). β3 knockout mice display deficits in inhibitory synaptic transmission in granule cells but not mitral cells of the olfactory bulb (Nusser et al., 2001). In order to determine the relative contribution of each β subunit to inhibitory synaptic transmission in the hippocampus, we expressed individual sgRNAs for the β subunits (Figure 25a). Knockout of neither β1 nor β2 had a significant effect on inhibitory transmission (Figure 25b, 25c and 25e). This is consistent with the low expression of β2 in the hippocampus (Laurie et al., 1992; Sperk et al., 1997). Knockout of β3 resulted in a significant impairment of inhibitory currents (Figure 25d and 25e), indicating its importance for inhibitory transmission.

We proceeded to knockout two different subunits at once in order to determine the properties of the endogenous subunit that was left (Figure 26a). Knockout of both β1 and β2 did not result in a significant change to inhibitory currents, suggesting that the endogenous β3 subunit remaining is fully able to maintain proper inhibitory synaptic transmission (Figure 26b and 26e). While the currents observed after knockout of β1 and β3 were not significantly different than control cells, the effect was significantly different than that seen with knockout of both β1 and β2, suggesting that the presence of β2 alone may not be sufficient to maintain inhibitory transmission (Figure 26c and 26e). Knockout of β2 and β3 resulted in a significant depression of inhibitory currents, suggesting that the presence of β1 alone is not sufficient to maintain inhibitory transmission (Figure 26d and 26e). Overall, these results show that β3 is necessary for maintaining proper inhibitory transmission and is the most able to compensate for the loss of the other β subunits.

Knockout of β3 preferentially affects PV and not SOM inputs

It was interesting that neither our single nor double knockout manipulations fully recapitulated the dramatic elimination of all inhibitory current observed with the triple knockout. Since CA1 pyramidal cells receive inhibitory inputs from a multitude of interneuron subtypes, we wondered whether there are subtype specific effects in our knockout manipulations which could underlie the partial reduction observed with single and double knockouts. In particular, we wanted to parse the inputs from parvalbumin (PV) positive interneurons, which target somatic and proximal dendritic regions, from somatostatin (SOM) positive interneurons, which target distal dendritic regions of pyramidal cells (Rudy et al., 2011; Xu et al., 2010). We focused on knockout of β3 since it was the only single knockout manipulation that had exhibited a significant reduction in inhibitory currents. We were encouraged by the occurrence of faster IPSC decay kinetics of the current remaining after knockout of either β3 or both β2 and β3 (Figure 28a and 28b), suggesting that the inhibitory synapses remaining are electrophysiologically distinct.

We utilized transgenic mice expressing Cre either under the PV or SOM promoter along with Cre-dependent Channelrhodopsin (ChR2). Experiments were performed wherein electrical stimulation was given to sample the population of inhibitory inputs followed by a brief pulse of blue light to stimulate the particular inputs from either PV or SOM cells. Using this approach, we found that β3 knockout significantly impaired responses mediated by PV interneurons while inputs from SOM interneurons were unaffected, suggesting that loss of β3 preferentially affects PV but not SOM inputs (Figure 27b and 27c, 27e and 27f). Importantly, electrical stimulation of slices from both PV-ChR2

and SOM-ChR2 mice still showed a deficit in inhibitory currents due to loss of β3, consistent with what we observed in rat slices (Figure 27a and 27c, 27d and 27f).

Expression of β3 alone is sufficient to restore inhibitory transmission

To follow up on our result that knockout of both β1 and β2 did not change inhibitory synaptic transmission, we expressed a human homolog of β3 that would not be recognized by our CRISPR guide-RNA in combination with the triple β subunit knockout. Inhibitory currents recorded from these cells did not show a significant change compared to control cells, indicating that expression of β3 alone is able to restore inhibitory synaptic currents (Figure 29a and 29b). Converse to what we observed with β3 knockout, these rescued currents displayed slower kinetics (Figure 28c). We also looked to see if expression of the β3 subunit alone is also able to restore extrasynaptic currents as well, since we see no response after applying a puff of GABA onto cells expressing the triple β subunit knockout (Figure 29c). Indeed, expression of β3 on the background of the triple β subunit knockout is able to fully restore responses to control levels (Figure 29d).

Discussion

Dissection of the molecular and circuit mechanisms of inhibitory neurotransmission is difficult due to the diversity in subunit composition of $GABA_A$ receptors, in addition to the diversity in population of the inhibitory interneurons themselves. The emergence of new tools to hone in on the precise workings of native receptors within defined neuronal circuits hold much promise toward accelerating progress in understanding inhibition in the brain.

Here we utilize both CRISPR/Cas9 as well as optogenetic approaches to dissect the involvement of the β subunits of the $GABA_A$ receptor in inhibitory transmission. We find that the presence of the β subunit is absolutely required for the assembly of functional $GABA_A$ receptors. In addition, we find that knockout of β3 preferentially affects PV but not SOM-mediated inhibitory synapses onto CA1 pyramidal cells. Finally, we show that expression of β3 alone is sufficient to rescue the complete loss of inhibition observed in the triple β subunit knockout. Together these results highlight the crucial role of the β subunit, especially β3, of the $GABA_A$ receptor in inhibitory transmission both at the level of individual circuits and in overall transmission.

Efficacy of CRISPR/Cas9

CRISPR/Cas9 works with a remarkable efficiency in eliminating the expression of synaptic proteins in post-mitotic neurons (Incontro et al., 2014; Straub et al., 2014). A key question in further applying this technology for genetic manipulations concerns whether this approach can be used to target multiple different gene targets at once while maintaining

the same efficacy and efficiency as seen with single targets. Previous work characterizing the expression of four sgRNAs targeting four distinct genomic loci in one lentiviral vector into HEK293T and human fibroblast cells observed about a 30% efficacy in eliminating all four targets at once (Kabadi et al., 2014). In our approach, we were able to observe >90% co-expression and functionality of all three sgRNAs after about 3 weeks. It is possible that by using post-mitotic cells we maintain high expression of the Cas9 and sgRNAs, enabling multiple rounds of gene editing until expression of the target is effectively eliminated.

Previous attempts to utilize CRISPR to target $GABA_A$ receptor subunits showed that knockout of the γ2 subunit of the $GABA_A$ receptor abolished miniature IPSCs (Uezu et al., 2016). The γ2 subunit is an obligatory subunit for synaptic $GABA_A$ receptors (Essrich et al., 1998). Our knockout of all three β subunits eliminated all inhibitory current, both synaptic and extrasynaptic. This manipulation can be used in future studies as a way to eliminate all inhibition postsynaptically. It is possible that other cell types in other brain regions have different requirements for $GABA_A$ receptor functional assembly. Our approach provides a guide and framework in which to address this possibility and many other remaining questions regarding the assembly and function of $GABA_A$ receptors.

The critical requirement of the β subunit

We were able to show that native assembly of a functional $GABA_A$ receptor requires the inclusion of the β subunit. This is consistent with what has been proposed from observations in heterologous systems that $GABA_A$ receptors are composed of two α

subunits, two β subunits, and one other subunit (Chang et al., 1996; Sieghart and Sperk, 2002). Furthermore, our results show that expression of just one β subunit isoform, in this case β3, is able to restore the deficits seen when all three are eliminated, suggesting that within the complex of 2 α, 2 β, and a γ subunit the two β subunits can be the same isoform. While biochemical studies have suggested the existence of two different β subunit isoforms in the same $GABA_A$ receptor, our results show that this criteria does not prevent functional assembly (Jechlinger et al., 1998; Li and De Blas, 1997).

β3 is critical for proper inhibitory transmission

We found in both our single and double knockout manipulations that it was only when β3 is knocked out, either alone or in combination with another β isoform, that inhibitory currents are depressed, suggesting that out of the three β subunits, β3 is most important for proper inhibitory transmission. β3 was also observed to be sufficient to maintain inhibitory currents, both in the absence of β1 or β2 or upon rescue on the triple β subunit knockout.

Another indication of the unique nature of β3 containing synapses is the faster kinetics observed in the β3 knockout and slower kinetics seen with β3 rescue in the triple β subunit knockout (Figure 28a, 28b, and 28c). The gating kinetics of the $GABA_A$ receptor depend on expression of the particular α subunit isoform, with α1 containing receptors having faster kinetics than α2/3 containing receptors (Gingrich et al., 1995). Previous characterization of neurons from β3 knockout mice found faster mIPSC decay kinetics due to the reduction in expression of α2/3 subunits (Ramadan et al., 2003). Our results

corroborate this finding and suggest that the β3 subunit preferentially associates with α2/3 subunits to mediate slower IPSC kinetics.

The β3 subunit has been highly associated with a number of disorders including autism and epilepsy, and knockout mice for β3 experience frequent seizures (DeLorey et al., 1998; Homanics et al., 1997; Vien et al., 2015). Our results showing that knockout of β3 preferentially affects PV but not SOM inputs onto pyramidal cells further refines the mechanisms by which β3 functions at inhibitory synapses and defines potential avenues for further investigation in determining how disruptions to β3 expression and function can eventually lead to disease.

Towards a model

From our results, we can assemble a possible model for $GABA_A$ receptor β subunit localization that can explain our observations (Figure 30). It is of particular interest that none of our single and double knockout manipulations fully recapitulated the dramatic elimination of inhibitory responses seen in the triple knockout. To illustrate these findings, our model proposes the existence of two different types of inhibitory synapses: one that has $GABA_A$ receptors with β3 as the only β subunit and one that has receptors comprised of all three β isoforms. In manipulations where either β1 or β2 or both are knocked out, β3 is present to maintain proper inhibitory transmission. It is only in instances where β3 is knocked out do we see a deficit owing to the fact that the presence of either β1 or β2 or both is not enough to compensate for the loss of β3 in synapses containing only β3. This also explains why we only see a partial deficit when β3 is knocked out since β1 and/or β2 is able to compensate at synapses where all three isoforms are present.

How does this model fit into our observation that loss of β3 preferentially affects PV but not SOM synapses? While PV interneurons are a major subset of interneurons and account for 26% of GABAergic neurons in the CA1, they themselves can be subdivided into different of classes of interneurons including PV-positive basket cells, bistratified cells, and axo-axonic (chandelier) cells (Kosaka et al., 1987; Somogyi and Klausberger, 2005). It is therefore possible that the effect we see on PV inputs is due to changes from one particular type of PV-pyramidal cell connection and future experiments can be performed to refine our findings even further to hone in on this possibility.

Our work highlights the critical role of the β subunits in inhibitory transmission and identifies the β3 subunit as an important subunit regulating $GABA_A$ receptor channel function at both the molecular and circuit level. These findings and approach will provide multiple avenues for future study in elucidating mechanisms of $GABA_A$ receptor function and how its dysfunction can lead to disease.

Figure 24: $GABA_A$ β 1-3 subunits are necessary for inhibitory transmission

a) Diagram of the vector constructs used to express the chained sgRNAs for β1, β2, and β3 along with Cas9. CBh: promoter; NLS: nuclear localization sequence; 2A: protease site; U6: promoter; hUbC: promoter. b) Western blot of rat dissociated hippocampal cultures infected with lentiviruses containing individually the constructs in a or control untransfected cultures. Lysates were probed for expression of β1, β2/3, and actin. c) Representative traces of an untransfected cell (in black) and cell transfected with the sgRNAs for β1-3 and Cas9 (in green). d) Varying absolute amplitudes were observed in control untransfected cells while transfected cells displayed no inhibitory current (***p = 0.0002, n = 18) e) Scatter plot showing reduction in IPSCs in β1-3 CRISPR transfected neurons compared to untransfected controls (***p = 0.0002, n = 18). Open circles are individual pairs, filled circle is mean ± s.e.m.

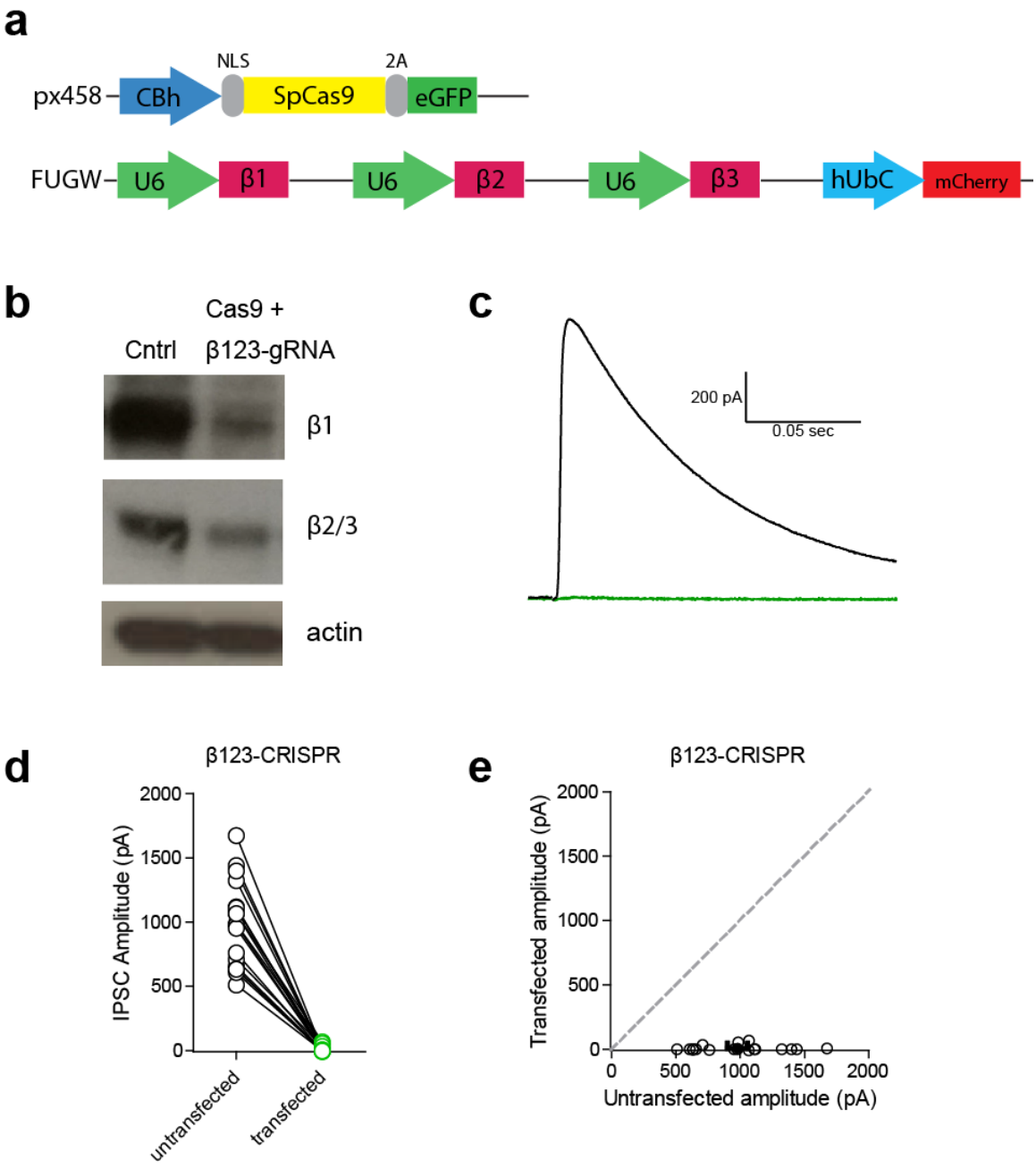
a
NLS
2A
px458
CBh
SpCas9
eGFP
FUGW
U6
β1
U6
β2
U6
β3
hUbC
mCherry
b
Cas9 +
Cntrl
β123-gRNA
β1
β2/3
actin
c
200 pA
0.05 sec
d
β123-CRISPR
IPSC Amplitude (pA)
2000
1500
1000
500
0
untransfected
transfected
e
β123-CRISPR
Transfected amplitude (pA)
2000
1500
1000
500
0
0
500
1000
1500
2000
Untransfected amplitude (pA)

Figure 25: $GABA_A$ β3 subunit is critical for proper inhibitory transmission

a) Diagram of the vector constructs used to express the individual sgRNAs for β1, β2, and β3. b) Scatter plot showing no reduction in IPSCs in β1 CRISPR transfected neurons compared to untransfected controls ($p = 0.4$, $n = 13$). c) Scatter plot showing no reduction in IPSCs in β2 CRISPR transfected neurons compared to untransfected controls ($p = 0.2$, $n = 10$). d) Scatter plot showing reduction in IPSCs in β3 CRISPR transfected neurons compared to untransfected controls (*$p = 0.037$, $n = 10$). e) Summary graph of b-d. For panels b-d, open circles are individual pairs, filled circle is mean ± s.e.m. Black sample traces are control, green are transfected. Scale bars represent 100 pA and 50 ms. For panel e summary graph plots mean transfected amplitude ± s.e.m, expressed as a percentage of control amplitude. Significance above each column represents pairwise comparison between transfected and untransfected cells.

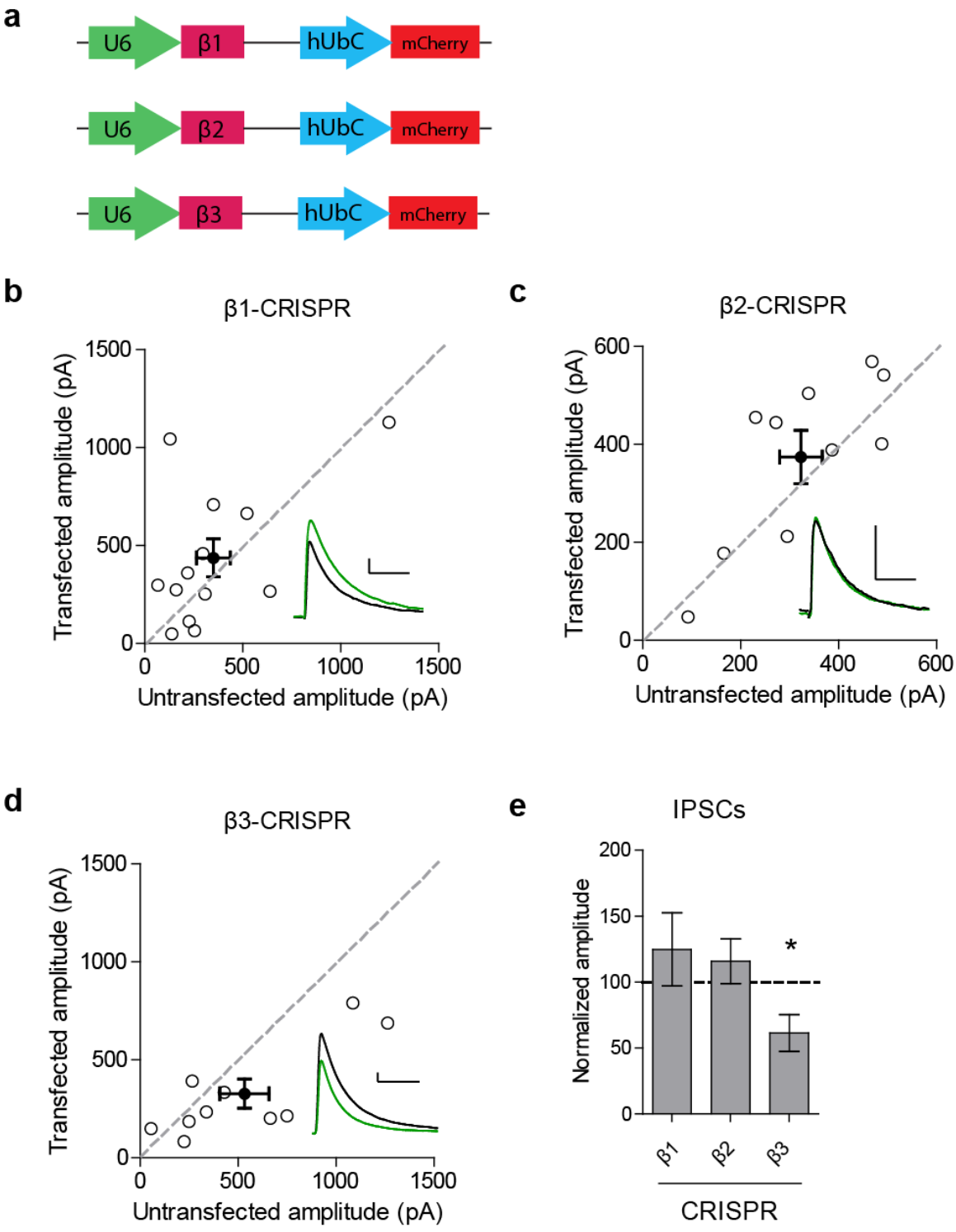
a
U6
β1
hUbC
mCherry
U6
β2
hUbC
mCherry
U6
β3
hUbC
mCherry
b
β1-CRISPR
Transfected amplitude (pA)
Untransfected amplitude (pA)
0
500
1000
1500
c
β2-CRISPR
Transfected amplitude (pA)
Untransfected amplitude (pA)
0
200
400
600
d
β3-CRISPR
Transfected amplitude (pA)
Untransfected amplitude (pA)
0
500
1000
1500
e
IPSCs
Normalized amplitude
0
50
100
150
200
*
β1
β2
β3
CRISPR

Figure 26: $GABA_A$ β3 subunit is important for maintaining proper inhibition

a) Diagram of the vector constructs used to express two of the sgRNAs for β1, β2, and β3 at once. b) Scatter plot showing no reduction in IPSCs in β1 and β2 CRISPR transfected neurons compared to untransfected controls ($p = 0.8$, $n = 7$). c) Scatter plot showing inhibitory currents in β1 and β3 CRISPR transfected neurons were not significantly different compared to untransfected control cells ($p = 0.1$, $n = 11$). d) Scatter plot showing reduction in IPSCs in β2 and β3 CRISPR transfected neurons compared to untransfected controls (**$p = 0.0024$, $n = 17$). e) Summary graph of b-d. Knockout of both β1 and β3 or both β2 and β3 resulted in currents that were significantly reduced compared to those seen in knockout of both β1 and β2 (*$p = 0.046$, **$p = 0.0052$). For panels b-d, open circles are individual pairs, filled circle is mean ± s.e.m. Black sample traces are control, green are transfected. Scale bars represent 100 pA and 50 ms. For panel e summary graph plots mean transfected amplitude ± s.e.m, expressed as a percentage of control amplitude. Significance above each column represents pairwise comparison between transfected and untransfected cells.

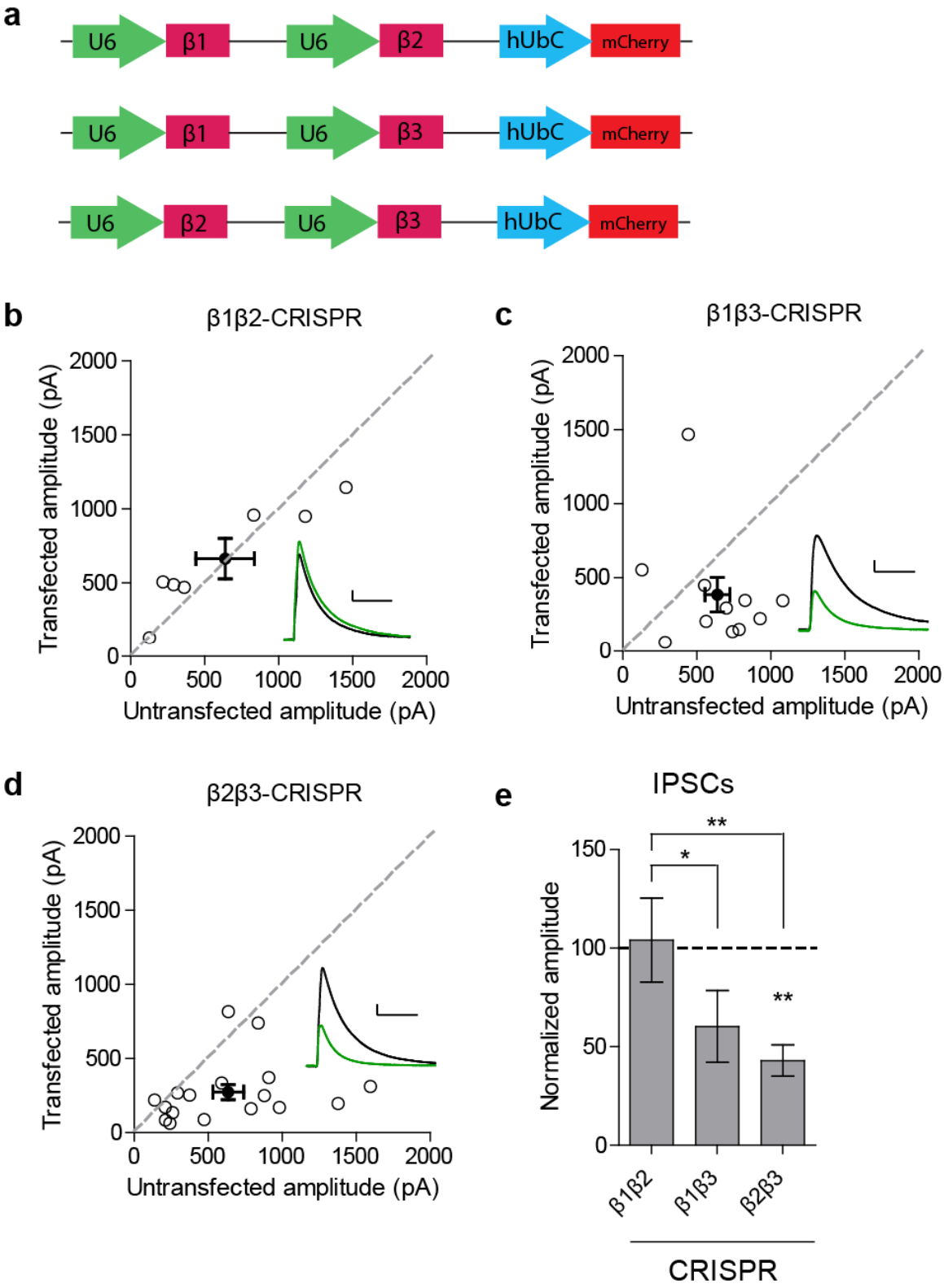
a
U6
β1
U6
β2
hUbC
mCherry
U6
β1
U6
β3
hUbC
mCherry
U6
β2
U6
β3
hUbC
mCherry
b
β1β2-CRISPR
Transfected amplitude (pA)
Untransfected amplitude (pA)
0
500
1000
1500
2000
c
β1β3-CRISPR
Transfected amplitude (pA)
Untransfected amplitude (pA)
d
β2β3-CRISPR
Transfected amplitude (pA)
Untransfected amplitude (pA)
e
IPSCs
Normalized amplitude
150
100
50
0
*
**
**
β1β2
β1β3
β2β3
CRISPR

Figure 27: Knockout of $GABA_A$ β3 subunit preferentially affects PV not SOM inputs

a) Scatter plot showing electrical stimulation of hippocampal organotypic slices from SOM-ChR2 transgenic mice still displayed a deficit in inhibitory transmission in cells transfected with β3 CRISPR compared to untransfected controls (***p = 0.0005, n = 13). b) Scatter plot showing no reduction in IPSCs in β3 CRISPR transfected neurons when SOM currents are specifically elicited with blue light (p = 0.3, n = 13). c) Summary graph of a-b. d) Scatter plot showing electrical stimulation of hippocampal organotypic slices from PV-ChR2 transgenic mice still displayed a deficit in inhibitory transmission in cells transfected with β3 CRISPR compared to untransfected controls (*p = 0.04, n = 17). e) Scatter plot showing reduction in IPSCs in β3 CRISPR transfected neurons when PV currents are specifically elicited with blue light (p = 0.01, n = 17). f) Summary graph of d-e. For panels a-b and d-e, open circles are individual pairs, filled circle is mean ± s.e.m. Black sample traces are control, green are transfected. Scale bars represent 100 pA and 50 ms. For panel c and f summary graph plots mean transfected amplitude ± s.e.m, expressed as a percentage of control amplitude. Significance above each column represents pairwise comparison between transfected and untransfected cells.

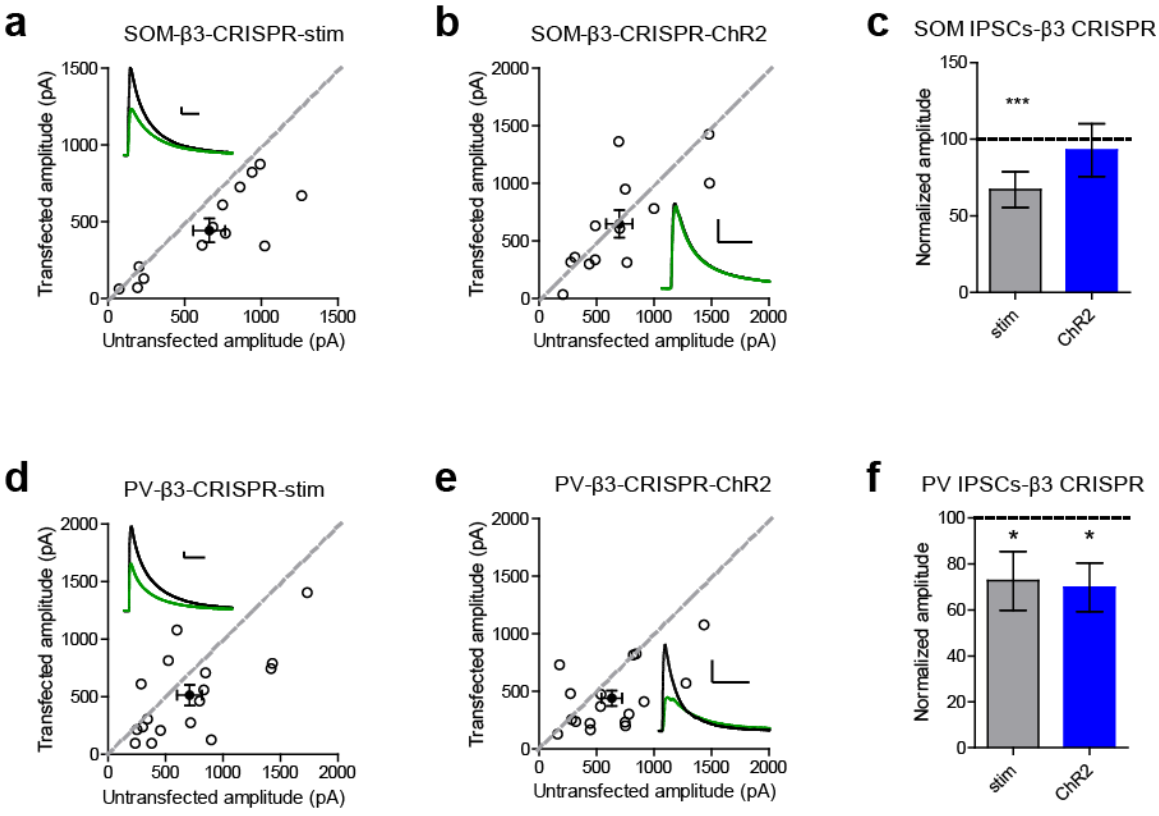
a
SOM-β3-CRISPR-stim
Transfected amplitude (pA)
Untransfected amplitude (pA)
b
SOM-β3-CRISPR-ChR2
Transfected amplitude (pA)
Untransfected amplitude (pA)
c
SOM IPSCs-β3 CRISPR
Normalized amplitude
***
stim
ChR2
d
PV-β3-CRISPR-stim
Transfected amplitude (pA)
Untransfected amplitude (pA)
e
PV-β3-CRISPR-ChR2
Transfected amplitude (pA)
Untransfected amplitude (pA)
f
PV IPSCs-β3 CRISPR
Normalized amplitude
*
*
stim
ChR2

Figure 28: IPSC decay kinetics are altered in β3 manipulations

a) Cells where β3 is knocked out display faster kinetics compared to control untransfected cells (*p = 0.04, n = 10). b) Cells where β2 and β3 are knocked out display faster kinetics compared to control untransfected cells (*p = 0.003, n = 15). c) Cells where replacement with β3 on the background of the triple β subunit CRISPR display slower kinetics (*p = 0.01, n = 12).

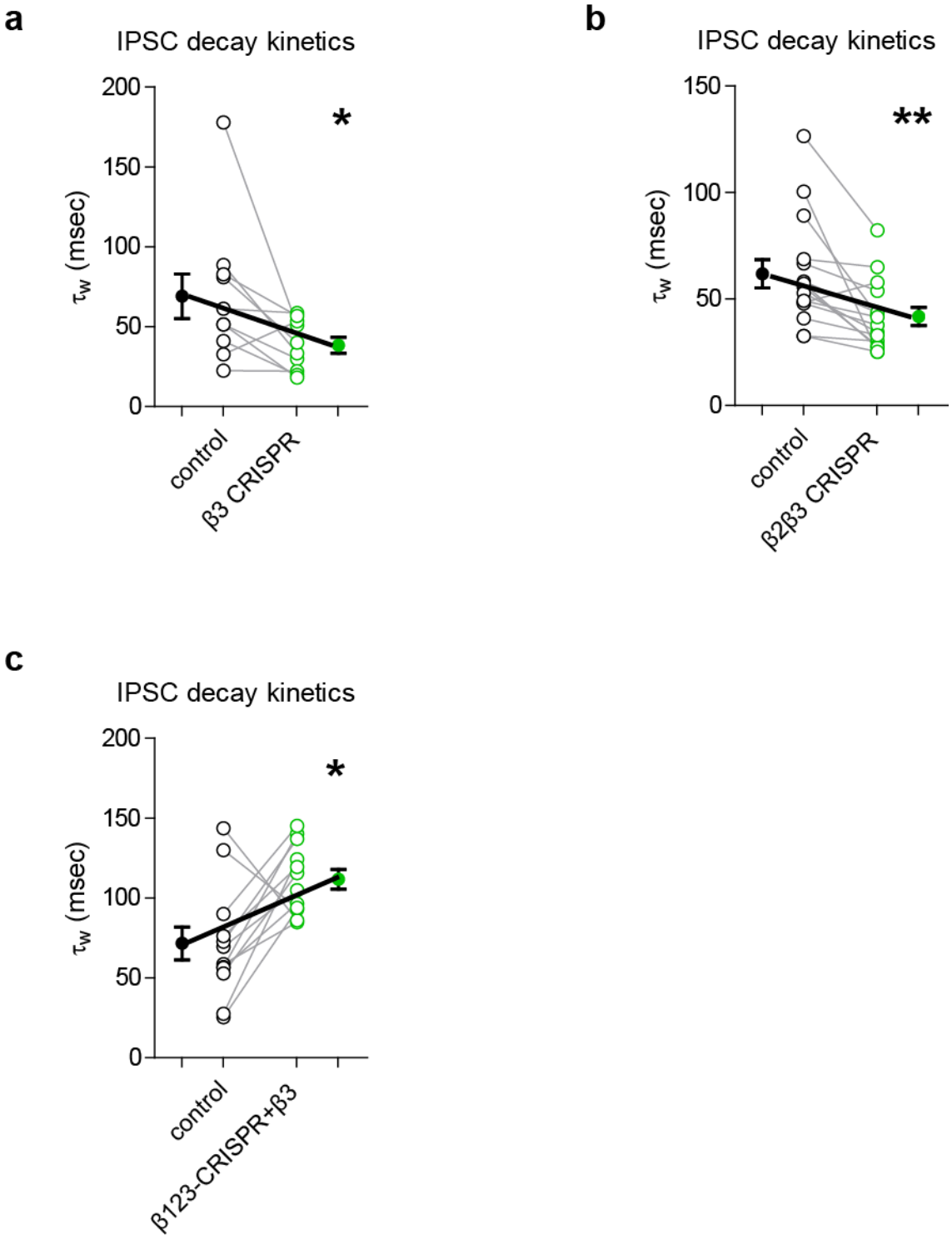
a
IPSC decay kinetics
200
150
100
50
0
τw (msec)
*
control
β3 CRISPR
b
IPSC decay kinetics
150
100
50
0
τw (msec)
**
control
β2β3 CRISPR
c
IPSC decay kinetics
200
150
100
50
0
τw (msec)
*
control
β123-CRISPR+β3

Figure 29: $GABA_A$ β3 subunit is sufficient to restore inhibitory transmission

a) Scatter plot showing expression of β3 on the background of triple β subunit CRISPR is able to restore inhibitory synaptic currents ($p = 0.06$, $n = 14$). b) Summary graph of a. c) Scatter plot showing no responses to a puff of GABA in cells transfected with the triple β subunit CRISPR compared to untransfected controls ($*p = 0.0156$, $n = 7$). d) Scatter plot showing rescue of responses to a puff of GABA in cells transfected with the triple β subunit CRISPR and β3 ($p = 0.5$, $n = 8$). For panels a and c-d, open circles are individual pairs, filled circle is mean ± s.e.m. Black sample traces are control, green are transfected. Scale bars represent 100 pA and 50 ms. For panel b summary graph plots mean transfected amplitude ± s.e.m, expressed as a percentage of control amplitude.

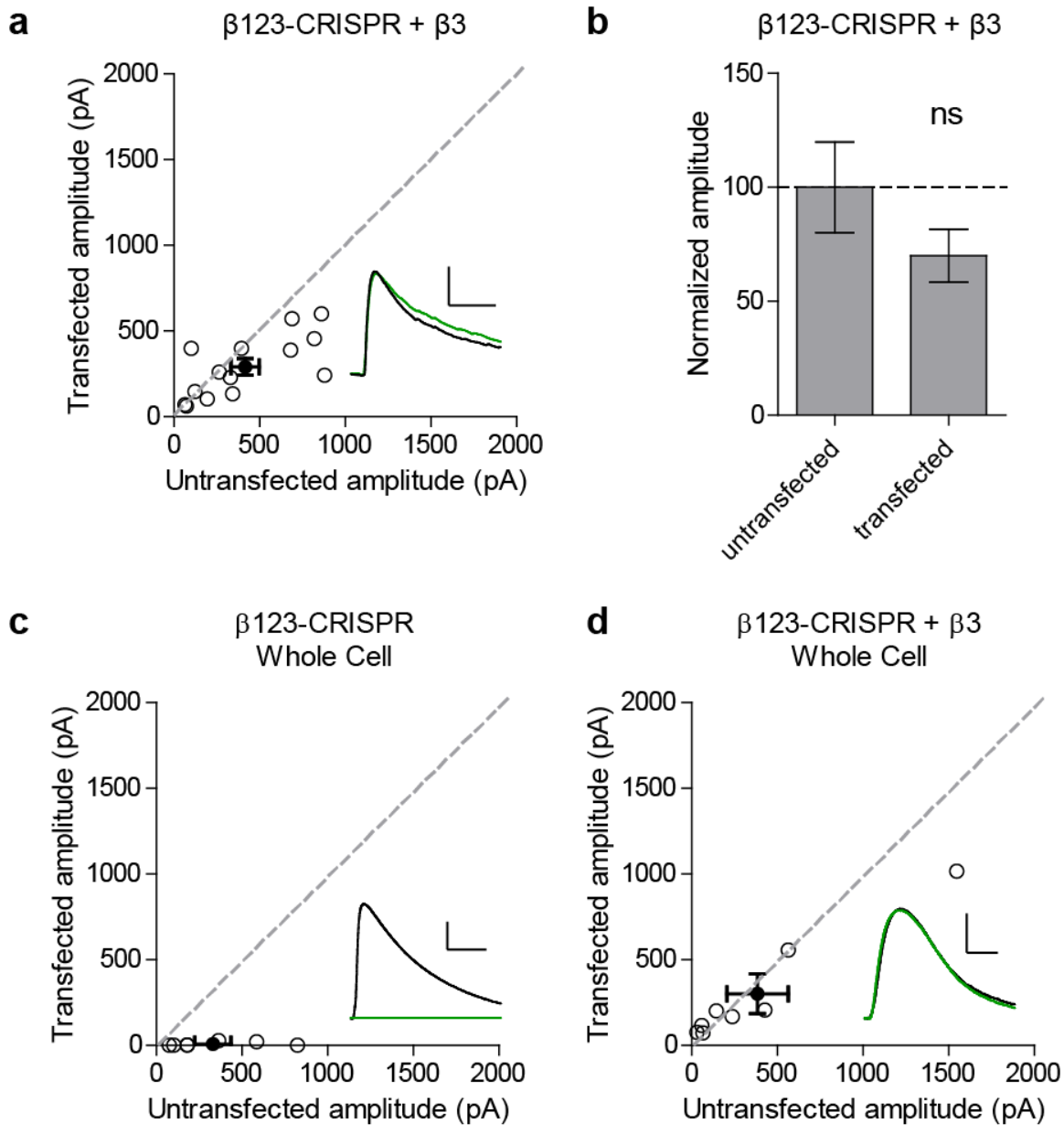
a
β123-CRISPR + β3
Transfected amplitude (pA)
Untransfected amplitude (pA)
0
500
1000
1500
2000
b
β123-CRISPR + β3
Normalized amplitude
ns
150
100
50
0
untransfected
transfected
c
β123-CRISPR
Whole Cell
Transfected amplitude (pA)
Untransfected amplitude (pA)
d
β123-CRISPR + β3
Whole Cell
Transfected amplitude (pA)
Untransfected amplitude (pA)

Figure 30: Model for synapse-specific $GABA_A$ receptor β subunit localization

Our model proposes the existence of two different types of inhibitory synapses. One that has $GABA_A$ receptors with β3 as the only β subunit and one that receptors comprised of all three β isoforms.

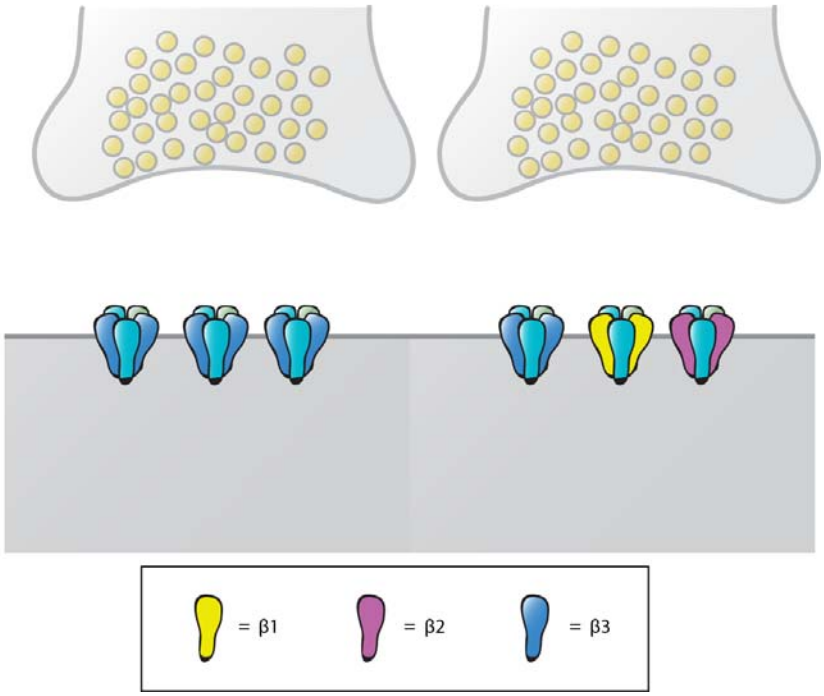
= β1
= β2
= β3

CHAPTER 6:

General Conclusions

This body of work has aimed to tackle the question of how molecular diversity specifies function of a synapse. I showed that two different neuroligin isoforms which are both expressed at inhibitory synapses have different requirements for their ability to enhance inhibitory synaptic transmission (Chapter 3). I showed that a single point mutation in one neuroligin isoform at inhibitory synapses has no effect (Chapter 3) but the same analogous point mutation in another neuroligin isoform at excitatory synapses has profound effects (Chapter 4). I show that the general need for the presence of one subunit family for proper assembly of a $GABA_A$ receptor can be further refined for particular isoforms of that subunit and at particular synapses (Chapter 5).

Neuroligin 3 has distinct functions at inhibitory vs excitatory synapses

The neuroligin family of cell adhesion molecules encompass multiple isoforms and alternative splicing generates even more variants (Ichtchenko et al., 1996). This vast diversity suggests that each variant could have a specialized function, and indeed this is largely the case with neuroligin 1 and neuroligin 2 which are localized to excitatory and inhibitory synapses respectively (Song et al., 1999; Varoqueaux et al., 2004). Neuroligin 3 is expressed at both inhibitory and excitatory synapses but it was previously unclear whether its function was the same at both (Budreck and Scheiffele, 2007). Previous work had shown that overexpression of neuroligin 3 is able to enhance synaptic responses at excitatory synapses even when expression of all endogenous neuroligins are knocked down (Shipman et al., 2011). Here we have shown that neuroligin 3 function at inhibitory synapses requires the presence of neuroligin 2 and this requirement is separate from its ability to function at excitatory synapses.

A key question that remains is what exactly is the nature of this requirement? The basic functional arrangement of the neuroligins is in the form of a dimer. This was previously proposed by examining the similarity between the neuroligins and acetylcholinesterase and subsequent biochemical, functional, and structural studies have confirmed the formation of neuroligins into dimers (Arac et al., 2007; Comoletti et al., 2003; Comoletti et al., 2007; Dean et al., 2003; Fabrichny et al., 2007; Koehnke et al., 2008; Shipman and Nicoll, 2012a). Does neuroligin 3 need to heterodimerize with neuroligin 2 in order to function at inhibitory synapses or does it just need the presence but not direct interaction with neuroligin 2?

There is evidence both for and against the formation of neuroligin 2-neuroligin 3 heteromers (Budreck and Scheiffele, 2007; Poulopoulos et al., 2012). We attempted to determine whether neuroligin 2 and neuroligin 3 can interact directly using biochemical pull down assays from HEK cells expressing neuroligin 2 and neuroligin 3 (Figure 31). HEK cells were transfected with constructs for either GFP, neuroligin 2, neuroligin 3, or both neuroligin 2 and neuroligin 3. The neuroligin 2 construct contained an HA tag that we immunoprecipitated for and then blotted for neuroligin 3 to determine if the two bind. We see robust neuroligin 3 signal in the IP samples from cells expressing both neuroligin 2 and neuroligin 3. We can also see that we did enrich for HA-associated protein complexes since the neuroligin 3 signal in the input lane from cells expressing only neuroligin 3 goes away in the IP lane. We see some signal in the neuroligin 2 only samples in the IP lane and this is due to the fact that the antibody we use can also detect other neuroligins when they are highly overexpressed. Therefore, neuroligin 2 and neuroligin 3 can indeed directly interact. It is unclear whether this direct interaction is necessary for the function of neuroligin 3 at

inhibitory synapses since it would be difficult to separate the binding of neuroligin 3 to neuroligin 2 from the basic necessity of dimerization for function.

Neuroligin 2 is the critical neuroligin at inhibitory synapses

We found that of the neuroligins expressed at inhibitory synapses, neuroligin 2 seems to be most critical for proper inhibitory synaptic transmission. It was only when we knocked down neuroligin 2 but not neuroligin 3 did we see a comparable deficit of inhibitory currents to the knockdown of all three neuroligins. A key question arising from this finding is what exactly makes neuroligin 2 different from neuroligin 3 to enable it to have such an important role at the inhibitory synapse? Our results suggest that the difference may reside in the extracellular domain, at a region between the 52nd and 180th amino acid of neuroligin 2. Could neuroligin 2 bind something within that region that neuroligin 3 can't? While there have been some biochemical and proteomic studies of the various molecules at inhibitory synapses and identification of protein interactions among these molecules, there are no clear candidates that interact with neuroligin 2 but not neuroligin 3 to account for the differences in their function at inhibitory synapses (Kang et al., 2014; Loh et al., 2016).

Based on the idea that the diversity in both neuroligin and its presynaptic binding partner neurexins mediate a type of synaptic code for defining neuronal connections, the most viable candidate for differential binding to the extracellular domain of neuroligin 2 and neuroligin 3 is a neurexin molecule. Unfortunately, it would be difficult to hone in on exactly which neurexin is responsible due to the large diversity of neurexin isoforms and

splice variants possible. However, we have attempted to characterize our critical extracellular domain further by looking at the crystal structure of neuroligin 2 which has previously been resolved (Koehnke et al., 2008). We aligned the structure of neuroligin 2 (3BL8) to the crystal structure of the neuroligin 1/neurexin 1β complex (3BIW, (Arac et al., 2007)) to approximate the location at which neurexin would bind to neuroligin 2 (Figure 32). Highlighted in red is our critical extracellular domain, which appears to be on the side of the neuroligin opposite the neurexin-binding interface, suggesting that molecular partners other than neurexins underlie the ability of this domain to confer neuroligin function at inhibitory synapses. One caveat of this structural prediction is that the neurexin binding sites are based on the neuroligin 1/neurexin 1β complex and it is possible that neurexins at inhibitory synapses bind to neuroligin 2 at a different site. In addition, we noticed that the published crystal structure of neuroligin 2 is missing 14 amino acids around and within the splice site A site, which could affect the true structure of the protein. We were unable to characterize and align neuroligin 3 to our analysis due to the lack of a crystal structure and the inability of structure prediction software to fully predict the sequence of our protein due to the highly disordered region around splice site A.

Gephyrin-independent modes of inhibitory synaptic function

Our finding that even on the background of a gephyrin knockdown a neuroligin 2 lacking all known interaction domains in its intracellular region could still potentiate inhibitory responses was very surprising. Our subsequent results showing that there are gephyrin-dependent and gephyrin-independent pathways for neuroligin function at

inhibitory synapses provides a new avenue of study for identifying and characterizing other scaffolding molecules which could play a role at inhibitory synapses.

It is imperative to make the distinction that our results do not suggest that gephyrin is not important for proper function of inhibitory synapses. Our observation that knockdown of gephyrin reduced inhibitory synaptic current by about 50% suggests that indeed, gephryin is important. Gephyrin is thought to be the major synaptic organizer for GABAergic synapses (Tretter et al., 2012). What we would like to propose is that there are other molecules besides gephyrin that can interact with the intracellular region of the neuroligins to mediate inhibitory synaptic function. Since neuroligin 2 is such a critical component for proper function of inhibitory synapses it would be no surprise that it has multiple pathways in which to carry out its function.

To support this proposition, we have observed firsthand that the interaction between neuroligin 2 and gephyrin is indeed quite weak (Figure 33). We transfected HEK cells with gephyrin and neuroligin 2. We then immunoprecipitated for the HA-tagged neuroligin 2 and blotted for gephyrin to observe the extent of gephyrin interaction with neuroligin 2. Our results show that the gephyrin-neuroligin 2 interaction itself is quite weak. As shown in our blots, we see robust gephyrin signal in our input lanes. However, when we enrich for neuroligin 2, we see about 90% less signal suggesting that most of the gephyrin being overexpressed is not binding to neuroligin 2. A remaining question is what other molecules are interacting at the intracellular domain of neuroligin 2? Future studies utilizing our identified point mutant at S714 which can modulate the gephyrin-independent pathway will need to be performed to answer this question.

Phosphorylation regulates neuroligin function differentially at inhibitory versus excitatory synapses

In chapter 3 I showed that an autism-associated mutation had no effect on neuroligin 2 function on its own. In chapter 4 I showed that the same mutation in neuroligin 4X, where it was initially found, had profound effects on the ability of neuroligin 4X to enhance excitatory responses when overexpressed on a neuroligin knockdown background. These differential results between excitatory and inhibitory responses suggest that the local environment plays a role in determining the consequences of phosphorylation at functional sites. This is consistent with previous results showing that a point mutation which abolished the function of neuroligin 3 and neuroligin 1 at excitatory synapses had no effect on inhibitory synaptic transmission when introduced into neuroligin 2 (Shipman et al., 2011).

To determine whether the same phosphorylation residue has differential effects within the same protein at excitatory versus inhibitory synapses, we looked at our neuroligin 4X manipulations and their effects on inhibitory synaptic transmission (Figure 34). Surprisingly we found that compared to full-length neuroligin 4X which potentiated inhibitory responses, the single autism-associated mutation completely blocked this potentiation. This result suggests that even within the same synaptic environment phosphorylation could have differential effects on different isoforms of the same protein family. One caveat to this is that the unique nature of neuroligin 4X, including its lack of endogenous expression in rats and its low conservation between species, may make it special in terms of its function. We also found no consequence of expressing phospho-null or phospho-mimic mutations for the PKC site we had identified on the ability of neuroligin

4X to potentiate inhibitory responses. This suggests that the ability of neuroligin 4X to enhance inhibitory responses does not depend on phosphorylation by PKC.

The importance of the β3 subunit for $GABA_A$ receptor function

There are two findings with respect to our manipulations involving the β3 subunit. First, β3 knockout in pyramidal cells affects PV but not SOM inputs onto the cells. Second, the presence or absence of the β3 subunit can bidirectionally control kinetics of the $GABA_A$ receptor. These two observations may be independent of each other since we expect inhibitory currents to get slower if there are less PV inputs onto the cell but instead they are faster with β3 knockout.

While differences have been observed for the subcellular distribution of α subunit isoforms, attempts using immunocytochemistry and high-resolution immunogold labeling to determine the distribution of β subunit isoforms utilized antibodies that recognized both β2 and β3, preventing the ability to distinguish different localization patterns between the two isoforms (Baude et al., 1992; Nusser et al., 1995; Nusser et al., 1996). More recently, experiments using antibodies specific for the individual isoforms have shown that all axon-initial segment and somatic synapses in CA1 contain β1, β2, and β3 subunits (Kerti-Szigeti and Nusser, 2016). These areas are thought to be where PV interneurons make their targets and further supports our observation that β3 knockout affects inputs from these cells. It would be of interest to isolate the PV responses from cells lacking β1 or β2 to see if there is also a deficit, though our results showing no change in electrically evoked inhibitory responses suggests there might be compensation by β3.

Differences in the kinetics of the $GABA_A$ receptor are thought to underlie distinct modes of information processing. Fast inhibitory currents are effective at reducing spiking activity early in a train and can modulate the threshold of input-output transfer within a circuit (Crowley et al., 2009). On the other hand, slow currents are effective at suppressing late spikes and can modulate both the gain and threshold of input-output transfer in a circuit (Crowley et al., 2009; Mitchell and Silver, 2003; Prescott and De Koninck, 2003). These changes to information processing could underlie the variable effects in sensory processing seen in heterozygous β3 knockout mice (DeLorey et al., 2011). A more thorough dissection of the consequences of β3 knockout on specific circuit and network functions is needed to tie these changes in receptor kinetics with behavioral effects. These findings combined with our observations and the subsequent model we built from our results could help explain why knockout of β3 is so lethal.

E/I balance and the interplay of inhibition and excitation

While we tend to group synapses into either inhibitory or excitatory, the manipulations on one type of synapse can indeed affect function of the other type. For example, neurons incubated in bicuculline, a $GABA_A$ receptor antagonist, experience a homeostatic reduction in the amplitude of AMPA-mediated excitatory currents (Turrigiano et al., 1998). Blockade of $GABA_A$ receptors causes an increase in the firing rate of the neuron and it responds accordingly to modulate the strength of its excitatory inputs and stabilize firing (Turrigiano, 2008).

Some of our manipulations to proteins at inhibitory synapses do indeed affect excitatory transmission, but in an unexpected and non-canonical manner. We see no change in AMPA-mediated currents with knockdown of gephyrin, but we see a significant reduction in NMDA-mediated currents (Figure 35). This is recapitulated in our triple β subunit knockout, suggesting a common mechanism downstream of reducing most or all inhibitory inputs. This result is surprising since we expected a reduction in AMPA-mediated currents if homeostatic mechanisms were taking place to account for the loss of inhibitory inputs and subsequent increase in the firing rate of the cell. However, this result is in line with what has been observed previously in mice lacking receptors for excitatory transmission. Mice lacking all AMPA and NMDA receptors experience a significant reduction in GABAergic inhibitory transmission (Lu et al., 2013). This effect was recapitulated only in mice lacking NMDA receptors, not in mice lacking only AMPA receptors (Gu et al., 2016). Thus, these results suggest that there is bidirectional interplay between NMDA-receptor mediated excitatory and GABAergic inhibitory transmission. It is possible these effects are occurring at immature synapses which possess specializations for both inhibitory and excitatory synapses (Cserep et al., 2012). In addition, the existence of inhibitory synapses on or near dendritic spines indicate that there could be enough close proximity between excitatory and inhibitory synapses to mediate interactions (Chen et al., 2012; Chiu et al., 2013). While the downstream mechanisms underlying these effects remain to be elucidated, neuronal activity and the activation of calmodulin seem to be required for these effects ((Gu et al., 2016) and Figure 35).

Potential Caveats

There are multiple caveats to our conclusions. The first is the large extent of overexpression we are utilizing in our manipulations. This high degree of overexpression of introduced constructs could explain why the neuroligin manipulations which were classified as not functional still rescued currents back to baseline. We surmise that this is due to incomplete knockdown of endogenous proteins and therefore the remaining endogenous neuroligin can heterodimerize with the overexpressed neuroligin isoform to rescue currents back to baseline. This high degree of overexpression may also cause us to miss more subtle effects that are present when proteins are expressed at more endogenous levels.

While our results are applicable to the experimental system and brain region we are studying, there is a need to determine whether our findings are applicable to other areas of the brain and in different stages of development as well. For example, knockout of neuroligin 3 impairs synaptic inhibition on striatal medium spiny neurons (Rothwell et al., 2014). The hippocampus is particularly unique in its low expression of the β2 subunit compared to the rest of the brain (Mohler et al., 1995; Sperk et al., 1997; Stephenson, 1995). Thus, it would be of importance to determine whether the effects we observe in our β subunit knockouts are also present in other brain regions where the subunit expression profile is different.

Concluding remarks

The vast diversity in synaptic proteins, receptor subunits, and interneuron cell types presents an increasingly complex biological system in which to study inhibitory synaptic transmission. Our results show that this diversity conveys unique functions and helps refine and distinguish individual synapses. By establishing a basic mechanism for how changes to particular synaptic proteins affect inhibitory transmission overall and within a set of defined circuits, we can extrapolate our findings to investigate how these changes affect neuronal processing on a network and region-specific level. The development and evolution of molecular tools to dissect specific inputs and more efficiently change and regulate the expression of particular proteins will be invaluable in helping to tackle the understanding of this complex system.

Figure 31: Neuroligin 2 associates with neuroligin 3

HEK293T cells were transfected with either GFP, NLGN2, NLGN3, or NLGN2+NLGN3. After 2 days lysates were harvested and incubated in HA-conjugated agarose beads to immunoprecipitate HA-tagged protein complexes. Samples were run on a 4-12% Bis-Tris gel and probed for HA, NLGN3, and actin. Input samples are 3% of IP samples. Blot are representative of at least 2 experimental and technical replicates. Size indicated on left in kDa.

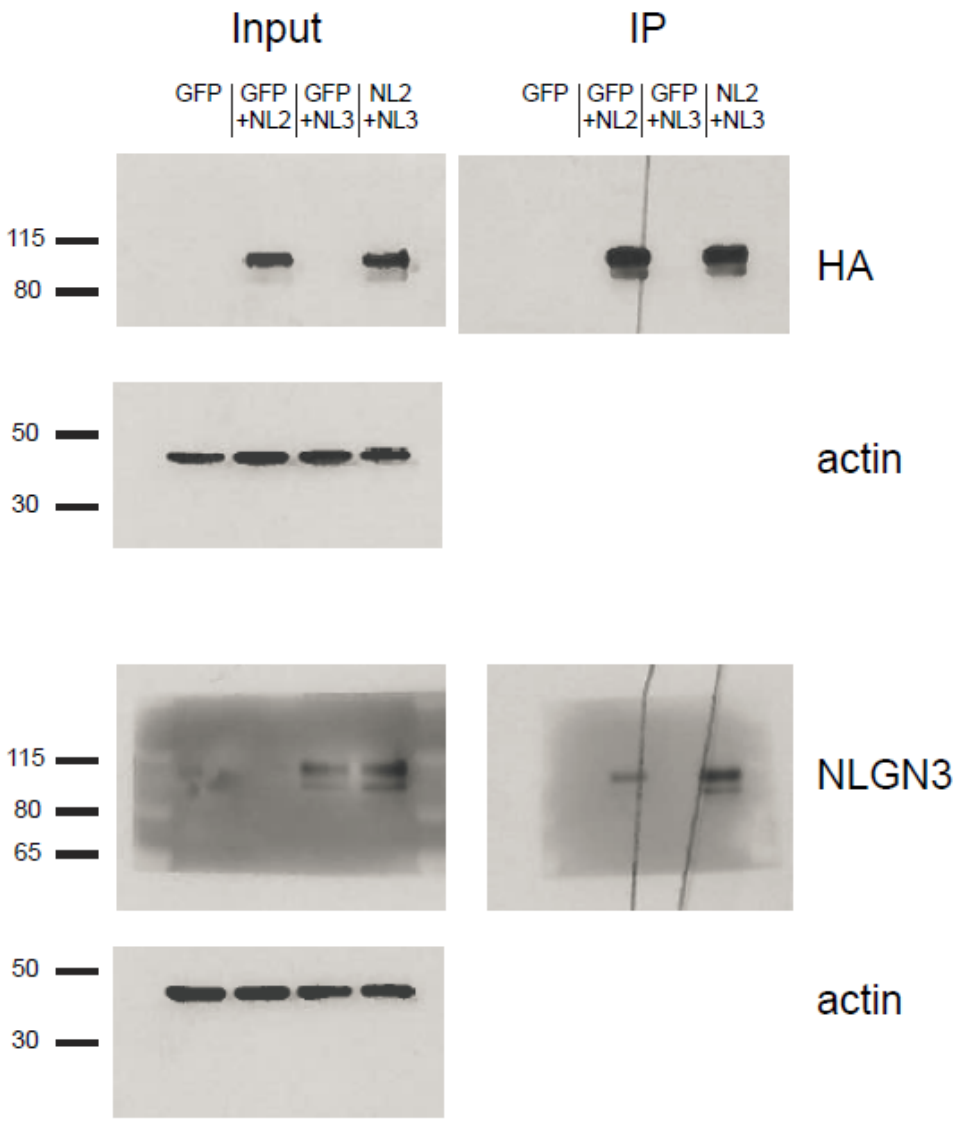
Input
IP
GFP
GFP +NL2
GFP +NL3
NL2 +NL3
115
80
HA
50
30
actin
115
80
65
NLGN3
50
30
actin

Figure 32: Structural visualization of critical extracellular domain

Crystal structure of neuroligin 2 (in blue) aligned with neurexin 1β structure (in orange). In red is the critical extracellular domain in neuroligin 2 identified in our study.

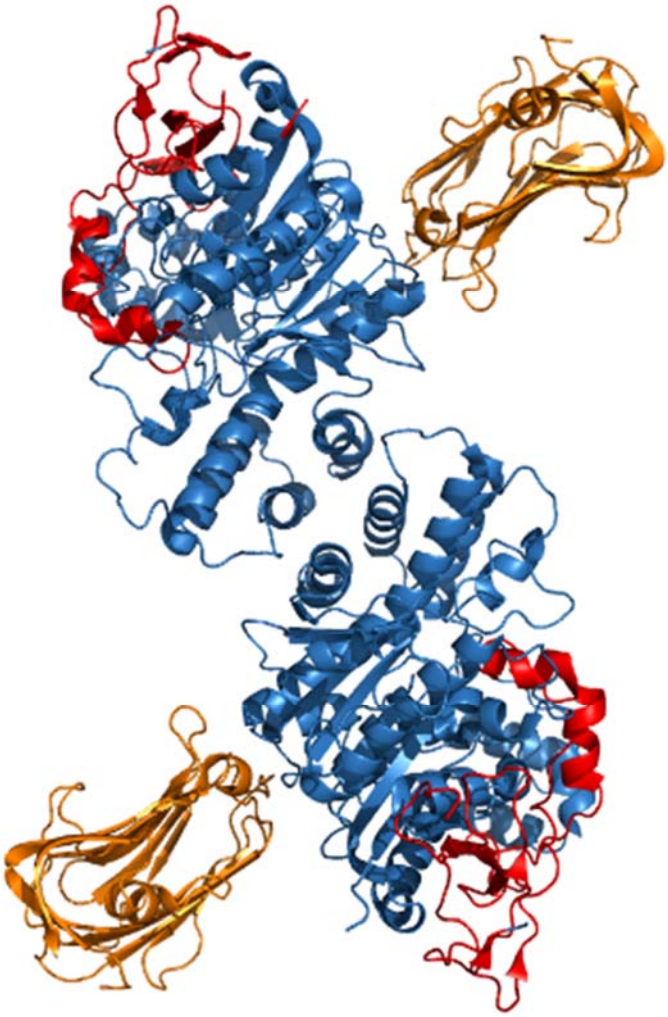

Figure 33: Weak binding of neuroligin 2 to gephyrin

HEK293T cells were transfected with either GFP or neuroligin 2. After 2 days lysates were harvested and incubated in HA-conjugated agarose beads to immunoprecipitate HA-tagged protein complexes. . Samples were run on a 4-12% Bis-Tris gel and probed for HA, gephyrin, and actin. Input samples are 3% of IP samples. Blots are representative of at least 2 technical replicates. Size indicated on left in kDa.

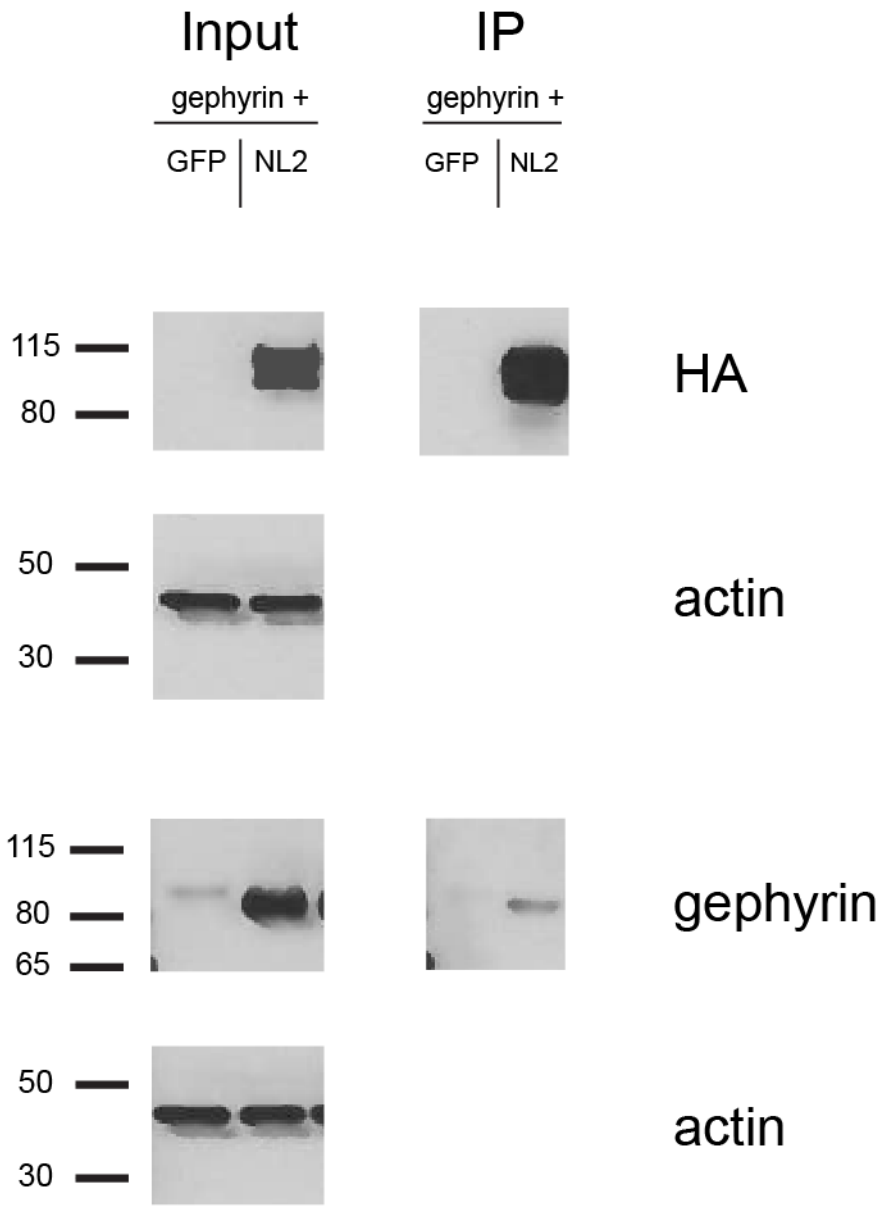
Input
IP
gephyrin +
GFP
NL2
gephyrin +
GFP
NL2
115
80
HA
50
30
actin
115
80
65
gephyrin
50
30
actin

Figure 34: NLGN4X-R704C effect on inhibitory transmission does not depend on PKC residue

a) Scatter plot showing expression of NLGN4X potentiates inhibitory responses (**p = 0.009). b) Scatter plot showing expression of NLGN4X-R704C does not potentiate inhibitory responses (p = 0.7). c) Scatter plot showing expression of NLGN4X-T707A potentiates inhibitory responses (**p = 0.0039). d) Scatter plot showing expression of NLGN4X- T707D potentiates inhibitory responses (**p = 0.002). e) Summary graph of a-d. Expression of full-length NLGN4X, NLGN4-T707A and NLGN4X-T707D results in greater enhancement of IPSCs compared to expression of NLGN4-R704C (*p = 0.0457, **p = 0.0084, **p = 0.0011). For panels a-d, open circles are individual pairs, filled circle is mean ± s.e.m. Black sample traces are control, green are transfected. Scale bars represent 100 pA and 50 ms. For panel e summary graph plots mean transfected amplitude ± s.e.m, expressed as a percentage of control amplitude.

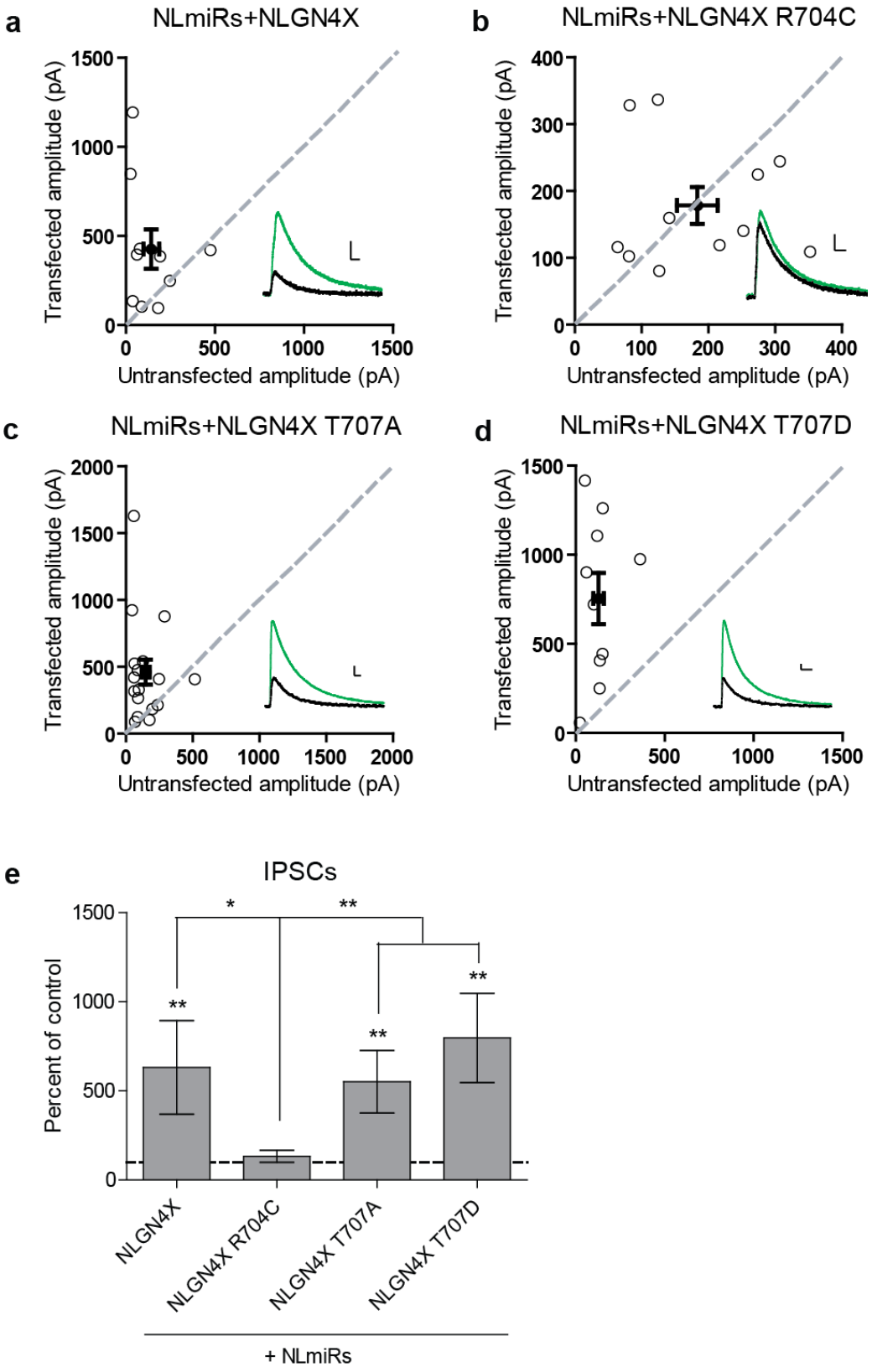
a
NLmiRs+NLGN4X
Transfected amplitude (pA)
Untransfected amplitude (pA)
0
500
1000
1500
b
NLmiRs+NLGN4X R704C
Transfected amplitude (pA)
Untransfected amplitude (pA)
0
100
200
300
400
c
NLmiRs+NLGN4X T707A
Transfected amplitude (pA)
Untransfected amplitude (pA)
0
500
1000
1500
2000
d
NLmiRs+NLGN4X T707D
Transfected amplitude (pA)
Untransfected amplitude (pA)
0
500
1000
1500
e
IPSCs
Percent of control
0
500
1000
1500
*
**
**
**
**
NLGN4X
NLGN4X R704C
NLGN4X T707A
NLGN4X T707D
+ NLmiRs

Figure 35: Gephyrin knockdown and CRISPR β1-3 knockout affects NMDA but not AMPA currents

a) Scatter plot showing knockdown of gephyrin did not reduce AMPA currents but significantly reduced NMDA currents ($p = 0.52$, $^{**}p = 0.0059$). b) Scatter plot showing knockout of β1-3 did not reduce AMPA currents but significantly reduced NMDA currents ($p = 0.24$, $^{*}p = 0.0156$). c) Scatter plot showing incubation of cells expressing gephyrin knockdown with TTX prevented the decrease in NMDA currents ($p = 0.3$).For panels a-c, open circles are individual pairs, filled circle is mean ± s.e.m. Black sample traces are control, green are transfected. Scale bars represent 100 pA and 50 ms. Summary graph plots mean transfected amplitude ± s.e.m, expressed as a percentage of control amplitude.

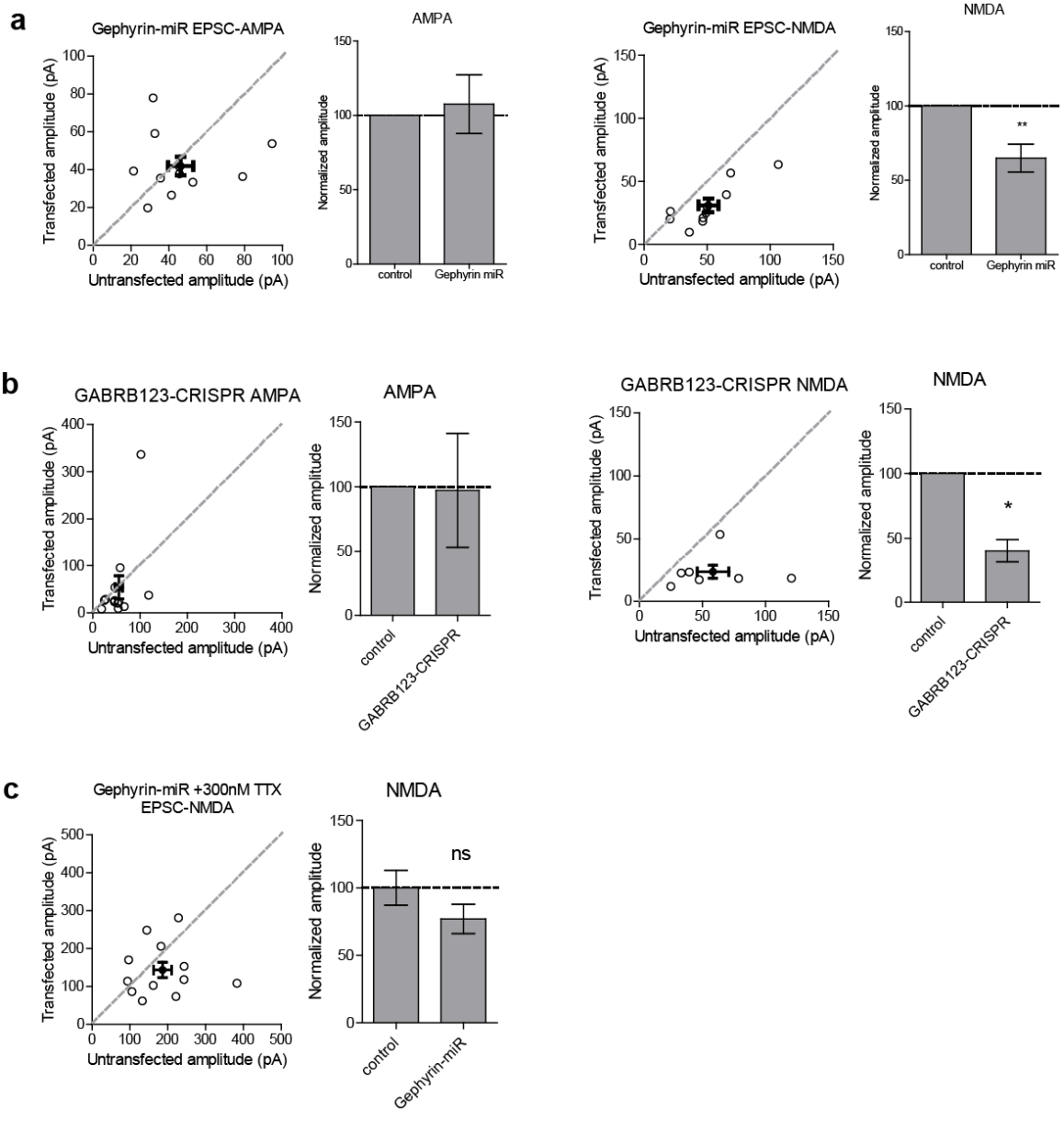
a
Gephyrin-miR EPSC-AMPA
Transfected amplitude (pA)
Untransfected amplitude (pA)
AMPA
Normalized amplitude
control
Gephyrin miR
Gephyrin-miR EPSC-NMDA
NMDA
**
b
GABRB123-CRISPR AMPA
GABRB123-CRISPR NMDA
*
GABRB123-CRISPR
c
Gephyrin-miR +300nM TTX
EPSC-NMDA
ns
Gephyrin-miR

References

Abrahams, B.S., and Geschwind, D.H. (2008). Advances in autism genetics: on the threshold of a new neurobiology. Nat Rev Genet *9*, 341-355.

Antonelli, R., Pizzarelli, R., Pedroni, A., Fritschy, J.M., Del Sal, G., Cherubini, E., and Zacchi, P. (2014). Pin1-dependent signalling negatively affects GABAergic transmission by modulating neuroligin2/gephyrin interaction. Nat Commun *5*, 5066.

Arac, D., Boucard, A.A., Ozkan, E., Strop, P., Newell, E., Sudhof, T.C., and Brunger, A.T. (2007). Structures of neuroligin-1 and the neuroligin-1/neurexin-1 beta complex reveal specific protein-protein and protein-Ca2+ interactions. Neuron *56*, 992-1003.

Bang, M.L., and Owczarek, S. (2013). A matter of balance: role of neurexin and neuroligin at the synapse. Neurochem Res *38*, 1174-1189.

Baude, A., Sequier, J.M., McKernan, R.M., Olivier, K.R., and Somogyi, P. (1992). Differential subcellular distribution of the alpha 6 subunit versus the alpha 1 and beta 2/3 subunits of the GABAA/benzodiazepine receptor complex in granule cells of the cerebellar cortex. Neuroscience *51*, 739-748.

Bemben, M.A., Nguyen, Q.A., Wang, T., Li, Y., Nicoll, R.A., and Roche, K.W. (2015a). Autism-associated mutation inhibits protein kinase C-mediated neuroligin-4X enhancement of excitatory synapses. Proc Natl Acad Sci U S A *112*, 2551-2556.

Bemben, M.A., Shipman, S.L., Hirai, T., Herring, B.E., Li, Y., Badger, J.D., 2nd, Nicoll, R.A., Diamond, J.S., and Roche, K.W. (2014). CaMKII phosphorylation of neuroligin-1 regulates excitatory synapses. Nat Neurosci *17*, 56-64.

Bemben, M.A., Shipman, S.L., Nicoll, R.A., and Roche, K.W. (2015b). The cellular and molecular landscape of neuroligins. Trends Neurosci *38*, 496-505.

Bezaire, M.J., Raikov, I., Burk, K., Vyas, D., and Soltesz, I. (2016). Interneuronal mechanisms of hippocampal theta oscillation in a full-scale model of the rodent CA1 circuit. Elife *5*.

Bolliger, M.F., Pei, J., Maxeiner, S., Boucard, A.A., Grishin, N.V., and Sudhof, T.C. (2008). Unusually rapid evolution of Neuroligin-4 in mice. Proc Natl Acad Sci U S A *105*, 6421-6426.

Brickley, S.G., and Mody, I. (2012). Extrasynaptic GABA(A) receptors: their function in the CNS and implications for disease. Neuron *73*, 23-34.

Budreck, E.C., Kwon, O.B., Jung, J.H., Baudouin, S., Thommen, A., Kim, H.S., Fukazawa, Y., Harada, H., Tabuchi, K., Shigemoto, R.*, et al.* (2013). Neuroligin-1 controls synaptic abundance of NMDA-type glutamate receptors through extracellular coupling. Proc Natl Acad Sci U S A *110*, 725-730.

Budreck, E.C., and Scheiffele, P. (2007). Neuroligin-3 is a neuronal adhesion protein at GABAergic and glutamatergic synapses. Eur J Neurosci *26*, 1738-1748.

Chang, Y., Wang, R., Barot, S., and Weiss, D.S. (1996). Stoichiometry of a recombinant GABAA receptor. J Neurosci *16*, 5415-5424.

Chen, J.L., Villa, K.L., Cha, J.W., So, P.T., Kubota, Y., and Nedivi, E. (2012). Clustered dynamics of inhibitory synapses and dendritic spines in the adult neocortex. Neuron *74*, 361-373.

Cherubini, E. (2012). Phasic GABAA-Mediated Inhibition. In Jasper's Basic Mechanisms of the Epilepsies, J.L. Noebels, M. Avoli, M.A. Rogawski, R.W. Olsen, and A.V. Delgado-Escueta, eds. (Bethesda (MD)).

Chih, B., Engelman, H., and Scheiffele, P. (2005). Control of excitatory and inhibitory synapse formation by neuroligins. Science *307*, 1324-1328.

Chih, B., Gollan, L., and Scheiffele, P. (2006). Alternative splicing controls selective trans-synaptic interactions of the neuroligin-neurexin complex. Neuron *51*, 171-178.

Chiu, C.Q., Lur, G., Morse, T.M., Carnevale, N.T., Ellis-Davies, G.C., and Higley, M.J. (2013). Compartmentalization of GABAergic inhibition by dendritic spines. Science *340*, 759-762.

Choii, G., and Ko, J. (2015). Gephyrin: a central GABAergic synapse organizer. Exp Mol Med *47*, e158.

Chubykin, A.A., Atasoy, D., Etherton, M.R., Brose, N., Kavalali, E.T., Gibson, J.R., and Sudhof, T.C. (2007). Activity-dependent validation of excitatory versus inhibitory synapses by neuroligin-1 versus neuroligin-2. Neuron *54*, 919-931.

Comoletti, D., Flynn, R., Jennings, L.L., Chubykin, A., Matsumura, T., Hasegawa, H., Sudhof, T.C., and Taylor, P. (2003). Characterization of the interaction of a recombinant soluble neuroligin-1 with neurexin-1beta. J Biol Chem *278*, 50497-50505.

Comoletti, D., Grishaev, A., Whitten, A.E., Tsigelny, I., Taylor, P., and Trewhella, J. (2007). Synaptic arrangement of the neuroligin/beta-neurexin complex revealed by X-ray and neutron scattering. Structure *15*, 693-705.

Craig, A.M., and Kang, Y. (2007). Neurexin-neuroligin signaling in synapse development. Curr Opin Neurobiol *17*, 43-52.

Crowley, J.J., Fioravante, D., and Regehr, W.G. (2009). Dynamics of fast and slow inhibition from cerebellar golgi cells allow flexible control of synaptic integration. Neuron *63*, 843-853.

Cserep, C., Szabadits, E., Szonyi, A., Watanabe, M., Freund, T.F., and Nyiri, G. (2012). NMDA receptors in GABAergic synapses during postnatal development. PLoS One *7*, e37753.

Danglot, L., Triller, A., and Bessis, A. (2003). Association of gephyrin with synaptic and extrasynaptic GABAA receptors varies during development in cultured hippocampal neurons. Mol Cell Neurosci *23*, 264-278.

Dean, C., and Dresbach, T. (2006). Neuroligins and neurexins: linking cell adhesion, synapse formation and cognitive function. Trends Neurosci *29*, 21-29.

Dean, C., Scholl, F.G., Choih, J., DeMaria, S., Berger, J., Isacoff, E., and Scheiffele, P. (2003). Neurexin mediates the assembly of presynaptic terminals. Nat Neurosci *6*, 708-716.

DeLorey, T.M., Handforth, A., Anagnostaras, S.G., Homanics, G.E., Minassian, B.A., Asatourian, A., Fanselow, M.S., Delgado-Escueta, A., Ellison, G.D., and Olsen, R.W. (1998). Mice lacking the beta3 subunit of the GABAA receptor have the epilepsy phenotype and many of the behavioral characteristics of Angelman syndrome. J Neurosci *18*, 8505-8514.

DeLorey, T.M., Sahbaie, P., Hashemi, E., Li, W.W., Salehi, A., and Clark, D.J. (2011). Somatosensory and sensorimotor consequences associated with the heterozygous disruption of the autism candidate gene, Gabrb3. Behav Brain Res *216*, 36-45.

Developmental Disabilities Monitoring Network Surveillance Year Principal, I., Centers for Disease, C., and Prevention (2014). Prevalence of autism spectrum disorder among children aged 8 years - autism and developmental disabilities monitoring network, 11 sites, United States, 2010. MMWR Surveill Summ *63*, 1-21.

Essrich, C., Lorez, M., Benson, J.A., Fritschy, J.M., and Luscher, B. (1998). Postsynaptic clustering of major GABAA receptor subtypes requires the gamma 2 subunit and gephyrin. Nat Neurosci *1*, 563-571.

Etherton, M.R., Tabuchi, K., Sharma, M., Ko, J., and Sudhof, T.C. (2011). An autism-associated point mutation in the neuroligin cytoplasmic tail selectively impairs AMPA receptor-mediated synaptic transmission in hippocampus. EMBO J *30*, 2908-2919.

Fabrichny, I.P., Leone, P., Sulzenbacher, G., Comoletti, D., Miller, M.T., Taylor, P., Bourne, Y., and Marchot, P. (2007). Structural analysis of the synaptic protein neuroligin and its beta-neurexin complex: determinants for folding and cell adhesion. Neuron *56*, 979-991.

Farrant, M., and Nusser, Z. (2005). Variations on an inhibitory theme: phasic and tonic activation of GABA(A) receptors. Nat Rev Neurosci *6*, 215-229.

Fekete, C.D., Chiou, T.T., Miralles, C.P., Harris, R.S., Fiondella, C.G., Loturco, J.J., and De Blas, A.L. (2015). In vivo clonal overexpression of neuroligin 3 and neuroligin 2 in neurons of the rat cerebral cortex: Differential effects on GABAergic synapses and neuronal migration. J Comp Neurol *523*, 1359-1378.

Foldy, C., Malenka, R.C., and Sudhof, T.C. (2013). Autism-associated neuroligin-3 mutations commonly disrupt tonic endocannabinoid signaling. Neuron *78*, 498-509.

Fritschy, J.M., and Panzanelli, P. (2014). GABAA receptors and plasticity of inhibitory neurotransmission in the central nervous system. Eur J Neurosci *39*, 1845-1865.

Fu, Z., Washbourne, P., Ortinski, P., and Vicini, S. (2003). Functional excitatory synapses in HEK293 cells expressing neuroligin and glutamate receptors. J Neurophysiol *90*, 3950-3957.

Fuccillo, M.V., Foldy, C., Gokce, O., Rothwell, P.E., Sun, G.L., Malenka, R.C., and Sudhof, T.C. (2015). Single-Cell mRNA Profiling Reveals Cell-Type-Specific Expression of Neurexin Isoforms. Neuron *87*, 326-340.

Futai, K., Doty, C.D., Baek, B., Ryu, J., and Sheng, M. (2013). Specific trans-synaptic interaction with inhibitory interneuronal neurexin underlies differential ability of neuroligins to induce functional inhibitory synapses. J Neurosci *33*, 3612-3623.

Giannone, G., Mondin, M., Grillo-Bosch, D., Tessier, B., Saint-Michel, E., Czondor, K., Sainlos, M., Choquet, D., and Thoumine, O. (2013). Neurexin-1beta binding to neuroligin-1 triggers the preferential recruitment of PSD-95 versus gephyrin through tyrosine phosphorylation of neuroligin-1. Cell Rep *3*, 1996-2007.

Gibson, J.R., Huber, K.M., and Sudhof, T.C. (2009). Neuroligin-2 deletion selectively decreases inhibitory synaptic transmission originating from fast-spiking but not from somatostatin-positive interneurons. J Neurosci *29*, 13883-13897.

Gingrich, K.J., Roberts, W.A., and Kass, R.S. (1995). Dependence of the GABAA receptor gating kinetics on the alpha-subunit isoform: implications for structure-function relations and synaptic transmission. J Physiol *489 (Pt 2)*, 529-543.

Graf, E.R., Zhang, X., Jin, S.X., Linhoff, M.W., and Craig, A.M. (2004). Neurexins induce differentiation of GABA and glutamate postsynaptic specializations via neuroligins. Cell *119*, 1013-1026.

Gu, X., Zhou, L., and Lu, W. (2016). An NMDA Receptor-Dependent Mechanism Underlies Inhibitory Synapse Development. Cell Rep *14*, 471-478.

Herd, M.B., Haythornthwaite, A.R., Rosahl, T.W., Wafford, K.A., Homanics, G.E., Lambert, J.J., and Belelli, D. (2008). The expression of GABAA beta subunit isoforms in synaptic and extrasynaptic receptor populations of mouse dentate gyrus granule cells. J Physiol *586*, 989-1004.

Hoffman, R.C., Jennings, L.L., Tsigelny, I., Comoletti, D., Flynn, R.E., Sudhof, T.C., and Taylor, P. (2004). Structural characterization of recombinant soluble rat neuroligin 1: mapping of secondary structure and glycosylation by mass spectrometry. Biochemistry *43*, 1496-1506.

Homanics, G.E., DeLorey, T.M., Firestone, L.L., Quinlan, J.J., Handforth, A., Harrison, N.L., Krasowski, M.D., Rick, C.E., Korpi, E.R., Makela, R.*, et al.* (1997). Mice devoid of gamma-aminobutyrate type A receptor beta3 subunit have epilepsy, cleft palate, and hypersensitive behavior. Proc Natl Acad Sci U S A *94*, 4143-4148.

Hoon, M., Soykan, T., Falkenburger, B., Hammer, M., Patrizi, A., Schmidt, K.F., Sassoe-Pognetto, M., Lowel, S., Moser, T., Taschenberger, H.*, et al.* (2011). Neuroligin-4 is localized to glycinergic postsynapses and regulates inhibition in the retina. Proc Natl Acad Sci U S A *108*, 3053-3058.

Ichtchenko, K., Nguyen, T., and Sudhof, T.C. (1996). Structures, alternative splicing, and neurexin binding of multiple neuroligins. J Biol Chem *271*, 2676-2682.

Incontro, S., Asensio, C.S., Edwards, R.H., and Nicoll, R.A. (2014). Efficient, complete deletion of synaptic proteins using CRISPR. Neuron *83*, 1051-1057.

Irie, M., Hata, Y., Takeuchi, M., Ichtchenko, K., Toyoda, A., Hirao, K., Takai, Y., Rosahl, T.W., and Sudhof, T.C. (1997). Binding of neuroligins to PSD-95. Science *277*, 1511-1515.

Jacob, T.C., Moss, S.J., and Jurd, R. (2008). GABA(A) receptor trafficking and its role in the dynamic modulation of neuronal inhibition. Nat Rev Neurosci *9*, 331-343.

Jamain, S., Quach, H., Betancur, C., Rastam, M., Colineaux, C., Gillberg, I.C., Soderstrom, H., Giros, B., Leboyer, M., Gillberg, C.*, et al.* (2003). Mutations of the X-linked genes encoding neuroligins NLGN3 and NLGN4 are associated with autism. Nature genetics *34*, 27-29.

Jechlinger, M., Pelz, R., Tretter, V., Klausberger, T., and Sieghart, W. (1998). Subunit composition and quantitative importance of hetero-oligomeric receptors: GABAA receptors containing alpha6 subunits. J Neurosci *18*, 2449-2457.

Kabadi, A.M., Ousterout, D.G., Hilton, I.B., and Gersbach, C.A. (2014). Multiplex CRISPR/Cas9-based genome engineering from a single lentiviral vector. Nucleic Acids Res *42*, e147.

Kang, Y., Ge, Y., Cassidy, R.M., Lam, V., Luo, L., Moon, K.M., Lewis, R., Molday, R.S., Wong, R.O., Foster, L.J.*, et al.* (2014). A combined transgenic proteomic analysis and regulated trafficking of neuroligin-2. J Biol Chem *289*, 29350-29364.

Kawaguchi, Y., and Kubota, Y. (1997). GABAergic cell subtypes and their synaptic connections in rat frontal cortex. Cereb Cortex *7*, 476-486.

Kerti-Szigeti, K., and Nusser, Z. (2016). Similar GABAA receptor subunit composition in somatic and axon initial segment synapses of hippocampal pyramidal cells. Elife *5*.

Kins, S., Betz, H., and Kirsch, J. (2000). Collybistin, a newly identified brain-specific GEF, induces submembrane clustering of gephyrin. Nat Neurosci *3*, 22-29.

Klausberger, T., Magill, P.J., Marton, L.F., Roberts, J.D., Cobden, P.M., Buzsaki, G., and Somogyi, P. (2003). Brain-state- and cell-type-specific firing of hippocampal interneurons in vivo. Nature *421*, 844-848.

Klausberger, T., Marton, L.F., Baude, A., Roberts, J.D., Magill, P.J., and Somogyi, P. (2004). Spike timing of dendrite-targeting bistratified cells during hippocampal network oscillations in vivo. Nat Neurosci *7*, 41-47.

Klausberger, T., and Somogyi, P. (2008). Neuronal diversity and temporal dynamics: the unity of hippocampal circuit operations. Science *321*, 53-57.

Kneussel, M., Brandstatter, J.H., Gasnier, B., Feng, G., Sanes, J.R., and Betz, H. (2001). Gephyrin-independent clustering of postsynaptic GABA(A) receptor subtypes. Mol Cell Neurosci *17*, 973-982.

Knuesel, I., Mastrocola, M., Zuellig, R.A., Bornhauser, B., Schaub, M.C., and Fritschy, J.M. (1999). Short communication: altered synaptic clustering of GABAA receptors in mice lacking dystrophin (mdx mice). Eur J Neurosci *11*, 4457-4462.

Ko, J., Zhang, C., Arac, D., Boucard, A.A., Brunger, A.T., and Sudhof, T.C. (2009). Neuroligin-1 performs neurexin-dependent and neurexin-independent functions in synapse validation. EMBO J *28*, 3244-3255.

Koehnke, J., Jin, X., Budreck, E.C., Posy, S., Scheiffele, P., Honig, B., and Shapiro, L. (2008). Crystal structure of the extracellular cholinesterase-like domain from neuroligin-2. Proc Natl Acad Sci U S A *105*, 1873-1878.

Kosaka, T., Katsumaru, H., Hama, K., Wu, J.Y., and Heizmann, C.W. (1987). GABAergic neurons containing the Ca2+-binding protein parvalbumin in the rat hippocampus and dentate gyrus. Brain Res *419*, 119-130.

Laumonnier, F., Bonnet-Brilhault, F., Gomot, M., Blanc, R., David, A., Moizard, M.P., Raynaud, M., Ronce, N., Lemonnier, E., Calvas, P., *et al.* (2004). X-linked mental retardation and autism are associated with a mutation in the NLGN4 gene, a member of the neuroligin family. American journal of human genetics *74*, 552-557.

Laurie, D.J., Wisden, W., and Seeburg, P.H. (1992). The distribution of thirteen GABAA receptor subunit mRNAs in the rat brain. III. Embryonic and postnatal development. J Neurosci *12*, 4151-4172.

Lavoie, A.M., Tingey, J.J., Harrison, N.L., Pritchett, D.B., and Twyman, R.E. (1997). Activation and deactivation rates of recombinant GABA(A) receptor channels are dependent on alpha-subunit isoform. Biophys J *73*, 2518-2526.

Lawson-Yuen, A., Saldivar, J.S., Sommer, S., and Picker, J. (2008). Familial deletion within NLGN4 associated with autism and Tourette syndrome. Eur J Hum Genet *16*, 614-618.

Lee, K., Kim, Y., Lee, S.J., Qiang, Y., Lee, D., Lee, H.W., Kim, H., Je, H.S., Sudhof, T.C., and Ko, J. (2013). MDGAs interact selectively with neuroligin-2 but not other neuroligins to regulate inhibitory synapse development. Proc Natl Acad Sci U S A *110*, 336-341.

Levi, S., Logan, S.M., Tovar, K.R., and Craig, A.M. (2004). Gephyrin is critical for glycine receptor clustering but not for the formation of functional GABAergic synapses in hippocampal neurons. J Neurosci *24*, 207-217.

Levy, D., Ronemus, M., Yamrom, B., Lee, Y.H., Leotta, A., Kendall, J., Marks, S., Lakshmi, B., Pai, D., Ye, K.*, et al.* (2011). Rare de novo and transmitted copy-number variation in autistic spectrum disorders. Neuron *70*, 886-897.

Li, M., and De Blas, A.L. (1997). Coexistence of two beta subunit isoforms in the same gamma-aminobutyric acid type A receptor. J Biol Chem *272*, 16564-16569.

Loh, K.H., Stawski, P.S., Draycott, A.S., Udeshi, N.D., Lehrman, E.K., Wilton, D.K., Svinkina, T., Deerinck, T.J., Ellisman, M.H., Stevens, B.*, et al.* (2016). Proteomic Analysis of Unbounded Cellular Compartments: Synaptic Clefts. Cell *166*, 1295-1307 e1221.

Lu, W., Bushong, E.A., Shih, T.P., Ellisman, M.H., and Nicoll, R.A. (2013). The cell-autonomous role of excitatory synaptic transmission in the regulation of neuronal structure and function. Neuron *78*, 433-439.

Macdonald, R.L., and Olsen, R.W. (1994). GABAA receptor channels. Annu Rev Neurosci *17*, 569-602.

Mackowiak, M., Mordalska, P., and Wedzony, K. (2014). Neuroligins, synapse balance and neuropsychiatric disorders. Pharmacol Rep *66*, 830-835.

Marei, H.E., Ahmed, A.E., Michetti, F., Pescatori, M., Pallini, R., Casalbore, P., Cenciarelli, C., and Elhadidy, M. (2012). Gene expression profile of adult human olfactory bulb and embryonic neural stem cell suggests distinct signaling pathways and epigenetic control. PLoS One *7*, e33542.

Marshall, C.R., Noor, A., Vincent, J.B., Lionel, A.C., Feuk, L., Skaug, J., Shago, M., Moessner, R., Pinto, D., Ren, Y.*, et al.* (2008). Structural variation of chromosomes in autism spectrum disorder. American journal of human genetics *82*, 477-488.

Mitchell, S.J., and Silver, R.A. (2003). Shunting inhibition modulates neuronal gain during synaptic excitation. Neuron *38*, 433-445.

Mohler, H. (2006). GABAA receptors in central nervous system disease: anxiety, epilepsy, and insomnia. J Recept Signal Transduct Res *26*, 731-740.

Mohler, H., Knoflach, F., Paysan, J., Motejlek, K., Benke, D., Luscher, B., and Fritschy, J.M. (1995). Heterogeneity of GABAA-receptors: cell-specific expression, pharmacology, and regulation. Neurochem Res *20*, 631-636.

Nguyen, T., and Sudhof, T.C. (1997). Binding properties of neuroligin 1 and neurexin 1beta reveal function as heterophilic cell adhesion molecules. J Biol Chem *272*, 26032-26039.

Niwa, F., Bannai, H., Arizono, M., Fukatsu, K., Triller, A., and Mikoshiba, K. (2012). Gephyrin-independent GABA(A)R mobility and clustering during plasticity. PLoS One *7*, e36148.

Nusser, Z., Kay, L.M., Laurent, G., Homanics, G.E., and Mody, I. (2001). Disruption of GABA(A) receptors on GABAergic interneurons leads to increased oscillatory power in the olfactory bulb network. J Neurophysiol *86*, 2823-2833.

Nusser, Z., Roberts, J.D., Baude, A., Richards, J.G., Sieghart, W., and Somogyi, P. (1995). Immunocytochemical localization of the alpha 1 and beta 2/3 subunits of the GABAA receptor in relation to specific GABAergic synapses in the dentate gyrus. Eur J Neurosci *7*, 630-646.

Nusser, Z., Sieghart, W., Benke, D., Fritschy, J.M., and Somogyi, P. (1996). Differential synaptic localization of two major gamma-aminobutyric acid type A receptor alpha subunits on hippocampal pyramidal cells. Proc Natl Acad Sci U S A *93*, 11939-11944.

Olsen, R.W., and Sieghart, W. (2008). International Union of Pharmacology. LXX. Subtypes of gamma-aminobutyric acid(A) receptors: classification on the basis of subunit composition, pharmacology, and function. Update. Pharmacol Rev *60*, 243-260.

Pettem, K.L., Yokomaku, D., Takahashi, H., Ge, Y., and Craig, A.M. (2013). Interaction between autism-linked MDGAs and neuroligins suppresses inhibitory synapse development. J Cell Biol *200*, 321-336.

Poulopoulos, A., Aramuni, G., Meyer, G., Soykan, T., Hoon, M., Papadopoulos, T., Zhang, M., Paarmann, I., Fuchs, C., Harvey, K.*, et al.* (2009). Neuroligin 2 drives postsynaptic assembly at perisomatic inhibitory synapses through gephyrin and collybistin. Neuron *63*, 628-642.

Poulopoulos, A., Soykan, T., Tuffy, L.P., Hammer, M., Varoqueaux, F., and Brose, N. (2012). Homodimerization and isoform-specific heterodimerization of neuroligins. Biochem J *446*, 321-330.

Prescott, S.A., and De Koninck, Y. (2003). Gain control of firing rate by shunting inhibition: roles of synaptic noise and dendritic saturation. Proc Natl Acad Sci U S A *100*, 2076-2081.

Ramadan, E., Fu, Z., Losi, G., Homanics, G.E., Neale, J.H., and Vicini, S. (2003). GABA(A) receptor beta3 subunit deletion decreases alpha2/3 subunits and IPSC duration. J Neurophysiol *89*, 128-134.

Ran, F.A., Hsu, P.D., Wright, J., Agarwala, V., Scott, D.A., and Zhang, F. (2013). Genome engineering using the CRISPR-Cas9 system. Nat Protoc *8*, 2281-2308.

Roche, K.W., O'Brien, R.J., Mammen, A.L., Bernhardt, J., and Huganir, R.L. (1996). Characterization of multiple phosphorylation sites on the AMPA receptor GluR1 subunit. Neuron *16*, 1179-1188.

Rothwell, P.E., Fuccillo, M.V., Maxeiner, S., Hayton, S.J., Gokce, O., Lim, B.K., Fowler, S.C., Malenka, R.C., and Sudhof, T.C. (2014). Autism-associated neuroligin-3 mutations commonly impair striatal circuits to boost repetitive behaviors. Cell *158*, 198-212.

Rudolph, U., and Mohler, H. (2004). Analysis of GABAA receptor function and dissection of the pharmacology of benzodiazepines and general anesthetics through mouse genetics. Annu Rev Pharmacol Toxicol *44*, 475-498.

Rudy, B., Fishell, G., Lee, S., and Hjerling-Leffler, J. (2011). Three groups of interneurons account for nearly 100% of neocortical GABAergic neurons. Dev Neurobiol *71*, 45-61.

Sanders, S.J., Ercan-Sencicek, A.G., Hus, V., Luo, R., Murtha, M.T., Moreno-De-Luca, D., Chu, S.H., Moreau, M.P., Gupta, A.R., Thomson, S.A., *et al.* (2011). Multiple recurrent de novo CNVs, including duplications of the 7q11.23 Williams syndrome region, are strongly associated with autism. Neuron *70*, 863-885.

Sanjana, N.E., Shalem, O., and Zhang, F. (2014). Improved vectors and genome-wide libraries for CRISPR screening. Nat Methods *11*, 783-784.

Scheyltjens, I., and Arckens, L. (2016). The Current Status of Somatostatin-Interneurons in Inhibitory Control of Brain Function and Plasticity. Neural Plast *2016*, 8723623.

Schnell, E., Sizemore, M., Karimzadegan, S., Chen, L., Bredt, D.S., and Nicoll, R.A. (2002). Direct interactions between PSD-95 and stargazin control synaptic AMPA receptor number. Proc Natl Acad Sci U S A *99*, 13902-13907.

Schweizer, C., Balsiger, S., Bluethmann, H., Mansuy, I.M., Fritschy, J.M., Mohler, H., and Luscher, B. (2003). The gamma 2 subunit of GABA(A) receptors is required for maintenance of receptors at mature synapses. Mol Cell Neurosci *24*, 442-450.

Shipman, S.L., and Nicoll, R.A. (2012a). Dimerization of postsynaptic neuroligin drives synaptic assembly via transsynaptic clustering of neurexin. Proc Natl Acad Sci U S A *109*, 19432-19437.

Shipman, S.L., and Nicoll, R.A. (2012b). A subtype-specific function for the extracellular domain of neuroligin 1 in hippocampal LTP. Neuron *76*, 309-316.

Shipman, S.L., Schnell, E., Hirai, T., Chen, B.S., Roche, K.W., and Nicoll, R.A. (2011). Functional dependence of neuroligin on a new non-PDZ intracellular domain. Nat Neurosci *14*, 718-726.

Sieghart, W. (1995). Structure and pharmacology of gamma-aminobutyric acidA receptor subtypes. Pharmacol Rev *47*, 181-234.

Sieghart, W. (2006). Structure, pharmacology, and function of GABAA receptor subtypes. Adv Pharmacol *54*, 231-263.

Sieghart, W., and Sperk, G. (2002). Subunit composition, distribution and function of GABA(A) receptor subtypes. Curr Top Med Chem *2*, 795-816.

Sigel, E., Baur, R., Trube, G., Mohler, H., and Malherbe, P. (1990). The effect of subunit composition of rat brain GABAA receptors on channel function. Neuron *5*, 703-711.

Sigel, E., and Steinmann, M.E. (2012). Structure, function, and modulation of GABA(A) receptors. J Biol Chem *287*, 40224-40231.

Simon, J., Wakimoto, H., Fujita, N., Lalande, M., and Barnard, E.A. (2004). Analysis of the set of GABA(A) receptor genes in the human genome. J Biol Chem *279*, 41422-41435.

Somogyi, P., and Klausberger, T. (2005). Defined types of cortical interneurone structure space and spike timing in the hippocampus. J Physiol *562*, 9-26.

Song, J.Y., Ichtchenko, K., Sudhof, T.C., and Brose, N. (1999). Neuroligin 1 is a postsynaptic cell-adhesion molecule of excitatory synapses. Proc Natl Acad Sci U S A *96*, 1100-1105.

Soykan, T., Schneeberger, D., Tria, G., Buechner, C., Bader, N., Svergun, D., Tessmer, I., Poulopoulos, A., Papadopoulos, T., Varoqueaux, F*., et al.* (2014). A conformational switch in collybistin determines the differentiation of inhibitory postsynapses. EMBO J *33*, 2113-2133.

Sperk, G., Schwarzer, C., Tsunashima, K., Fuchs, K., and Sieghart, W. (1997). GABA(A) receptor subunits in the rat hippocampus I: immunocytochemical distribution of 13 subunits. Neuroscience *80*, 987-1000.

Stephenson, F.A. (1995). The GABAA receptors. Biochem J *310 (Pt 1)*, 1-9.

Stoppini, L., Buchs, P.A., and Muller, D. (1991). A simple method for organotypic cultures of nervous tissue. J Neurosci Methods *37*, 173-182.

Straub, C., Granger, A.J., Saulnier, J.L., and Sabatini, B.L. (2014). CRISPR/Cas9-mediated gene knock-down in post-mitotic neurons. PLoS One *9*, e105584.

Sudhof, T.C. (2008). Neuroligins and neurexins link synaptic function to cognitive disease. Nature *455*, 903-911.

Sur, C., Wafford, K.A., Reynolds, D.S., Hadingham, K.L., Bromidge, F., Macaulay, A., Collinson, N., O'Meara, G., Howell, O., Newman, R.*, et al.* (2001). Loss of the major GABA(A) receptor subtype in the brain is not lethal in mice. J Neurosci *21*, 3409-3418.

Tabuchi, K., Blundell, J., Etherton, M.R., Hammer, R.E., Liu, X., Powell, C.M., and Sudhof, T.C. (2007). A neuroligin-3 mutation implicated in autism increases inhibitory synaptic transmission in mice. Science *318*, 71-76.

Thomas, N.S., Sharp, A.J., Browne, C.E., Skuse, D., Hardie, C., and Dennis, N.R. (1999). Xp deletions associated with autism in three females. Human genetics *104*, 43-48.

Tretter, V., Mukherjee, J., Maric, H.M., Schindelin, H., Sieghart, W., and Moss, S.J. (2012). Gephyrin, the enigmatic organizer at GABAergic synapses. Front Cell Neurosci *6*, 23.

Turrigiano, G.G. (2008). The self-tuning neuron: synaptic scaling of excitatory synapses. Cell *135*, 422-435.

Turrigiano, G.G., Leslie, K.R., Desai, N.S., Rutherford, L.C., and Nelson, S.B. (1998). Activity-dependent scaling of quantal amplitude in neocortical neurons. Nature *391*, 892-896.

Tyagarajan, S.K., and Fritschy, J.M. (2014). Gephyrin: a master regulator of neuronal function? Nat Rev Neurosci *15*, 141-156.

Uezu, A., Kanak, D.J., Bradshaw, T.W., Soderblom, E.J., Catavero, C.M., Burette, A.C., Weinberg, R.J., and Soderling, S.H. (2016). Identification of an elaborate complex mediating postsynaptic inhibition. Science *353*, 1123-1129.

Ullrich, B., Ushkaryov, Y.A., and Sudhof, T.C. (1995). Cartography of neurexins: more than 1000 isoforms generated by alternative splicing and expressed in distinct subsets of neurons. Neuron *14*, 497-507.

Varoqueaux, F., Aramuni, G., Rawson, R.L., Mohrmann, R., Missler, M., Gottmann, K., Zhang, W., Sudhof, T.C., and Brose, N. (2006). Neuroligins determine synapse maturation and function. Neuron *51*, 741-754.

Varoqueaux, F., Jamain, S., and Brose, N. (2004). Neuroligin 2 is exclusively localized to inhibitory synapses. Eur J Cell Biol *83*, 449-456.

Vien, T.N., Modgil, A., Abramian, A.M., Jurd, R., Walker, J., Brandon, N.J., Terunuma, M., Rudolph, U., Maguire, J., Davies, P.A.*, et al.* (2015). Compromising the phosphodependent regulation of the GABAAR beta3 subunit reproduces the core phenotypes of autism spectrum disorders. Proc Natl Acad Sci U S A *112*, 14805-14810.

Walker, M.C., and Kullmann, D.M. (2012). Tonic GABAA Receptor-Mediated Signaling in Epilepsy. In Jasper's Basic Mechanisms of the Epilepsies, J.L. Noebels, M. Avoli, M.A. Rogawski, R.W. Olsen, and A.V. Delgado-Escueta, eds. (Bethesda (MD)).

Wang, T., Allie, R., Conant, K., Haughey, N., Turchan-Chelowo, J., Hahn, K., Rosen, A., Steiner, J., Keswani, S., Jones, M.*, et al.* (2006). Granzyme B mediates neurotoxicity through a G-protein-coupled receptor. FASEB J *20*, 1209-1211.

Washbourne, P., Dityatev, A., Scheiffele, P., Biederer, T., Weiner, J.A., Christopherson, K.S., and El-Husseini, A. (2004). Cell adhesion molecules in synapse formation. J Neurosci *24*, 9244-9249.

Woo, J., Kwon, S.K., Nam, J., Choi, S., Takahashi, H., Krueger, D., Park, J., Lee, Y., Bae, J.Y., Lee, D.*, et al.* (2013). The adhesion protein IgSF9b is coupled to neuroligin 2 via S-SCAM to promote inhibitory synapse development. J Cell Biol *201*, 929-944.

Xu, X., Roby, K.D., and Callaway, E.M. (2010). Immunochemical characterization of inhibitory mouse cortical neurons: three chemically distinct classes of inhibitory cells. J Comp Neurol *518*, 389-404.

Yamagata, M., Sanes, J.R., and Weiner, J.A. (2003). Synaptic adhesion molecules. Curr Opin Cell Biol *15*, 621-632.

Yan, J., Oliveira, G., Coutinho, A., Yang, C., Feng, J., Katz, C., Sram, J., Bockholt, A., Jones, I.R., Craddock, N.*, et al.* (2005). Analysis of the neuroligin 3 and 4 genes in autism and other neuropsychiatric patients. Molecular psychiatry *10*, 329-332.

Zhang, B., Chen, L.Y., Liu, X., Maxeiner, S., Lee, S.J., Gokce, O., and Sudhof, T.C. (2015). Neuroligins Sculpt Cerebellar Purkinje-Cell Circuits by Differential Control of Distinct Classes of Synapses. Neuron *87*, 781-796.

Zhang, J.H., Sato, M., and Tohyama, M. (1991). Different postnatal ontogenic profiles of neurons containing beta (beta 1, beta 2 and beta 3) subunit mRNAs of GABAA receptor in the rat thalamus. Brain Res Dev Brain Res *58*, 289-292.

Zoghbi, H.Y., and Bear, M.F. (2012). Synaptic dysfunction in neurodevelopmental disorders associated with autism and intellectual disabilities. Cold Spring Harb Perspect Biol *4*.

Publishing Agreement

It is the policy of the University to encourage the distribution of all theses, dissertations, and manuscripts. Copies of all UCSF theses, dissertations, and manuscripts will be routed to the library via the Graduate Division. The library will make all theses, dissertations, and manuscripts accessible to the public and will preserve these to the best of their abilities, in perpetuity.

I hereby grant permission to the Graduate Division of the University of California, San Francisco to release copies of my thesis, dissertation, or manuscript to the Campus Library to provide access and preservation, in whole or in part, in perpetuity.

Author Signature  Date 4/30/17